NOTICE

The quality of this microform is heavily dependent upon the quality of the original thesis submitted for microfilming. Every effort has been made to ensure the highest quality of reproduction possible.

If pages are missing, contact the university which granted the degree.

Some pages may have indistinct print especially if the original pages were typed with a poor typewriter ribbon or if the university sent us an inferior photocopy.

Reproduction in full or in part of this microform is governed by the Canadian Copyright Act, R.S.C. 1970, c. C-30, and subsequent amendments.

AVIS

La qualité de cette microforme dépend grandement de la qualité de la thèse soumise au microfilmage. Nous avons tout fait pour assurer une qualité supérieure de reproduction.

S'il manque des pages, veuillez communiquer avec l'université qui a conféré le grade.

La qualité d'impression de certaines pages peut laisser à désirer, surtout si les pages originales ont été dactylographiées à l'aide d'un ruban usé ou si l'université nous a fait parvenir une photocopie de qualité inférieure.

La reproduction, même partielle, de cette microforme est soumise à la Loi canadienne sur le droit d'auteur, SRC 1970, c. C-30, et ses amendements subséquents.

Canada

PROPOSED CODE PROVISIONS FOR SLAB SPAN THICKNESS LIMITATIONS INCLUDING EARLY-AGE CONSTRUCTION LOADS AND TIME-DEPENDENT EFFECTS

By

Kwabena Ofosu-Asamoah

A Ph.D. Thesis

submitted to the School of Graduate Studies and Research
in partial fulfillment of the requirements
for the Doctor of Philosophy of
Civil Engineering Degree*

DEPARTMENT OF CIVIL ENGINEERING
University of Ottawa
Ottawa, Ontario, Canada
May, 1993

*The Doctor of Philosophy of Civil Engineering Program
is a joint program with Carleton University
administered by the Ottawa-Carleton
Institute for Civil Engineering

ISBN 0-315-89701-5

UNIVERSITÉ D'OTTAWA
UNIVERSITY OF OTTAWA

TO JOYCE, DENNIS, & KRISTINA

ACKNOWLEDGEMENTS

The author wishes to extend his sincere gratitude and thanks to his research supervisor, Professor N.J. Gardner for the valuable discussions and continued guidance throughout all phases of this study. His friendship, patience and constant encouragement over the years are most graciously acknowledged.

The author is similarly grateful to Professors J.J. Salinas, of Carleton University, M. Saatcioglu, S.F. Ng and H. Tanaka, for serving as members of his Advisory Committee. Their useful suggestions and constructive criticisms during the research process proved a great asset.

The author is also grateful to Mr. Chris Carruthers of the Computing Center, Mr. Francis Ofori Berkoh of Carleton University, and Miss Jiehong Zhang of the University of Ottawa for their diverse assistance during the research period.

A special word of thanks is extended to Professor A.G. Razaqpur of Carleton University and Professor D. Redekop of the Mechanical Engineering Department for their valuable consultations on the Finite Element Method.

Lastly, but certainly not the least, the author extends his thanks to his family and friends for their support, love and understanding in his quest for yet another degree.

ABSTRACT

A typical construction procedure for a multi-storey reinforced concrete building involves supporting newly cast slabs on a number of previously cast floors through a reshore system. The loads transferred by the forms to the previously cast partially cured supporting slabs may appreciably exceed the design capacity.

A further complication is that large early-age construction loads applied to immature slabs will cause large immediate deflections and extensive flexural cracking. The large ratio of applied stress to developed strength, coupled with the low elastic moduli of the immature slabs, will cause significant creep, mostly non-recoverable, resulting in large longterm deflections. Shrinkage, though a non-stress originated concrete deformation phenomena, also affects concrete deformation and needs to be accounted for in calculations to predict longterm deflections.

Most cases of deflection damage occur as a result of exceeding the permissible deflection of slabs supporting non-structural elements. This creates serviceability problems such as cracked partitions, jamming of doors and windows, and an uneven placement of furniture. In most cases, the visual impact of cracks and sagging floors may cause concern for safety of the structure even if the structure has adequate strength.

Problems related to excessive slab deflection constitutes a serviceability limit state. Current deflection control provisions of the ACI and CSA codes do not address the sensitivity of slab deflections to early-age construction loading and schedule.

The present study develops a more realistic span-thickness criterion which includes the effect of early-age construction loads, concrete strength and panel aspect ratio.

Undesirable slab deflections can be reduced by appropriately chosen camber in the formwork. The concept is to use a prescribed camber to offset the immediate deflections. An equation is recommended for the estimation of the amount of camber needed for any given span.

Contents

List of Figures

List of Tables

NOMENCLATURE

A_s	area of tension steel
A'_s	area of compression steel
$[B]$	strain matrix
b	width of strip
b_{ef}	effective width of an equivalent beam
C_t	creep coefficient
C_u	ultimate creep coefficient
CL	maximum construction load in multiples of slab dead load
D	dead load
$[D]$	elastic matrix
$[D]$	$= Eh^3/12(1-\nu^2)$
d	effective depth of concrete section
E_c	modulus of elasticity of concrete
E_{con}	modulus of elasticity of concrete at casting
E_s	modulus of elasticity of steel
EI	flexural rigidity
F	force vector
f'_c	uniaxial compressive strength of concrete
f'_ck28	characteristic concrete strength at 28 days
f'_cm28	mean concrete strength at 28 days
f'_cmto	mean concrete strength at age of loading
f'_t	uniaxial tensile strength of concrete

f_y	yield strength of steel
G'	shear modulus
h	slab thickness
h_{min}	minimum slab thickness
$[K]$	stiffness matrix
K_w	shrinkage coefficient
k_r	deflection reduction factor due compression reinforcement
L	Live Load
l	clear span
l/d	span-to-depth ratio
$[N]$	matrix of shape function
n	modular ratio
P	load vector
plf	peak load factor
q	load per unit area
t_c	age of concrete at casting
UL	ultimate design load
u	displacement vector
u, v, w	displacements in x,y,z directions
W_{max}	maximum construction load
W_{sd}	service dead load
w_s	sustained slab load per unit length
w_v	variable slab load per unit length

β	panel aspect ratio
Δ_{cs}	additional deflection due to creep and shrinkage
Δ_{ic}	initial deflection based on cracked section
Δ_t	longterm deflection
δ	deflection
δ_{sd}	service dead load deflection
δ'_{max}	deflection caused by maximum construction load
δ_{sl}	sustained load deflection
δ_{sh}	shrinkage deflection
δ_{sus}	sustained service load deflection
δ_{tot}	total deflection
$\{\varepsilon\}$	strain vector
ϵ_{iu}	equivalent uniaxial strain
ε_{sh}	shrinkage strain
ε_{shu}	ultimate shrinkage strain
λ	longterm deflection multiplication factor
ν	Poisson's ratio
ρ	percentage of tension reinforcement
ρ'	percentage of compression reinforcement
ρ_{sh}	shrinkage curvature
σ_1, σ_2	principal stresses
$\sigma_{ic}, \epsilon_{ic}$	maximum compressive stress and corresponding strain of concrete

Chapter 1

INTRODUCTION

1.1 General Remarks

Currently, design of reinforced concrete structures is based on the limit state philosophy which takes into account the fundamental functional requirements of safety and serviceability.

Safety requires structures to have sufficient strength to carry the prescribed design loads with an appropriately small likelihood of collapse. Serviceability requires that under service load conditions structures perform satisfactorily for their intended use, by keeping such factors as deflections, cracks and vibrations within acceptable limits. The assessment of structural performance at the service load stage is an important consideration when members are designed on the basis of their required strength.

Serviceability problems with reinforced concrete slabs have long been a concern to

structural engineers. Nevertheless this concern has not translated into anything more than design rules governing span-to-depth ratios based on prior experience. A symposium on serviceability organized by the National Research Council of Canada in 1989 identified the following points.

1. Serviceability is easy to identify in the abstract, as a problem requiring consideration in design, but is difficult to deal with by specific prescriptive requirements.

2. Most of the problems requiring attention in buildings are serviceability problems by definition, inasmuch as safety seldom is a consideration in a completed building.

3. The serviceability limit state should be identified in codes to encourage more consideration by architects and engineers.

4. Serviceability requirements should be reasonably flexible and should permit engineers to pursue a range of options in structural design.

The introduction of the limit state design method in recent years has separated the design criteria for safety from serviceability. This puts more emphasis on slab deflections. However, the analytical determination of deflection responses is complicated because of the three-dimensional nature of the problem and the nonlinear time-dependent behaviour of concrete. This thesis is concerned with the deflection serviceability limit state of flat slab and flat plate structures (see Fig. 1.1).

The construction of reinforced concrete flat slabs in multi-storey buildings involves the use of flying forms and reshores; which is a rapid, high quality, repetitive, construction process. The procedure involves casting the slabs onto forms, which

are in turn supported on one or more previously cast floors. The construction loads on the supporting slabs are determined by the construction schedule, stripping and reshoring procedure, and the load-deflection characteristics of the supporting floors.

The loads occuring through the process of sequential casting of fresh slabs and stripping of reshores can be significantly higher than the nominal design capacity of the supporting slabs. If these construction loads exceed the developed structural strength, failure (collapse) occurs during the construction process, violating the safety limit state.

These construction loads occur before the supporting slabs have achieved their full design strength and stiffness. These relatively large, early-age construction loads applied to immature slabs, having low elastic moduli and tensile strength, will cause large immediate deflections and extensive flexural cracking. The high ratio of applied stress versus developed strength of the supporting slabs will cause significant creep, mostly non-recoverable, resulting in large longterm deflections. Shrinkage, which is a non-stress originated concrete deformation property also contributes to the longterm deflections. The occurance of such longterm deflections constitutes a serviceability limit problem.

1.2 Problem Statement

In reinforced concrete multi-storey construction, contractors prefer to remove formwork and proceed to the next stage of construction as quickly as is safely possible. The method of sequential casting and stripping of formwork generally used in reinforced concrete flat slab construction causes loads which are larger

than the occupancy load. The early-age construction loads often occur before the slabs acquire their specified design strength and stiffness. Consequently, the slabs are subjected to extensive early-age flexural cracking, high non-recoverable creep and large longterm deflections.

The Canadian Standard CAN3-A23.3-M84, Code for the Design of Concrete Structures for Buildings [15], and the American code ACI 318-89, Building Code Requirements for Reinforced Concrete [1], provide deflection control for reinforced concrete slabs by limiting their span-thickness ratios. Unfortunately, this format does not adequately address the sensitivity of slab deflection to early-age construction loading. Calculating member depths based upon the thickness equations of CSA and ACI may not be adequate to prevent excessive slab deflections.

1.3 Deflection of Reinforced Concrete Slabs

1.3.1 General Remarks

Estimating the deflection of reinforced concrete flat slabs is difficult. The three-dimensional nature of the problem, the influence of cracking and tension stiffening, and the development of biaxial creep and shrinkage strains are some of the contributing factors. Accurate prediction of deflections, therefore, depends on a good understanding of the different factors involved. A complete solution to the problem would require a reliable knowledge of the load history, a method that relates load to deflection, with full recognition of the actual properties of the materials involved, and an understanding of what constitutes an objectionable deflection.

Deflection of reinforced concrete slabs consists of an immediate deflection occur-

ing on the application of load. and a longterm deflection resulting from creep and shrinkage. Various methods proposed for the calculation of both types of deflections are discussed in Chapter 2.

1.3.2 Construction Loads on Flat Slabs

The forms and reshores procedure used to construct reinforced concrete flat slab structures lead to the imposition of early-age loads on the partially cured supporting slabs. These slabs are therefore subjected to undesirable stress levels and deformations. This may be detrimental to the subsequent performance of the structure. Consequently, it is appropriate that both design and construction loads be taken into account during the design phase of reinforced concrete floor slab construction.

The design, or occupancy, loads are generally specified with reasonable accuracy, but the construction loads are usually not well defined and can vary with the construction method. It is necessary, therefore, to determine the variation in magnitude of these loads which occur during the construction period. The loads applied to the slabs are dependent on the number of forms used, number of levels of reshores, and the stripping sequence. As a result, the analysis of any construction process must take into account the number of forms and levels of reshores.

The basic concept is to assume a possible construction procedure, number of forms and reshores, and a casting cycle to determine the load applied to the various slabs at the appropriate critical times. The factored construction loads are then compared with the available slab strengths. If the load applied is greater than the strength available, the proposed construction procedure cannot be used.

A typical construction procedure of a multi-floor building is illustrated in Fig. 1.2. The construction sequence shown is for the case where one level of shores and two levels of reshores are used. In the present study, the method of analysis developed by Grundy and Kabaila [30] and later extended by Agarwal and Gardner [5] is used to estimate construction loads.

1.4 Code Requirements for Serviceability

Current North American codes (ACI 318-83 and CSA A23.3-M84) provide two methods for the control of two-way slab deflections. Deflections may be calculated directly and the magnitudes compared with specified deflection limits. Alternatively, deflections need not be calculated if the slab thickness exceeds a specified minimum value. Equation (1.1) gives the ACI minimum thickness expression in U.S. Customary Units for two-way slabs without beams.

$$h_{min} = \frac{l_n(800 + 0.005 f_y)}{36,000} \tag{1.1}$$

where, f_y is in psi.

The Canadian provision as given in CAN3-A23.3 is of the form,

$$h_{min} = \frac{l_n(800 + f_y/1.5)}{36,000} \tag{1.2}$$

where, f_y is in MPa.

The two equations are effectively identical with the difference between calculated minimum thicknesses less than 2%.

The empirical minimum thickness provisions have evolved on the basis of experience with slab systems designed using these minimum thicknesses. Irrespective of the fact that this approach is simple and ideal for use in design, the selection of

the minimum thickness does not give the designer any idea of the magnitude of the actual deflections.

Most European countries recommend permissible maximum deflection values to which analytically calculated deflections are to be compared. The countries of the former Council of Mutual Economic Assistance, COMECON, impose the following deflection limitation: for apartment building slabs, the deflection due to dead load should be less than $l/200$ and the increase due to every $100kN/m^2$ of live load should be

$$\delta_{100kN} \leq \frac{l}{5000} \leq 0.7mm$$

where, l is the clear span and δ_{100kN}, the deflection caused by a $100kN/m^2$ live load. The German Code, DIN-1045 [8], recommends a permissible deflection value of $l/250$.

As both the ACI and CSA minimum thickness equations do not indicate the magnitude of the actual deflections, they may not adequately ensure deflection control.

1.5 Objective and Scope

Current code provisions for maximum span-to-thickness ratios of reinforced concrete slabs omit terms relating to construction rate and the effects of early-age construction loads. The present research is designed to:

1. study the effects of early-age construction loading on the deflection of flat slabs;
2. determine whether slabs designed on the basis of the ACI and CSA minimum thickness equations result in calculated deflections that satisfy the codes maximum permissible limits;
3. use a computerized analytical procedure which takes into account the effects of early-age construction loading and the time-dependent effects of creep and shrinkage to estimate incremental slab deflections; and
4. set a new threshold for the prevention of deflection damage by developing a span-thickness equation based on the concept of *precambering [40]*.

The scope of the research consists of the following:

- the use of a layered finite element analysis to predict the deflection responses of reinforced concrete flat slabs
- the use of nonlinear methods of analysis to account for concrete cracking, nonlinear material properties and time-dependent concrete behaviour
- mathematical modelling of concrete creep and shrinkage behaviour using the recommendations of Gardner and Zhao [24]

- generation of creep compliance coefficients using a computer program CCCoef written by the author
- modification of computer program NOPARC to incorporate the revised time-dependent behaviour of concrete in serviceability analysis
- validation of the modified program by modelling and analyzing a series of experimentally tested slabs
- the use of the validated program in serviceability analysis
- development of a span-thickness criteria.

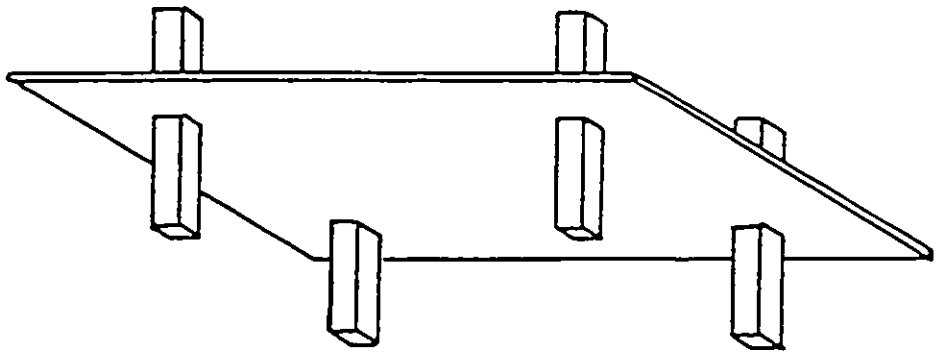

2-way slab without beams
(flat plate)

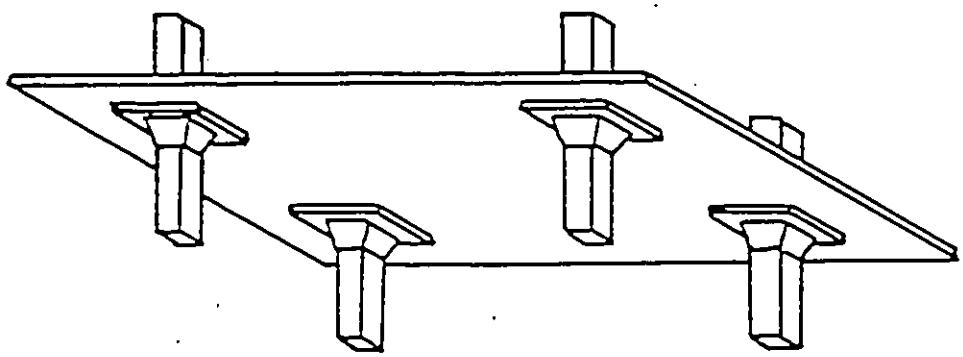

2-way slab without beams
(drop panels and column capitals)

Figure 1.1: Flat Plate and Flat Slab Structures

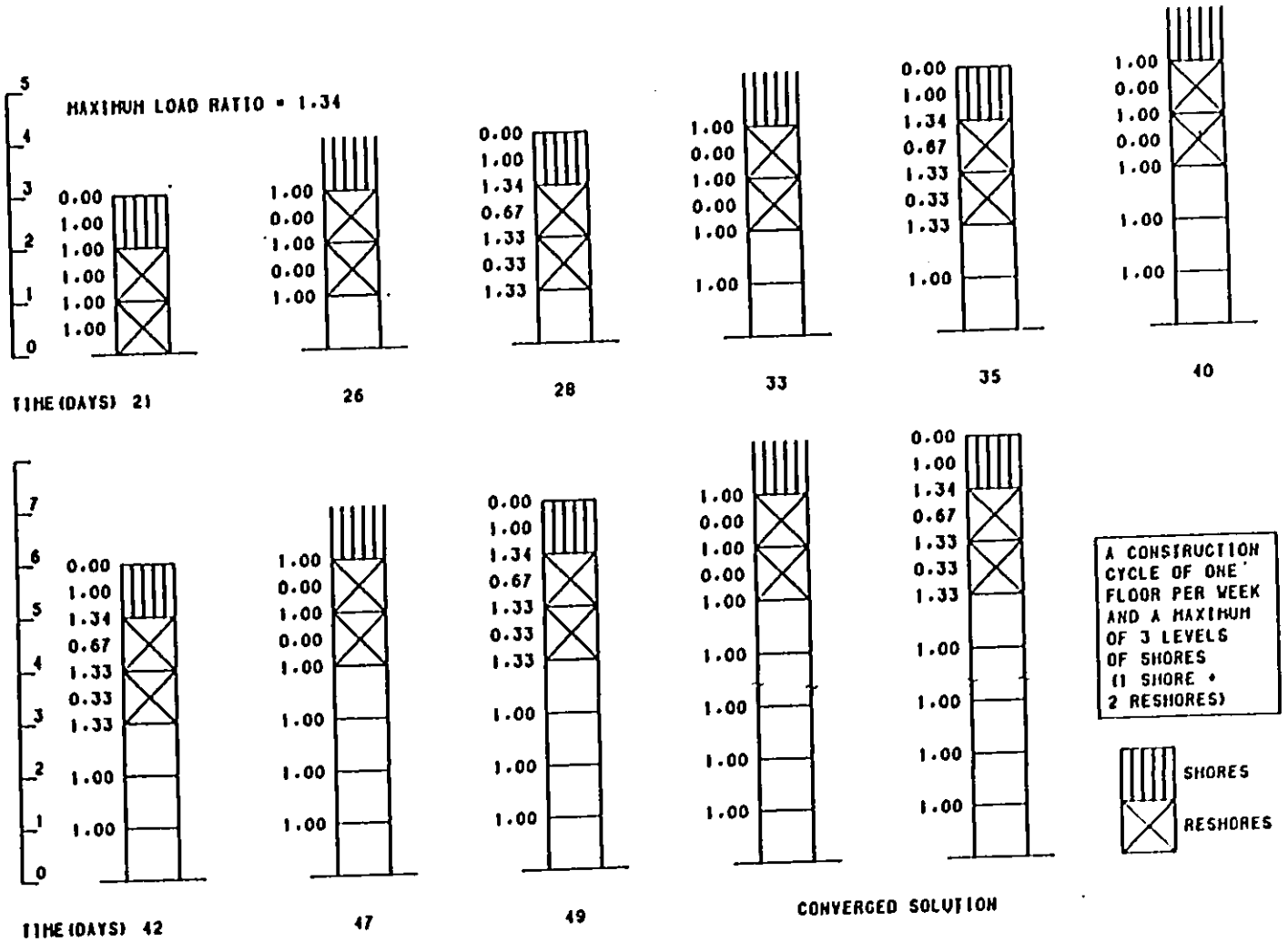

Figure 1.2: Construction Loads with 1 Shore and 2 Levels of Reshores

Chapter 2

LITERATURE REVIEW

2.1 General Remarks

Over the past three decades many research investigations have been carried out into the serviceability of reinforced concrete floor systems, but limited progress has been made in predicting longterm deflections. This is due to the sensitivity of slab deflections to factors such as early-age construction loading, degree of cracking, and the time-dependent effects of creep and shrinkage, which are difficult to model effectively. With the main emphasis of this study on how early-age construction loads and time-dependent concrete properties affect the serviceability of reinforced concrete flat slabs, the review of literature will be restricted to these topics.

2.1.1 Experimental Studies

Documentation of field-measured deflections for two-way slabs is very limited. A brief review of the available case studies known to the author is presented below.

C.S.I.R.O., Division of Building Research (Sydney), 1961 [16]

The Commonwealth Scientific and Industrial Research Organization, (C.S.I.R.O) reported the results of an experimental study conducted in Sydney, Australia by the Division of Building Research on a light-weight flat plate structure during and after erection.

The reinforced concrete flat plate slab was 90 mm (3.5 in) thick, and spanned three bays of 2.74 m (9 ft) in one direction and three bays of 3.66 m (12 ft) in the other direction with cantilevers of 1.83 m (6 ft) at each end of the longer span. No edge beams or torsional reinforcement were provided near the edge columns. The slab was subjected to its own weight of 1.53 kPa (32 psf) ten days after casting.

Progressive deflection of the slab continued for 52 days as a result of the slab dead load and an applied uniformly distributed load. Immediate deflections due to slab self-weight were not alarming, but the interior panel deflections observed 8 months later were as much as 12 times the initial elastic deflections. Of these unacceptably large longterm deflections, 20% was attributed to differential column settlements, 40% to cracking and local bond slip and the remainder to creep.

Taylor, 1970 [51]

Taylor reported the results of initial and longterm deflections measured on a flat plate roof construction in North Sydney, Australia. The 203 mm (8 in) thick slab, with a span-to-depth ratio of 31.0, was subjected to its full dead load 14 days after casting. Mid-panel deflections measured after 850 days for four interior panels ranged between 6.5 to 10 times the initial deflection. As the slabs were not subjected to construction loads, little cracking was expected. The large longterm multipliers were therefore attributed to high creep and shrinkage of the concrete used.

Taylor and Heiman 1970 [52]

Taylor and Heiman reported on measured deflections for a reinforced concrete flat plate roof system. The test slab was 203 mm (8 in) thick with a span-to-depth ratio of 31. The slab was designed for a total load of 8.86 kPa (185 psf), including slab dead weight of 5.27 kPa (110 psf). Formwork for the roof slab was stripped 14 days after construction.

The initial mid-panel deflection for an interior panel was 2.79 mm (0.11 in). The total deflection of the same panel, being in service 9 years after, measured 24.38 mm (0.96 in), i.e 8.7 times the initial deflection. This total deflection was considered to consist of 15% immediate deflection, 19% longterm deflection due to cracking, 40% creep deflection and 26% shrinkage deflection.

Sbarounis 1984, [45], [46]

Slab deflections were measured by Sbarounis in a multi-storey flat plate building in Chicago. The slabs had an average thickness of 184 mm (7.25 in) with center-to-center spans of 6.6 m and 6.8 m (21.6 ft and 22.4 ft). Lateral force resistance of the flat plate was assured by shear walls and a stiff system of beams and closely spaced wide columns. .

Midpanel deflections measured one year after construction for 175 bays on 13 floors ranged between 13.46 mm (0.53 in) and 54.86 mm (2.16 in) with a mean of 34.29 mm (1.35 in), and a standard deviation of 7.67 mm (0.29 in).

The calculated initial deflection for an identical reinforced concrete slab loaded to the service dead load of 4.17 kPa (87 psf) was 5.33 mm (0.21 in). Longterm deflections were also calculated using Sbarounis's analytical procedure and an assumed one-year multiplier of 4.2. The calculated and the mean one-year measured deflections were reported to be in good agreement.

Fu, 1985 [19]

Fu conducted an experimental investigation into the effects of early age construction loads on the immediate and longterm deflections of reinforced concrete slabs. Two sets of experimental slabs were cast and subjected to various construction load histories, followed by a constant sustained load over a long period of time.

The first set of slabs involved three identical flat plate models, 63.5 mm (2.5 in) thick, and supported by four 203 mm (8 in) square columns, with clear spans of 1.96 m (6.42 ft) in both directions. The design live load to dead load ratios were

1.0 for flat plate model 1, and 0.5 for flat plate models 2 and 3.

The second set of slabs were five nominally identical one-way slabs subjected to different load histories. All slabs were 63.5 mm (2.5 in) thick, 203 mm (8 in) wide, 1.96 m (6.42 ft) long, and designed for a live load to dead load ratio of 0.5. The load histories were modelled to represent different construction methods.

Mid-panel deflections were measured regularly for both sets of slabs for up to 10 months. The longterm deflections in all cases were significantly high, of the order of 5 to 7 times the immediate deflections.

Jokinen and Scanlon, 1987 [34]

Jokinen and Scanlon reported the results of an experimental study conducted on a twin-storey office complex during and after construction. The complex consisted of two towers, 20 and 28 storeys in height. The floor system consisted of a 200 mm thick two-way flat slab with 3000 × 3000 × 150 mm drop panels and 1520 × 1520 mm column capitals. Columns were spaced 9.0 m on center and the floor slabs were cambered 15 mm at bay centers and 10 mm on grid lines. The compressive strength of concrete used for the floor slabs was 30 MPa.

The floors were constructed using a system of flying formwork and three levels of reshores. Formwork was stripped 3 days after casting. Mean deflections (not including camber) measured one year after construction ranged from 32.53 to 39.05 mm with coefficients of variation between 24.8 and 31.0 percent.

2.1.2 Analytical Studies

Taylor, 1970 [50]

Taylor proposed two computational procedures for the determination of the longterm deflection of flat plates. The first method considered creep and shrinkage deflections separately and their contributions were added. The creep deflection is calculated as a product of a computed initial deflection and a creep factor. The shrinkage deflection is determined using the expression of Branson and Christianson [11].

$$\delta_{sh} = K_w \rho_{sh} L^2 \tag{2.1}$$

where,

K_w = shrinkage coefficient which depends on end constraints,

ρ_{sh} = shrinkage curvature, and

L = member span (center-to-center). The extent of the shrinkage curvature depends on the level of reinforcement. If $(\rho - \rho') \leq 3\%$,

$$\rho_{sh} = 0.7 \frac{\varepsilon_{sh}}{h} (\rho - \rho')^{\frac{1}{3}} \sqrt{\frac{(\rho - \rho')}{\rho}} \tag{2.2}$$

If $(\rho - \rho') > 3\%$,

$$\rho_{sh} = \frac{\varepsilon_{sh}}{h} \tag{2.3}$$

where,

ε_{sh} = shrinkage strain,

h = slab thickness,

ρ' = percentage or ratio of compression reinforcement, and

ρ = percentage or ratio of tensile reinforcement.

An alternative method also proposed by Taylor combines the effects of creep and shrinkage. The longterm deflection of a reinforced concrete member is calculated

using the following equations:

$$\Delta_t = \Delta_{ic} + \Delta_{cs} \tag{2.4}$$

$$\Delta_{cs} = k_r C_t \Delta_{ic} \tag{2.5}$$

where,

Δ_t = longterm deflection,

Δ_{ic} = initial deflection based on cracked section,

Δ_{cs} = additional deflection due to creep and shrinkage,

k_r = a factor which accounts for a reduction in longterm deflection due to the presence of compressive reinforcement, and

C_t = a combined shrinkage and creep multiplier which depends on the age of concrete at loading and the average relative humidity. It has a value of 3 after 10 years.

Sbarounis, 1984 [46]

A method developed by Sbarounis proposed calculating the longterm deflection of flat slabs as the product of an immediate secant service dead load deflection and a longterm multiplier.

$$\delta_{longterm} = \delta_{sd} \times Multiplier \tag{2.6}$$

The service dead load deflection, δ_{sd} is given by

$$\delta_{sd} = \delta'_{max} \left(\frac{W_{sd}}{W_{max}}\right) \tag{2.7}$$

where,

δ'_{max} = deflection caused by maximum construction load applied as a simple load increment.

W_{max} = maximum construction load, and

W_{sd} = service dead load.

The longterm multiplier which characterizes the effects of creep and shrinkage is expressed as

$$Multiplier = 1 + 2.S\,(\frac{C_u}{2.35}) + 1.2\,(\frac{\varepsilon_{shu}}{S00}) \qquad (2.S)$$

where, C_u is the ultimate creep coefficient and ε_{shu}, the ultimate shrinkage strain.

Gilbert, 1985 [26], [27]

A design oriented procedure for the control of deflection in reinforced concrete slab systems was proposed by Gilbert. The basis of Gilbert's procedure was a series of computer analyses of reinforced concrete slabs. The computer experiments were performed using a plate-bending finite element program developed to study the longterm service load behaviour of reinforced and prestressed concrete slabs.

According to Gilbert, the maximum allowable span-to-depth ratio for reinforced concrete slabs should be calculated using the relationship

$$\frac{l}{d} = K_1 K_2 K_3 [\frac{\Delta}{l}(\frac{\alpha b_{ef} E_c}{k(w_v + cw_s)})]^{0.33} \qquad (2.9)$$

where,

l/d = span-to-depth ratio,

K_1 = a factor which depends on support conditions,

K_2 = a constant which is equal to 1.0 for flat slabs,

K_3 = slab system factor which depends on the aspect ratio of the slab,

k = fraction of the total uniformly distributed load carried by an equivalent beam. For flat plates $k = 1.0$,

b_{ef} = effective width of the equivalent beam,

w_s = sustained slab load per unit length,

w_v = variable slab load per unit length,

E_c = modulus of elasticity of concrete, and

α = a factor that accounts for the effects of reinforcement ratio, ρ, and the modular ratio, n.

$$\alpha = 15\sqrt{\rho n} \leq 8.0 \tag{2.10}$$

for $\rho n \geq 0.045$, and

$$\alpha = \frac{1}{7\rho n} \tag{2.11}$$

for $\rho n \leq 0.045$.

If the member does not support non-structural elements likely to be damaged by deflection, Δ is the maximum permissible total deflection. In such a case $c = 1+\lambda$. For members supporting non-structural elements likely to be damaged by excessive deflection, Δ is the maximum permissible incremental deflection (i.e that part of the total deflection which occurs after the attachment of non-structural elements) and $c = \lambda$, where λ is a longterm deflection multiplication factor which is expressed as:

$$\lambda = 2.0 - 1.2\,\frac{A'_s}{A_s} \geq 0.6 \tag{2.12}$$

A'_s and A_s being areas of compression and tension steel respectively. Gilbert compared predictions made using his proposed equations with field measurements of several in-service slabs reported by Taylor and stated that the results were in good agreement.

Fu and Gardner, 1985 [20]

Fu and Gardner reviewed the literature reporting measured longterm deflections of reinforced concrete slabs. Unfortunately most of the published work reviewed

did not indicate the construction schedule used. Table 2.1 gives a summary of the published ratios of measured longterm deflection to initial deflections. Based on their studies, Fu and Gardner developed the following equation to calculate longterm deflections.

$$\delta_{longterm} = \delta_{elastic}(1 + c.c) + \delta_{sh} \tag{2.13}$$

where,

$$c.c = 3.3 + 5.5(plf - 0.55) \tag{2.14}$$

$$plf = \frac{P_{max}}{P_{ult}}\sqrt{\frac{f'_c}{f_c}} \tag{2.15}$$

In the above equations,

$\delta_{longterm}$ = longterm deflection,

$\delta_{elastic}$ = elastic deflection,

δ_{sh} = deflection due to shrinkage,

plf = peak load factor,

P_{max} = maximum load during construction,

P_{ult} = 28-day design ultimate load,

f'_c = 28-day concrete strength,

f_c = concrete strength when P_{max} is applied.

Graham and Scanlon, 1986 [29]

Using a parametric study, Graham and Scanlon developed a procedure using long-time multipliers to estimate deflections of two-way slabs subjected to construction loads, shrinkage, and irrecoverable creep. The analytical model used in developing the long-time multipliers treated construction loading history as a series of load increments, applied at specific times and associated with a particular construction sequence.

Immediate deflection for each load increment was calculated using a finite element plate bending program. Creep and shrinkage deflections were calculated based on the provisions of the ACI Building Code. Total instantaneous plus creep deflection at time, t, was obtained by summing deflections from all load increments. Shrinkage deflection was then added to the total instantaneous deflection and creep deflection to obtain the longterm deflection.

Current practice involves calculating an immediate deflection, taking into account the effects of cracking and then multiplying the instantaneous deflection by a factor to account for creep and shrinkage effects. Accordingly, Graham and Scanlon proposed an alternative simplified procedure which calculates a maximum deflection, Δ_{max}, due to construction loads, which is in turn scaled down to the sustained load level. The resulting sustained load deflection, Δ_{sl}, is then multiplied by a factor, λ_t, to obtain the total deflection.

For a multi-storey slab system using a typical shoring and reshoring procedure, Graham and Scanlon recommend the use of an effective modulus of rupture

$$(f_r)_{eff} = 0.3\sqrt{f'_c} \tag{2.16}$$

and a longterm multiplier of 3.50. It was, however, indicated that if the expected ultimate creep *and/or* shrinkage values are different from those recommended by ACI-209, the longterm multiplier is to be calculated using Sbarounis's equation

$$\lambda_{t(modified)} = 1 + \lambda_c(\frac{C_u}{2.35}) + \lambda_{sh}(\frac{\varepsilon_{sh}}{780 \times 10^{-6}}) \tag{2.17}$$

Gardner and Fu, 1987 [23]

Gardner and Fu proposed a method that included a construction load dependent creep term to calculate the longterm deflections of reinforced concrete flat slab

structures. The total deflection included deflections due to shrinkage and sustained live load.

$$\delta_{total} = \delta_{sh} + \delta_{sus}[1 + C_t(1 + \frac{CL}{UL})] \tag{2.18}$$

where,

δ_{total} = total deflection,

δ_{sh} = deflection due to shrinkage,

δ_{sus} = deflection due to sustained service load,

CL = maximum construction load in multiples of slab dead load,

UL = ultimate design load, and

C_t = ACI creep coefficient.

For shrinkage deflection, Gardner and Fu reported that Branson's equation gave reasonable prediction of their experimental results and, therefore, recommended its use.

The value UL is given by,

$$UL = 1.4D + 1.7L \tag{2.19}$$

where D is the slab dead load and L the applied live load.
The deflections calculated using Eq. (2.18) were compared with measured deflections and they showed good agreement. The results are summarized in Table (2.2).

Thompson and Scanlon 1988, [53]

Based on the results of a parametric study, Thompson and Scanlon proposed modifications to the code's serviceability provisions. The following is a summary of their recommended changes.

1. For two-way slabs without beams between interior supports, the minimum thickness should be governed by

$$h_{min} = \frac{l_n}{30} \tag{2.20}$$

for, $f_y \leq 60,000$ psi

2. For exterior panels with discontinuous edges, the slab thickness may be decreased by up to 5 percent if an edge beam with stiffness ratio, α, not less than 0.80 is provided.

3. The minimum thickness may be multiplied by a factor

$$(1.20 - 0.20\beta) \geq 0.9$$

to account for the effect of panel aspect ratio, β.

4. For flat slabs with drop panels the minimum thickness may be decreased by 10 percent if the thickness of the drop panel is greater than or equal to 1.25 times the slab thickness, or by 20 percent if the drop panel thickness is greater than or equal to 1.50 times the slab thickness.

5. Thickness smaller than h_{min} may be used if the deflections are computed, and if it can be shown that the deflections computed will not adversely affect the serviceability of the structure.
   Deflection computations should take into account the effects of construction loading and shrinkage stresses.

6. A limit of $l/200$ on total deflection should be included.

Table 2.1: Summary of Measured Longterm Deflections [20]

Source	Year	Longer Span (mm)	Age of Initial Defl. (Days)	Initial Defl. (mm)	Age of Final Defl. (Days)	Final Defl. (mm)	Longterm to Short-term Deflection Ratio
C.S.I.R.O.	1961	3937	10	1.27	8 months	12.7	10.0
Taylor & Heiman	1970	6293	14	2.80	9 years	24.4	8.7
Taylor	1971	8676	56	3.56	1 year	13.97	3.9
					3.5 years	22.35	6.3
					8.0 years	23.40	6.7
Taylor & Heiman	1972	7544	17	8.60	610 days	18.87	2.2
					3.5 years	21.80	2.5
Jenkins	1974	6477	10	2.00	1 year	7.90	4.0
					27 months	11.70	5.9
Yamamoto	1982	3600	1	1.29	112 days	5.71	4.4
		3600	2	0.95	112 days	5.35	5.6
		3600	3	0.81	112 days	5.46	6.7
		3600	7	0.77	112 days	4.92	6.4
		3600	28	0.72	112 days	3.92	5.4
		5000	3	4.15	112 days	19.62	4.7
		5000	28	4.05	112 days	14.78	3.6
Sbarounis	1984	6828	28	5.33	1 year	34.29	6.4
Fu	1985	2163	10	2.12	483 days	8.48	4.0

Table 2.2: Comparison of Eq. (2.18) with Measured Deflections

	Shrinkage Deflections mm	28-Day Sustained Load Deflection (mm)	CL/UL	Creep Factor	Calculated Deflection mm	Experimental Deflection mm
Slab 1	2.89	0.93	0.65	1.711	6.44	6.51
Slab 2	2.32	0.89	0.89	1.711	6.09	7.57
Slab 3	3.20	1.68	0.67	1.711	9.68	9.52

Chapter 3

METHOD OF ANALYSIS

3.1 General Remarks

General analytical solution methods do not exist for the analysis of surface structures such as flat plates and shells. The finite element method can model a continuous surface structure as a system of discrete elements joined at nodes. All the displacements, strains and stresses within an element are described in terms of the conditions at the node. The analysis of reinforced concrete structures is complicated by the concrete cracking in tension at discrete locations when the principal tension exceeds the tensile strength of the concrete.

Concrete creeps under load with the creep strains usually considered a multiple of the "elastic" strains. Consequently, for a reinforced concrete element under flexure, the creep strains under compression increase with distance from the neutral surface and, together with the concrete cracking under tension, a redistribution of internal strains and stresses is required for equilibrium and compatibility. Concrete also

experiences shrinkage with time. This shrinkage is restrained by the reinforcement causing additional redistribution of strains and stresses to maintain equilibrium and compatibility.

The finite element method is the only feasible method of analyzing the time dependent behaviour of cracked reinforced concrete flat slabs. The slab structure can be modelled by an appropriate number of triangular or rectangular elements. The reinforced concrete section is modelled as a layered system of concrete and *equivalent smeared* steel layers. The stiffness property of an element is obtained by integrating the contributions from all the layers in the system.

To model nonlinear effects due to load, the problem is treated as piece-wise linear with the load applied in a number of increments and the material properties dependent upon the level of strain. For each increment in load, the element properties are iterated and the strains, stresses, and displacements due to the load increment are added to those from the previous load increment.

Time dependent effects due to shrinkage and creep of the concrete for a specified time duration are modelled as follows. For each concrete layer in an element, the shrinkage and creep strains corresponding to the specified time interval are added to the existing strains of the layer. The lack of internal compatibility requires internal stresses and corresponding forces at the nodes. A time dependent nodal force vector, analogous to the applied load nodal force vector is created. The time dependent force vector can be divided into a number of increments. The problem is again treated as piece-wise linear, with the material properties and element state of strain dependent upon the cumulative level of strain.

However conceptually easy, the finite element method requires adequate modelling of the constitutive materials. This chapter describes the displacement formulation of the finite element method and presents the basic equations and the element models used.

Chapter 4 reviews the material models used to derive the constitutive relationships for concrete and steel.

Chapter 5 discusses the time dependent properties of creep and shrinkage and the equations used to model their effects.

Chapter 6 discusses the computer simulation process and presents the results of the analysis.

Chapter 7 presents the conclusions drawn from the study and the recommendations necessary to effect changes in the Building Codes.

3.2 Finite Element Analysis

The concept of the finite element method is an idealization of a continuous media by a discretized structural system to which the matrix methods of structural analysis are directly applicable. The validity of the method depends on how well the approximate solution converges to the exact solution. There are two basic matrix formulation approaches associated with the method;

- the **Force Method** which assumes the internal forces as the unknowns of the problem, or
- the **Displacement Method** which assumes the displacements of the nodes as the unknowns of the problem. This is the option used herein.

3.2.1 Displacement Formulation

The displacement formulation of the finite element method is equivalent to the minimization of the total potential energy of the continuum in terms of a prescribed displacement field. An appropriate choice of the displacement field ensures that convergence of the minimum potential energy of the continuum and of the nodal displacements to a correct solution occurs by increasing the number of the finite elements used in approximating the continuum. With the displacement method, compatibility requirements in and along elements are initially satisfied and the governing equations in terms of nodal displacements are written for each node using equilibrium conditions.

To obtain a solution to a given structural problem using the displacement approach, five steps are necessary.

(1) The elastic continuum with an infinite number of unknowns is discretized into an assemblage of elements having a finite number of unknowns. This requires selection of the type and size of the finite elements to generate the mesh of the system.

(2) Interpolation functions are used to approximate the variation of displacement within an element. These are in the form,

$$\{u\} = [N]\{w\} \tag{3.1}$$

where u = the displacement field,
N = interpolation (or shape) function, and
w = nodal displacements.

(3) From compatibility the strain vector, ε at any point within the element can be found in terms of the displacement vector u.

$$\{\varepsilon\} = [L]\{u\} \tag{3.2}$$

where L is a linear differential operator.

Substituting for u in Eq. (3.2) from Eq. (3.1), the strain vector becomes:

$$\{\varepsilon\} = [L][N]\{w\} = [B]\{w\} \tag{3.3}$$

where $[B] = [L][N]$ is a strain-displacement matrix called the B-matrix.

(4) Stresses are evaluated from strains using the constitutive relationship

$$\{\sigma\} = [D](\{\varepsilon\} - \{\varepsilon_o\}) + \{\sigma_o\} \tag{3.4}$$

where,

$[D]$ = constitutive matrix,

$\{\varepsilon_o\}$ = initial strain vector, and

$\{\sigma_o\}$ = initial stress vector.

(5) From the Principle of Virtual Work, the equilibrium equation for an initial stress-free state is given by:

$$\sum_e \int_v \{\varepsilon\}^T\{\sigma\}dv = \sum_e \int_v \{u\}^T\{f^B\}dv + \sum_e \int_s \{u\}^T\{f^S\}ds + \sum_e \{u^i\}^T\{F^i\} \tag{3.5}$$

where,

$\sum_e$ = summation over all elements,

v = volume of an element,

s = surface of an element,

$\{u\}$ = element displacement vector,

$\{\varepsilon\}$ = corresponding strain vector,

$\{\sigma\}$ = stress vector,

$\{f^B\}$ = vector for body forces,

$\{f^S\}$ = applied surface loads vector,

$\{u^i\}$ = virtual nodal displacements, and

$\{F^i\}$ = vector for externally applied forces at nodes.

Substituting for the element displacements, strains, and stress in Eq. (3.5) from Eqs. (3.1), (3.3), and (3.4) respectively, gives

$$\{u^i\}^T(\{Fi\} + \sum_e \int_v [N]^T\{f^B\}dv + \sum_e \int_s [N]^T\{f^S\}ds) = \{u^i\}^T \sum_e \int_v [B]^T\{[D](\{\varepsilon\} - \{\varepsilon_o\}) + \{\sigma_o\}\}dv \tag{3.6}$$

where,

$$\{F^b\} = \sum_e \int_v [N]^T\{f^B\}dv \tag{3.7}$$

$$\{F^s\} = \sum_e \int_s [N]^T\{f^S\}ds \tag{3.8}$$

$$\{F^{\varepsilon_o}\} = \sum_e \int_v [B]^T[D]\{\varepsilon_o\}dv \tag{3.9}$$

$$\{F^{\sigma_o}\} = \sum_e \int_v [B]^T\{\sigma_o\}dv \tag{3.10}$$

$$[K] = \sum_e \int_v [B]^T[D][B]dv \tag{3.11}$$

The equilibrium equation may simply be written as:

$$[K]\{u\} = \{F\} \tag{3.12}$$

with,

$$\{F\} = \{F^b\} + \{F^s\} + \{F^{\varepsilon_o}\} + \{F^{\sigma_o}\} \tag{3.13}$$

where,

$[K]$ = element stiffness matrix,

u = displacement field vector,

$\{F\}$ = equivalent nodal force vector, and

$\{F^b\}$, $\{F^s\}$, $\{F^{\varepsilon_o}\}$, $\{F^{\sigma_o}\}$ = equivalent nodal force vectors due to body forces, surface forces, initial strains, and initial stresses respectively.

The element stiffness matrix of Eq. (3.12) is generally evaluated by numerical integration.

In the application of the displacement formulation of the finite element method, an inherent assumption made is that the stress-strain function is linear. The assumption of a linear stress-strain relationship implies that the B-matrix is independent of the nodal displacement vector r, and that geometric nonlinearities are insignificant.

3.2.2 Finite Element Modelling

The accuracy and effectiveness of a solution routine will depend on the type of finite elements used for the analysis. To model the bending and membrane actions of reinforced concrete slabs, two finite elements are used. The selection of these elements was done on the basis of efficiency with regard to the computational effort required in forming the element stiffness matrix, the accuracy of the element displacement shape functions in representing the actual displacement field, and the ability of the element geometry to well represent the shapes of the structural members. Brief discussions of the elements used are presented below.

Triangular Shell Element

In the analysis of reinforced concrete column supported slabs, significant membrane forces develop as a result of large out-of-plane deflections. To account for both the plate bending action and the membrane effect, a triangular shell element is used. The element is formed by combining the 9-DOF Irons-Razzaque triangle with the Constant Strain Triangle (CST) to obtain a flat triangular element with five degrees of freedom at each node.

The Irons-Razzaque triangle is used to provide the plate bending action of the slab while the CST is used to model the membrane action developed as a result of the out-of-plane deflections. The shell element is three-dimensional in nature but Kirchoff assumptions reduce the problem to a two-dimensional problem.

Kirchoff's Assumptions

- normals to the plate middle surface remain normal and straight after deformation
- strains normal to the reference surface are neglected.

The advantages of the 5-DOF triangular shell element are:
(i) ability to model arbitrary geometric shapes,
(ii) mesh refinement capability for regions of high stress gradients,
(iii) element stiffness matrix is reasonably simple to calculate,
(iv) the assembled structural matrix has the minimum bandwidth for a particular nodal and element layout, and
(v) good bending capability provided by the Irons-Razzaque triangle.

A major disadvantage of the shell element is the inability of the CST to capture high stress gradients. The use of a refined mesh overcomes this problem.

Using Kirchoff's assumptions, the displacement at any point in the element can be written in terms of the displacements and their derivatives on the reference surface.

$$u(x,y,z) = u_o(x,y) + z\theta_y v(x,y,z) = v_o(x,y) - z\theta_x w(x,y,z) = w_o(x,y) \quad (3.14)$$

where,

u, v, w = displacements in the x,y,z -directions,

u_o, v_o, w_o = displacements on the element reference surface,

$\theta_x = \partial w/\partial y$ = rotation about the x-axis, and

$\theta_y = -\partial w/\partial x$ = rotation about the y-axis.

By choosing shape functions for the bending displacements (w, θ_x, θ_y), and the in-plane effects (u, v), the reference surface displacements (u_o, v_o, w_o) may be expressed as:

$$u_o = N_m(x,y)u \quad (3.15)$$

$$v_o = N_m(x,y)v \quad (3.16)$$

$$w_o = N_b(x,y)w \quad (3.17)$$

where,

N_m = shape functions for in-plane displacements, and

N_b = shape functions for bending displacements.

The nodal displacement vectors are:

$$u = [u_1 \cdot u_2 \cdot u_3]^T \quad (3.18)$$

$$v = [v_1 \cdot v_2 \cdot v_3]^T \quad (3.19)$$

$$w = [w_1 \cdot w_2 \cdot w_3]^T \quad (3.20)$$

$$\theta_x = [\theta_{x1} \cdot \theta_{x2} \cdot \theta_{x3}]^T \quad (3.21)$$

$$\theta_y = [\theta_{y1} \cdot \theta_{y2} \cdot \theta_{y3}]^T \quad (3.22)$$

The strain vector at any point in the element is given by:

$$\varepsilon = \left\{ \begin{array}{c} \frac{\partial u}{\partial x} \\ \frac{\partial v}{\partial y} \\ \frac{\partial u}{\partial y} + \frac{\partial v}{\partial x} \end{array} \right\} = \left\{ \begin{array}{c} \frac{\partial u_o}{\partial x} \\ \frac{\partial v_o}{\partial y} \\ \frac{\partial u_o}{\partial y} + \frac{\partial v_o}{\partial x} \end{array} \right\} - z \left\{ \begin{array}{c} \frac{\partial^2 w}{\partial x^2} \\ \frac{\partial^2 w}{\partial y^2} \\ 2\frac{\partial^2 w}{\partial x \partial y} \end{array} \right\} = \varepsilon_o - z\,\chi \tag{3.23}$$

where,

ε_o = in-plane strain vector at the reference surface, and

χ = curvature vector at the reference surface.

From Eq. (3.23), the strain and curvature vectors can be expressed as:

$$\varepsilon_o = \left[\begin{array}{cc} N,x & 0 \\ 0 & N,y \\ N,y & N,x \end{array} \right] \left\{ \begin{array}{c} u \\ v \end{array} \right\} = B_m \left\{ \begin{array}{c} u \\ v \end{array} \right\} \tag{3.24}$$

and,

$$\chi = \left[\begin{array}{c} M,xx \\ M,yy \\ M,xy \end{array} \right] \left\{ \begin{array}{c} w \\ \theta_x \\ \theta_y \end{array} \right\} = B_b \left\{ \begin{array}{c} w \\ \theta_x \\ \theta_y \end{array} \right\} \tag{3.25}$$

Substituting for ε_o and χ in Eq. (3.23), using the expressions of Eqs. (3.24) and (3.25), the strain-displacement relationship becomes:

$$\varepsilon = B_m\, r_m \;\; - z B_b\, r_b = B\, r \tag{3.26}$$

where,

$$r^T = [r_m^T \;\; r_b^T]$$

From Eq. (3.11), the element stiffness is given by:

$$[K] = \int_v B^T D B dv = \left[\begin{array}{cc} [K]_{mm} & [K]_{mb} \\ [K]_{bm} & [K]_{bb} \end{array} \right] \tag{3.27}$$

where, $[K]_{mm}$ is the membrane stiffness matrix, $[K]_{bb}$ is the bending stiffness matrix and $[K]_{mb}$ is the coupling stiffness matrix.

By definition,

$$[K]_{mm} = \int_v [B]_m^T [E][B]_m dv \tag{3.28}$$

$$[K]_{bb} = \int_v [B]_b^T [E][B]_b dv \tag{3.29}$$

$$[K]_{bm} = \int_v [B]_b^T [E][B]_m dv \tag{3.30}$$

In the element stiffness expression of Eq. (3.27),

$$[K]_{bm} = ([K]^T)_{mb}$$

The matrices $[B]_m$ and $[B]_b$ represent the strain-displacement relationship, which depends on the shape functions. The material constitutive matrices are $[D]_{mm}$ and $[D]_{bb}$. To evaluate the material matrices, the reinforced concrete composite section is considered as a layered system of concrete and *equivalent smeared* steel layers Fig. (3.2). The steel is converted to a uniform layer with an equivalent thickness of

$$t_s = \frac{A_s}{b} \tag{3.31}$$

where, A_s is the bar area and b the spacing between bars.

Each layer is assumed to be in a state of plane stress and the material matrix for an element is obtained by summing contributions from all layers as follows:

$$D_{mm} = \int_h C dz = \sum_{i=1}^{c} (z_{i+1} - z_i) C_{ci} + \sum_{j=1}^{s} C_{sj} t_{sj} \tag{3.32}$$

$$D_{bm} = \int_h -zC dz = -\sum_{i=1}^{c} \frac{1}{2}(z_{i+1}^2 - z_i^2) C_{ci} - \sum_{j=1}^{s} z_j C_{sj} t_{sj} \tag{3.33}$$

$$D_{bb} = \int_h z^2 C dz = \sum_{i=1}^{c} \frac{1}{3}(z_{i+1}^3 - z_i^3) C_{ci} + \sum_{j=1}^{s} z_j^2 C_{sj} t_{sj} \tag{3.34}$$

where C_{ci} = material matrix for concrete layer i,

C_{sj} = material matrix for steel layer j,

c, s = number of concrete and steel layers,

z_i, z_j = z-coordinates as illustrated in Fig. (3.2), and

t_{sj} = thickness of equivalent steel layer.

Support Element

A spring-type support element developed by Wilson [56] is used to provide linear-elastic supports for the nodes and to limit nodal displacements or rotations to prescribed values. The element is defined by a single directed axis through a specified nodal point and its assigned a linear extensional stiffness along the axis or a linear rotational stiffness about the axis. The element stiffnesses are added directly to the structural stiffness matrix. The forces in the support element are included in the calculation of the internal resisting load vector.

3.3 General Solution Algorithm

The solution procedure involves the use of an incremental approach and an iterative time-step integration scheme to find the load-displacement path. The duration for which the response history is to be analyzed is divided into a number of time steps. Externally applied loads are assumed to remain constant within a time step.

As an example, consider an external load vector R applied at time t_1. The load R_1 has been subdivided into three equal load steps, Fig. (3.3). The structure is then analyzed for each load step by an iterative solution procedure. The increments

calculated in the field variables (displacements, strains, and stresses) are added to previous totals to evaluate the current state of the structure. After all the externally applied load increments have been considered, the analysis for creep and shrinkage for a given time interval is carried out in a similar way. An algorithm describing the fundamental steps of the analysis is given below.

1. Input control parameters indicating the number of nodal points, element types, number of time steps, convergence criteria and the type of analysis to be performed.

2. Specify structural geometry, material properties, types of layer systems and layout, and element particulars. The element load vector is formed.

3. Input the control data for the current time, t_i, and time step $\Delta t_i = t_{i+1} - t_i$. Form the applied load vector, R^i, and the load step vector, ΔR^i, for time, t_i.

4. Form the structural load vector ΔR^j for time t_i from the external nodal increment vector R_E^j.

$$R_E^j = R_E^{j-1} + \Delta R^i \tag{3.35}$$

$$\Delta R_j = R_u^{j-1} + \Delta R^i \tag{3.36}$$

where j is the iteration number, and R_u^{j-1} is unbalanced load vector.
At the beginning of the problem, $R_E^o = R_u^o = 0$ and R_E is incremented only for external loads.
($j = 0$ means the last value for the previous load step).

5. Divide the structural load increment vector to obtain the load vector for each load step of the increment.

6. Create the material matrix for each concrete layer of an element, calculate the layer stiffnesses, and integrate to form the element stiffness matrix. Assemble the element stiffnesses into the global structural stiffness matrix and triangularize it.

7. Solve the equilibrium equation

$$K^j \Delta r^j = \Delta R^j \tag{3.37}$$

and back substitute to find the nodal displacement increment vector Δ^j. Add this to the previous total displacement vector to obtain the current total nodal displacement vector.

$$r^j = r^{j-1} + \Delta r^j \tag{3.38}$$

For the second and subsequent iterations, check for convergence using the displacement norm.

8. In the absence of a converged solution, repeat steps 5, 6, and 7 until convergence is obtained or the maximum number of iterations allowed is reached. If the equilibrium state has been found, continue to step 9.

9. Return to step 4 and repeat it through step 8 for a given time step if this is not the last load step. Otherwise, proceed to step 10.

10. At the end of a time step, calculate the material properties for the new time t_{i+1}.

11. For a time step, calculate creep and shrinkage strain increment vectors for each element and the equivalent nodal loads, treating the calculated strains as initial strains. Also, calculate the material properties at the end of the time step for the new time t_{i+1}.

12. Assemble the structural time-dependent load vector R_{Ti} and calculate the load step vector ΔR_{Ti} then return to step 4 and repeat it through step 8.

13. If time t_i is the last time considered, the solution is terminated. Otherwise, return to step 3 and continue the analysis for the next time step.

The steps outlined in the above algorithm are standard procedures in the computer program **TIDARCS** (discussed in section 3.5).

3.4 Procedure for Time-Dependent Effects

A stepwise integration method is used to analyze the time-dependent effects of creep and shrinkage. The nonlinear behaviour of the structure is modelled by dividing the entire analytical period into a number of time steps. An initial strain approach, which was discussed in detail by Zienkiewicz [57], and used in studies by van Greunen [54] and Kabir [35], was adopted to determine the response of the structure to creep and shrinkage strain increments occuring during a time step. The method is described below for a time step $\Delta t_i = t_{i+1} - t_i$.

1. It is assumed that all external loads are applied at the beginning of a time step and kept constant during the time step. The field variables (displacements, strains and stresses) for the elements are found by solving the equilibrium equations for the applied loads.

2. Based on the assumption that stresses remain constant for a given time step, the strain increments due to creep and shrinkage occuring in each concrete layer are calculated.

$$\Delta\varepsilon_{oi} = \Delta\varepsilon_i^c + \Delta\varepsilon_i^s \tag{3.39}$$

where $\Delta\varepsilon_i^c$ and $\Delta\varepsilon_i^s$ are the respective creep and shrinkage strain increment vectors in layer i, and $\Delta\varepsilon_{oi}$, the initial strain increment vector.

3. The equivalent nodal forces produced by the initial strain increment are calculated.

$$R_{ec} = \sum_{k=1}^{c} \int_A B_k^T D_k \Delta\varepsilon_{ok} dA \tag{3.40}$$

where, D_k is the material matrix for the concrete layer at time t_{i+1}. The resulting element load vectors are transformed into global coordinates and the time dependent load vector R_{ei}, due to creep and shrinkage strains, is assembled.

4. The structural stiffness matrix K is formed and the equilibrium equations are solved for the equivalent nodal load vector.

$$\Delta r = K^{-1} \Delta F_{e_o} \tag{3.41}$$

where, Δr is the nodal displacement increment vector.

5. From the nodal displacement increment, the corresponding strain increment vector $\Delta\varepsilon_i$ in every layer is obtained.

$$\Delta\varepsilon_i = B_i \Delta r \tag{3.42}$$

The stress increment vector is subsequently calculated as

$$\Delta\sigma_i = D_i(\Delta\varepsilon_i - \Delta\varepsilon_{io}) \tag{3.43}$$

6. Increments in the field variables are added to the total values from step 1 to obtain the current total values. Convergence is then checked and the solution completed for time step Δt_i.

7. Steps 1 through 6 are repeated for the next time step Δt_{i+1}.

3.5 Convergence Criteria

A step-by-step iterative approach is used to track the nonlinear response and the load-displacement profile of the structure. Displacement and a force convergence criteria can be used in the computer program to identify the equilibrium state of the structure. Convergence criteria are set such that iterations are terminated when the change in a response increment is reasonably small that further iterations would not improve the solution significantly.

The displacement criterion, used in this study involves the assessment of the accuracy of the total displacement vector by looking at the last displacement increment.

$$\Delta d = t_d \Delta\theta = t_r \tag{3.44}$$

where, t_d is the prescribed convergence tolerance for translational displacements and t_r, the prescribed convergence tolerance for rotations.

3.6 Computer Program

To perform the analytical investigations outlined in this study, a computer program TIDARCS (TIme Dependent Analysis of Reinforced Concrete Slabs) is

used. The program is a modified version of *NOPARC* which was developed at the University of California, Berkeley and used extensively by other researchers.

The program is based on the displacement formulation of the finite element method and a time step integration procedure. It is used to model the load-deformation response of reinforced concrete slabs and panels through the elastic, inelastic and ultimate regimes. The stress and strain states in concrete and steel can be determined for any stage of the response history. Time-dependent effects of creep and shrinkage are accounted for in tracing the deflection profile of the structure.

The program is coded in Fortran and was run on the University of Ottawa AMDAHL 5860 computer. It was first converted from CDC FORTRAN to IBM FORTRAN.

TIDARCS consists of a short main program and subroutines which perform the input and output functions, database management functions, and the numerical computations required for the time-dependent solution. A flow chart describing the logical structure of the program is presented in Fig. (3.4). A sample input file is presented in Appendix C with extracts of a typical output file given in Appendix D.

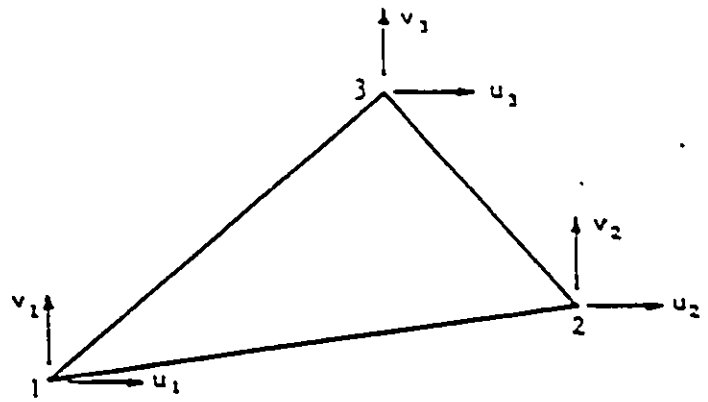

a. CONSTANT STRAIN TRIANGLE

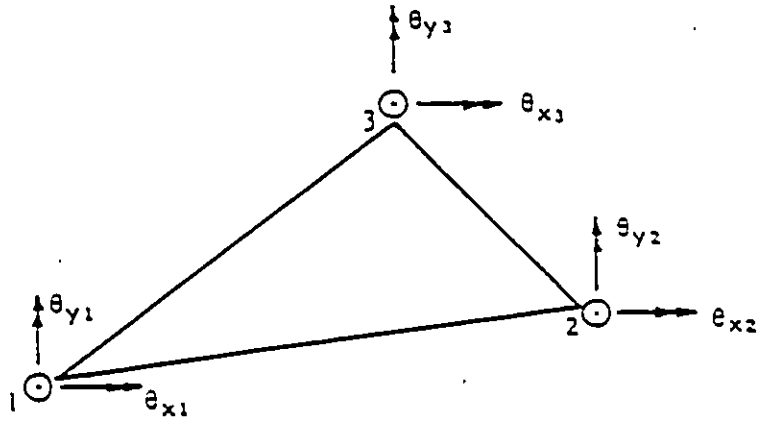

b. IRONS-RAZZAQUE PLATE BENDING TRIANGLE

Figure 3.1: Finite Elements Used in Present Study

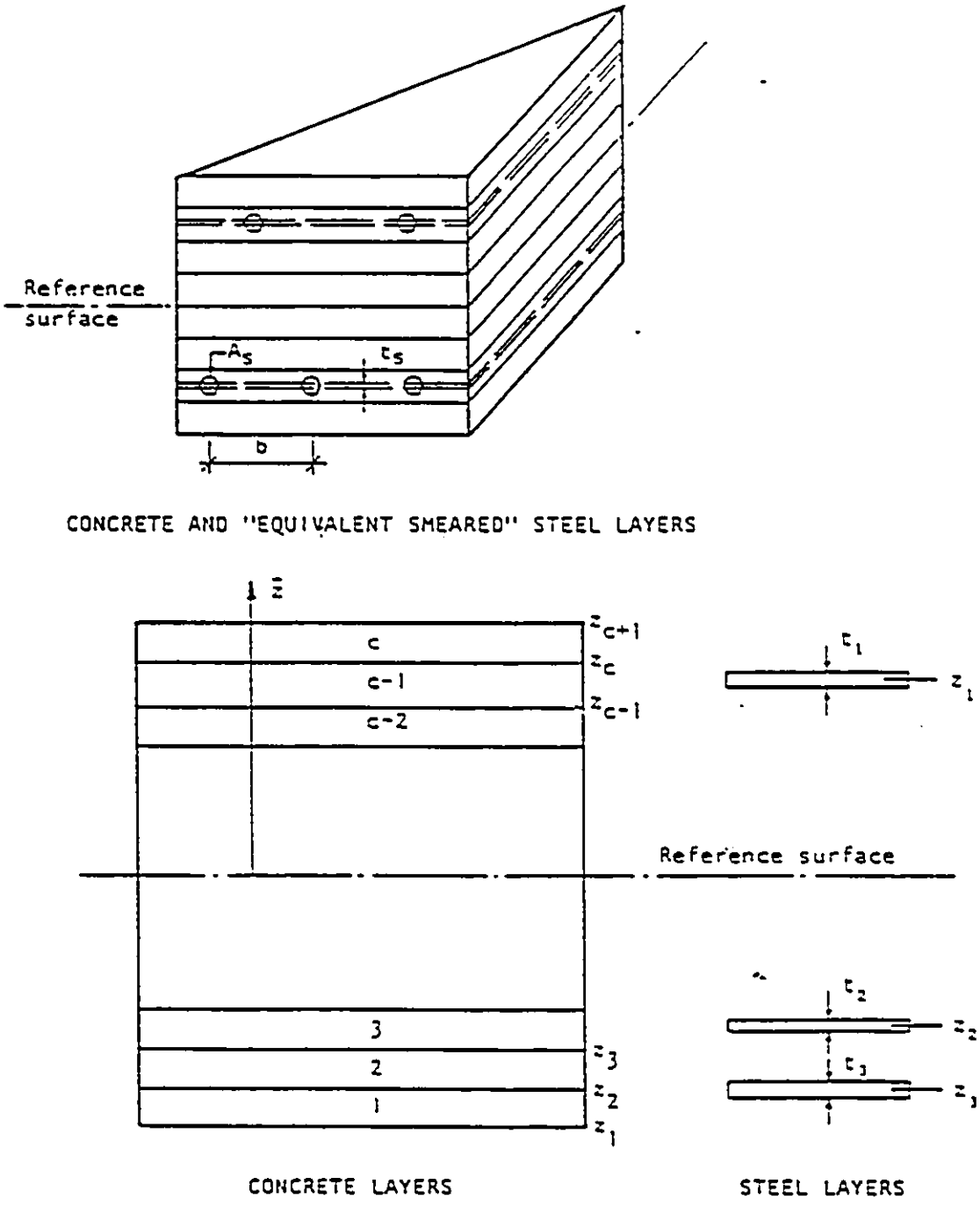

Figure 3.2: Layer System of a Triangular Finite Element

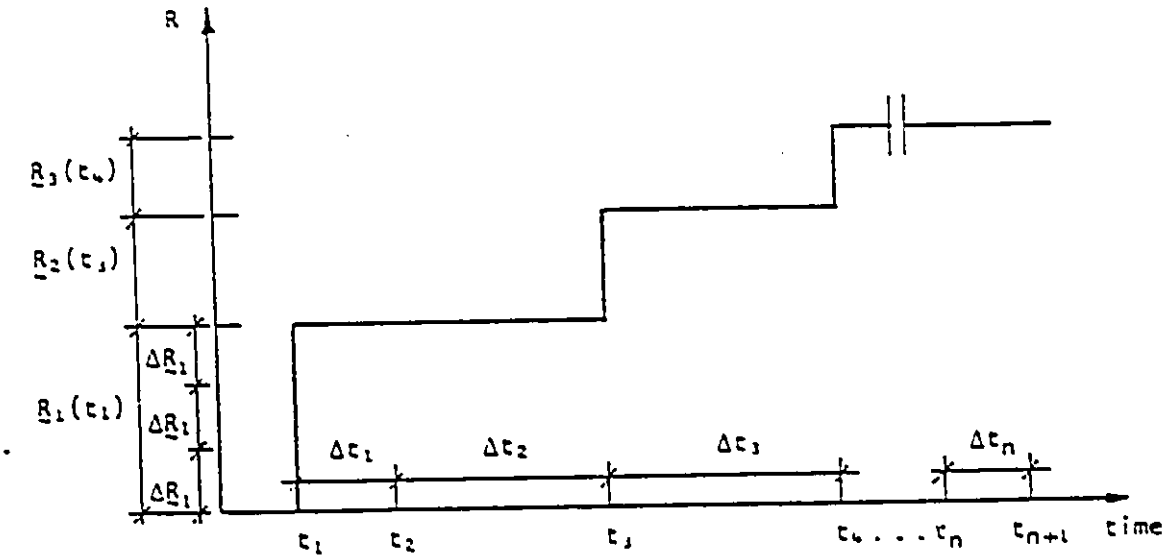

a. EXTERNAL LOAD HISTORY

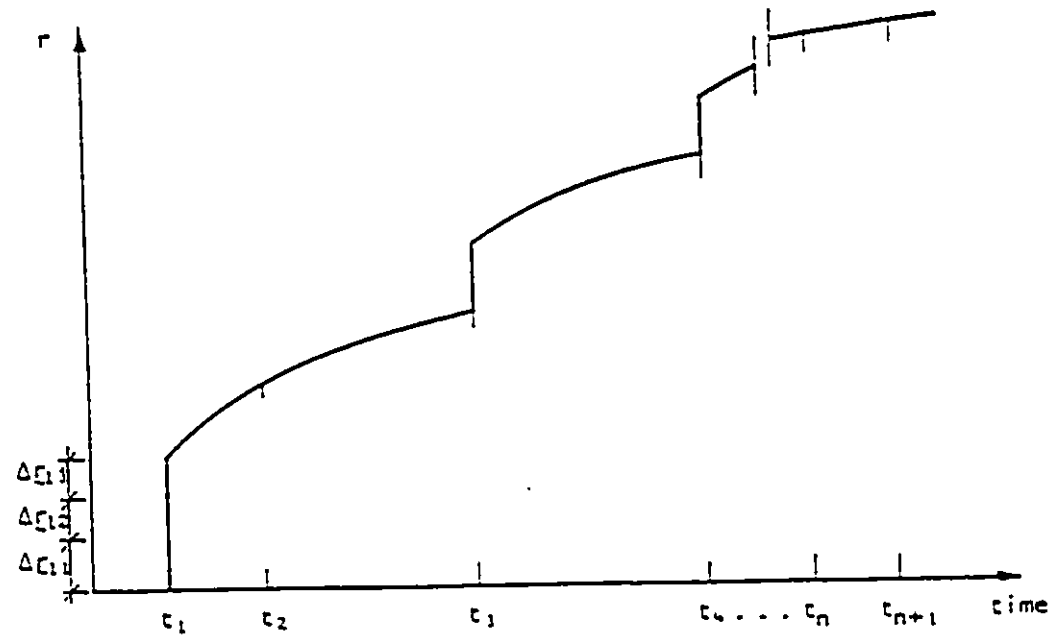

b. DISPLACEMENT HISTORY

Figure 3.3: Structural Response History Due to External Loads

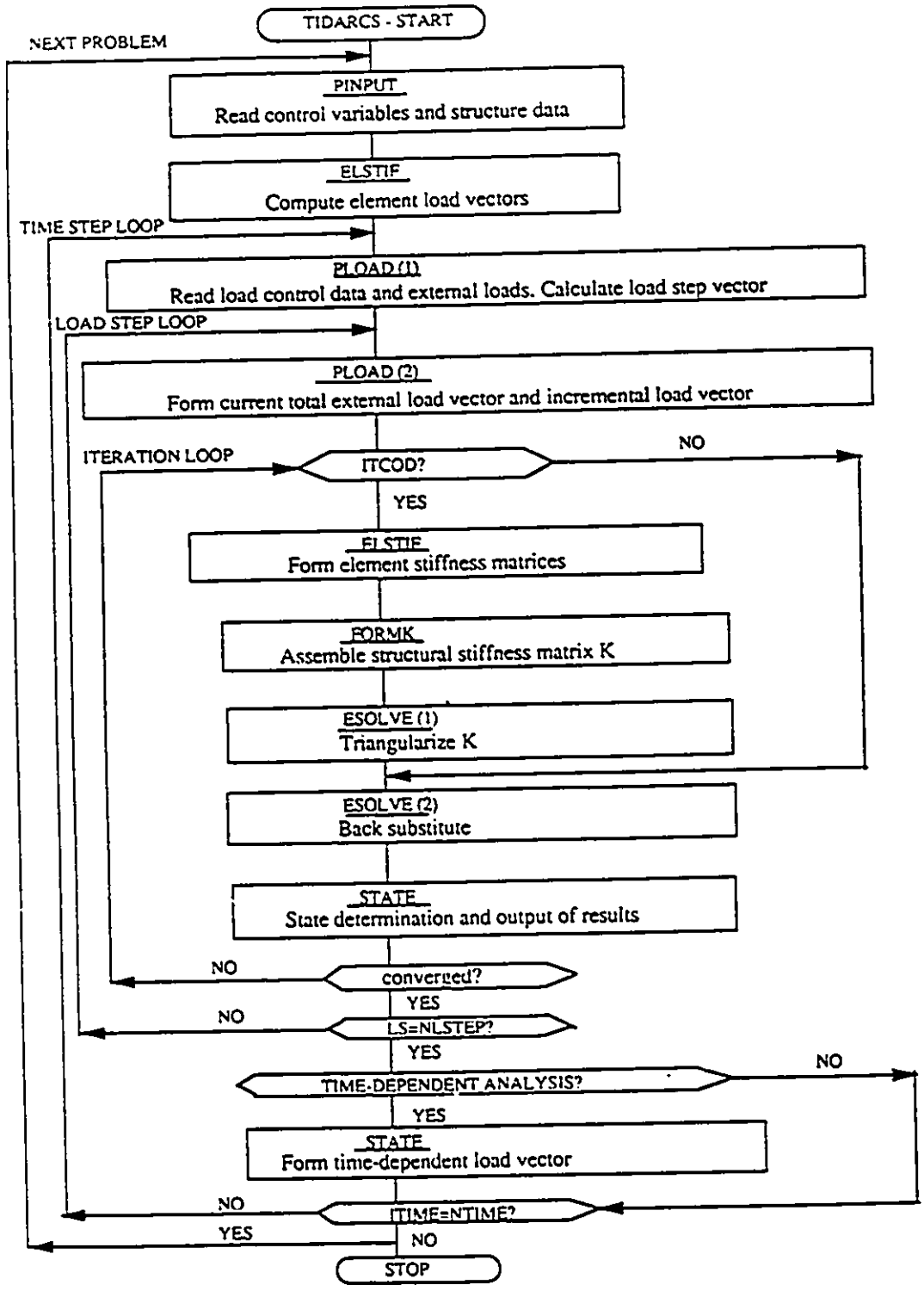

Figure 3.4: Structured Flow Chart of TIDARCS

Chapter 4

CONSTITUTIVE MODELS

4.1 General Remarks

Reinforced concrete is a composite of concrete and reinforcing steel. Accurate prediction of the structural behaviour will depend on adequate modelling of the constituent materials and the interface between them. The properties of reinforcing steel are generally well defined and can be modelled easily. Development of a suitable model for concrete is complicated due to the

- non-homogeneity of structural concrete,
- pronounced nonlinear behaviour of concrete at high stress levels,
- cracking of concrete in tension,
- absence of a well defined failure criteria, and
- time dependent influences of creep and shrinkage.

Extensive research effort has been directed towards establishing a generalized concrete theory, based on all experimental observations, which has led to the evolution

of several constitutive models. Detailed documentation and analysis of many of the existing models can be found in Ref. [35].

4.2 Behaviour of Concrete

A review of the deformation behaviour of concrete is important as one of the criteria for serviceability (deflection) depends on the extent of concrete deformation. The main factors generally considered in the deformation of concrete are applied stress, creep, shrinkage, and thermal variations. A general discussion of concrete deformation as the result of applied stress is presented in this section. Deformation resulting from the other phenomena will be discussed in Chapter 5.

4.2.1 Concrete under biaxial stress

Experimental findings indicate that concrete is seldom stressed in one direction, but simultaneously in a number of directions. Nevertheless, concrete is commonly treated as an orthotropic material with biaxial stress behaviour. In a detailed review of concrete subjected to biaxial stresses, Kupfer et al [37] presented experimental stress-strain curves for the following states:
(a) concrete under biaxial compression (see Fig. 4.1),
(b) concrete in combined tension and compression (see Fig. 4.2), and
(c) concrete subjected to biaxial tension (see Fig. 4.3).

The following conclusions were drawn from their study:

- a maximum compressive strength increase is realized for the biaxial compres-

sion state. Approximately 27% strength increase is achieved for a stress ratio $\sigma_2/\sigma_1 = 0.5$. This is reduced to about 16% at an equal biaxial compression state of $\sigma_2/\sigma_1 = 1$;

- under biaxial compression-tension, the compressive strength decreases almost linearly as the applied tensile stress increases
- the biaxial tensile strength is almost the same as that of the uniaxial tensile strength;
- stiffness of concrete increases in the presence of biaxial compression. This is mainly due to the confinement of microcracking in the cement paste;
- concrete undergoes an inelastic increase in volume as compressive stresses increase and its failure point is approached. This is attributed to the progressive growth of major microcracks.

4.2.2 Concrete model for present study

The model used to characterize concrete behaviour under biaxial stress is a modified version of Darwin and Pecknold's model [18]. The model (fig. 4.7), is based on an orthotropic hypoelastic formulation and was developed in such a way that the constitutive model.

1. can be easily incorporated into a finite-element program,

2. is applicable to cyclic loading,

3. accounts for strain softening in compression, and

4. is determined completely by conventional parameters rather than empirical constants.

For biaxial compression, a family of curves was suggested by Darwin and Pecknold [17], depending on the biaxial stress ratio, to express the constitutive relationship

$$\sigma_i = \frac{E_o \varepsilon_{iu}}{1 + [(\frac{E_o}{E_s} - 2)(\frac{\varepsilon_{iu}}{\varepsilon_{ic}}) + (\frac{\varepsilon_{iu}}{\varepsilon_{ic}})^2]} \tag{4.1}$$

where,

E_o = initial uniaxial tangent modulus,

E_s = secant modulus, $\frac{\sigma_{ic}}{\varepsilon_{ic}}$

ε_{iu} = *equivalent uniaxial strain* in the principal stress direction,

$\sigma_{ic}, \varepsilon_{ic}$ = maximum compressive stress and the corresponding strain in the principal direction i. These values are obtained from the biaxial failure envelope of Kupfer et al. [38], shown in Fig. 4.4.

For tension, the relationship is

$$\sigma_i = E_o \varepsilon_{iu}, \quad for \ \ \sigma_i \leq \sigma_{it} \tag{4.2}$$

where σ_{it} is the tensile strength of concrete in the principal stress direction.

The displacement formulation of the finite element method uses an incremental load step solution procedure to account for material and load-deformation nonlinearities. For an orthogonal material under biaxial stress, the incremental consti-

tutive matrix, with respect to the axes of orthotropy, is given by

$$\begin{Bmatrix} d\sigma_1 \\ d\sigma_2 \\ d\tau_{12} \end{Bmatrix} = \frac{1}{1-\nu_1\nu_2} \begin{bmatrix} E_1 & \nu_2 E_2 & 0 \\ \nu_2 E_2 & E_2 & 0 \\ 0 & 0 & (1-\nu_1\nu_2)G' \end{bmatrix} \begin{Bmatrix} d\varepsilon_1 \\ d\varepsilon_2 \\ d\gamma_{12} \end{Bmatrix} \tag{4.3}$$

where,

1 and *2* are the orthotropic material directions,

E_1, E_2 = uniaxial tangent moduli in directions *1* and *2*,

ν_1, ν_2 = Poisson's ratio in directions *1* and *2*,

G' = shear modulus for a material under plane stress.

The following assumptions are made in the modification process of the orthotropic constitutive relationship

- $\nu_1\ \nu_2 = \nu^2$, where ν is the effective Poisson's ratio under biaxial stress,
- $\nu_1 E_1 = \nu_2 E_2$ for symmetric material behaviour.

The value,

$$G' = \frac{1}{4(1-\nu^2)}[E_1 + E_2 - 2\nu\sqrt{E_1 E_2}] \tag{4.4}$$

is adopted as the shear modulus under a state of biaxial stress, as it has been demonstrated to show no bias in any particular direction with respect to shear stiffness [18]. Based on the above assumptions, the incrementally linear orthotropic constitutive relationship in the principal stress direction is given by:

$$\begin{Bmatrix} d\sigma_1 \\ d\sigma_2 \\ d\tau_{12} \end{Bmatrix} = \frac{1}{1-\nu^2} \begin{bmatrix} E_1 & \nu\sqrt{E_1 E_2} & 0 \\ \nu\sqrt{E_1 E_2} & E_2 & 0 \\ 0 & 0 & \frac{1}{4}(E_1 + E_2 - 2\nu\sqrt{E_1 E_2}) \end{bmatrix} \begin{Bmatrix} d\varepsilon_1 \\ d\varepsilon_2 \\ d\gamma_{12} \end{Bmatrix} \tag{4.5}$$

If the element coordinate system $x-y$ is such that the principal stress directions *1* and *2* make an angle θ with respect to $x-y$, then the constitutive relationship

in the element coordinate system is given by:

$$\begin{Bmatrix} d\sigma_{xx} \\ d\sigma_{yy} \\ d\tau_{xy} \end{Bmatrix} = \frac{1}{1-\nu^2} \begin{bmatrix} E_1c^2 + E_2s^2 & \nu\sqrt{E_1E_2} & \frac{1}{2}(E_1 - E_2)cs \\ & E_1s^2 + E_2c^2 & \frac{1}{2}(E_1 - E_2)cs \\ (sym.) & & \frac{1}{4}(E_1 + E_2 - 2\nu\sqrt{E_1E_2}) \end{bmatrix} \begin{Bmatrix} d\varepsilon_{xx} \\ d\varepsilon_{yy} \\ d\gamma_{xy} \end{Bmatrix} \tag{4.6}$$

where, c = cosθ and s = sinθ.

From Eq. (4.5), the concrete material properties needed in the solution process are the orthotropic elastic moduli E_1 and E_2, and the effective Poisson's ratio ν.

Work by Kupfer et al [37] suggested that, under biaxial stress there is a significant increase in stiffness which can not be attributed to Poisson's effect alone. The cause seems to be confinement of microcracking in the presence of biaxial compression. This makes the use of Eq. (4.5) inappropriate at high stress levels when microcracking confinement is present. The concept of *equivalent uniaxial strains* developed by Darwin and Pecknold can be adopted to help incorporate the effects of microcracking confinement in the constitutive equation.

4.2.3 Equivalent Uniaxial Strain

The equivalent uniaxial strain defines the variation of the elastic moduli E_1 and E_2 with respect to stress variation. If Poisson's effect is removed from experimental biaxial stress-strain curves in compression, a family of stress-strain curves can be constructed whose slopes would provide the values of E_1 and E_2. The curves are called *equivalent uniaxial* stress-strain curves, and the values of E_1 and E_2 account for the effects of microcracking confinement.

Equation (4.1) suggested by Darwin and Pecknold [18], was used to simulate the

biaxial stress-strain behaviour of concrete. Thus, the constitutive relationship for the compression part of the curve is given by,

$$\sigma_i = \frac{E_o \varepsilon_{iu}}{1 + [(\frac{E_o}{E_s} - 2)(\frac{\varepsilon_{iu}}{\varepsilon_{ic}}) + (\frac{\varepsilon_{iu}}{\varepsilon_{ic}})^2]} \tag{4.7}$$

where, all variables are as defined under Eq. (4.1).

For tension,

$$\sigma_i = E_o \varepsilon_{iu}, \quad for \ \ \sigma_i / \sigma_{it} \tag{4.8}$$

where σ_{it} is the tensile strength of concrete in the principal stress direction. The equivalent uniaxial strain ε_{iu} essentially removes Poisson's effect from the biaxial strains whereas increase in strength and ductility are accounted for by σ_{ic} and ε_{ic} respectively.

If concrete is biaxially compressed in the principal stress directions and assumed to be proportionally loaded with piece-wise linear material behaviour, the stress-strain relationship is defined as,

$$d\varepsilon_2 = \frac{d\sigma_2}{E_2} - \nu \frac{d\sigma_1}{E_1} \tag{4.9}$$

where,

$d\sigma_1$, $d\sigma_2$ = increment in stresses in principal directions 1 and 2 respectively E_1, E_2 = orthotropic tangent moduli.

Rearranging Eq. (4.9), gives

$$d\sigma_2 = E_2 \frac{d\varepsilon_2}{1 - \nu \alpha n} = E_2 \, d\varepsilon_{2u} \tag{4.10}$$

where,

$\alpha = \frac{\sigma_1}{\sigma_2}$ = biaxial stress ratio

$n = \frac{E_2}{E_1}$ = modular ratio

$d\varepsilon_{2u} = d\varepsilon_2 / (1 - \nu \, \alpha \, n)$ = uniaxial strain increment in principal direction 2.

For the stress-strain relationship of Eq. (4.10), the gradient E_2 does not contain Poisson's effect. Instead, a value $d\varepsilon_{2u}$ has been introduced to account for the effects of microcrack confinement. Subsequently, the value of E_2 can be used in the constitutive matrix of Eq. (4.5).

The total uniaxial strain at any point is obtained by summing all the strain increments up to that load point.

$$d\varepsilon_{iu} = \sum d\varepsilon_{iu} = \sum \frac{d\varepsilon_i}{1 - \nu\alpha n} = \sum \frac{d\sigma_i}{E_i} \tag{4.11}$$

The slope E_i of the equivalent uniaxial stress-strain curve at any point $(\sigma_i, \varepsilon_{iu})$ is given by differentiating equations (4.7) and (4.8).

For loading in compression,

$$E_i = \frac{\partial \sigma_i}{\partial \varepsilon_{iu}} = \frac{E_o(1 - q^2)}{(1 + [\frac{E_o}{E_s} - 2]q + q^2)^2} \tag{4.12}$$

where,

$$q = \frac{\varepsilon_{iu}}{\varepsilon_{ic}} \tag{4.13}$$

In the case of tension,

$$\frac{\partial \sigma_i}{\partial \sigma_{iu}} = E_o \tag{4.14}$$

The equivalent uniaxial stress-strain curve used is shown in Fig. 4.5. It has a slope E_s which passes through the point of maximum compressive stress and strain (σ_{ic}, ε_{ic}). For biaxial loading, the point $(\sigma_{ic}, \varepsilon_{ic})$ is a function of the principal stress ratio α, the uniaxial compressive strength f'_c, and the strain at the peak uniaxial stress ε_c. The values of the maximum stresses in the two principal directions $(\sigma_{1c}, \sigma_{2c})$ are obtained from the biaxial strength envelope of Kupfer et al. [38]. It is assumed that the maximum tensile stress the concrete can withstand is the uniaxial tensile stress, f'_t.

As shown in Fig. 4.4, the biaxial strength is divided into four regions, depending on the stress state represented by the stress ratio α. The principal stress directions are chosen such that $\sigma_1 \geq \sigma_2$ algebraically. A summary of the four regions of the strength envelope and the expressions for the maximum stresses σ_{1c}, σ_{2c} and their corresponding strains ε_{1c}, ε_{2c} is given below.

1. Compression-Compression Region

$$\sigma_{2c} = \frac{1 + 3.65\alpha}{(1+\alpha)^2} f'_c \tag{4.15}$$

$$\varepsilon_{2c} = \varepsilon_c(3\frac{\sigma_{2c}}{f'_c} - 2) \tag{4.16}$$

$$\sigma_{1c} = \alpha\sigma_{2c} \tag{4.17}$$

$$\varepsilon_{1c} = \varepsilon_c[-1.6(\frac{\sigma_{1c}}{f'_c})^3 + 2.25(\frac{\sigma_{1c}}{f'_c})^2 + 0.35\frac{\sigma_{1c}}{f'_c}] \tag{4.18}$$

2. Compression-Tension Region

$$\sigma_{2c} = \frac{1 + 3.28\alpha}{(1+\alpha)^2} f'_c \tag{4.19}$$

$$\varepsilon_{2c} = \varepsilon_c[4.42 - 8.38\frac{\sigma_{2c}}{f'_c} + 7.54(\frac{\sigma_{2c}}{f'_c})^2 - 2.58(\frac{\sigma_{2c}}{f'_c})^3] \tag{4.20}$$

$$\sigma_{1c} = \alpha\sigma_{2c} \tag{4.21}$$

$$\varepsilon_{1c} = \frac{\sigma_{1c}}{E_o} \tag{4.22}$$

3. Tension-Compression region

$$\sigma_{2c} = 0.65 f'_c \tag{4.23}$$

$$\varepsilon_{2c} = \varepsilon_c[4.42 - 8.38\frac{\sigma_{2c}}{f'_c} + 7.54(\frac{\sigma_{2c}}{f'_c})^2 - 2.58(\frac{\sigma_{2c}}{f'_c})^3] \tag{4.24}$$

$$\sigma_{1c} = f'_t \tag{4.25}$$

$$\varepsilon_{1c} = \frac{\sigma_{1c}}{E_o} \tag{4.26}$$

4. **Tension-Tension Region**

$$\sigma_{1c} = \sigma_{2c} = f'_t \tag{4.27}$$

$$\varepsilon_{1c} = \varepsilon_{2c} = \frac{f'_t}{E_o} \tag{4.28}$$

The biaxial stress-strain behaviour of concrete is treated as an equivalent uniaxial stress-strain relation. The strain increment in each principal direction is evaluated solely by the principal stress increment in the same direction. To construct the equivalent uniaxial stress-strain curve, only the following material properties of concrete are needed

- uniaxial initial tangent modulus, E_o
- uniaxial compressive strength, f'_c
- the corresponding strain for the uniaxial strength, ε_c
- uniaxial tensile strength, f'_t, and
- Poisson's ratio, ν.

Information on all five parameters may be readily obtained from experimental uniaxial load tests or from empirical expressions.

ACI Committee 209 [3] recommended the use of the following expressions for the uniaxial compressive strength, the uniaxial tensile strength, and the initial tangent modulus of concrete.

Compressive Strength

$$(f'_c)_t = \frac{t}{\alpha + \beta t}(f'_c)_{28} \tag{4.29}$$

where,

$(f'_c)_t$ = uniaxial compressive strength at time t,

$(f'_c)_{28}$ = 28-day concrete strength,

t = time in days after casting,

α, β = constants, which depend on cement type and method of curing.

Tensile Strength

$$f'(t) = g_t[w(f'_c)_t]^{\frac{1}{2}} \tag{4.30}$$

where,

$f'(t)$ = uniaxial tensile strength, and

w = unit weight of concrete in pcf. The value of g_t is equal to 1/3.

Modulus of Elasticity

$$E_c(t) = 33[w^3(f'_c)_t]^{\frac{1}{2}} \tag{4.31}$$

where,

$E_c(t)$ = initial tangent modulus, and

w = unit weight of concete in (pcf)

For the present study, a set of equations recommended by Gardner and Zhao [24] for compressive strength, tensile strength and modulus of elasticity are used as they represent concrete behaviour more realistically than those of ACI-209. The Gardner-Zhao compressive strength equation is of the form:

$$f_{cmt} = f_{cm28}\frac{t^{\frac{1}{2}}}{a + bt^{\frac{1}{2}}} \tag{4.32}$$

where,

$f_{cm,t}$ = mean concrete strength at age t,

f_{cm28} = mean concrete strength at 28 days,

a, b = constants, which depend on cement type.

The recommended coefficients for the various cement types are

- Type I or (Type 10) Cement concrete $a = 2.8$, $b = 0.77$
- Type II or (Type 20) Cement concrete $a = 3.4$, $b = 0.72$
- Type III or (Type 30) Cement concrete $a = 1.2$, $b = 0.90$.

The form of Eq.(4.32) is similar to the ACI-209 expression, which is limited in its ability to represent early age and longterm strength development. To relate the 28-day mean concrete strength, (f'_{cm28}) to the specified characteristic strength (f'_{ck28}), Gardner and Zhao adopted the recommended CEB-FIP 1990 Model Code [13] expression,

$$f_{cm28} = f_{ck28} + 8 \qquad (MPa) \tag{4.33}$$

For tensile strength calculations, Gardner and Zhao endorsed the use of the CEB-FIP 1990 Model Code [13] equation,

$$f'_{tk} = 0.30(f'_{ck})^{\frac{2}{3}} \qquad (MPa) \tag{4.34}$$

where,

f'_{tk} = characteristic tensile strength,

f'_{ck} = characteristic compressive strength.

The modulus of elasticity equation recommended by Gardner and Zhao is of the form:

$$E_c = 3500 + 4300(f'_{cm})^{1/2}$$

where, f'_{cm} is the concrete mean compressive strength. The relationship used to represent the strain corresponding to peak uniaxial compressive stress is the Hognestad expression [32],

$$\varepsilon_c(t) = 2\frac{f'_c(t)}{E_o(t)} \tag{4.35}$$

where, $\varepsilon_c(t)$ is strain corresponding to peak stress $f'_c(t)$ at t days.

Poisson's ratio is taken as 0.15 in this study and is assumed to be independent of age and stress. Experimental evidence [37] however indicates that at stress levels higher than 80% of peak stress, there is significant increase in value.

4.2.4 Cracking and tension stiffening

An important characteristic of concrete, which is in part responsible for the non-linear behaviour of reinforced concrete members, is its low tensile strength. In this study, a maximum stress criterion was used to determine the failure strain of concrete in tension.

When one of the principal stresses exceeds the tensile strength of concrete, an assumption of crack formation perpendicular to the direction of that stress is made. The modulus of elasticity in that direction is set to zero and a crack shear constant, β, is introduced. If there is crack formation in the principal stress direction 1 for

example, the constitutive relationship of Eq. (4.5) reduces to

$$\begin{Bmatrix} d\sigma_1 \\ d\sigma_2 \\ d\tau_{12} \end{Bmatrix} = \begin{bmatrix} 0 & 0 & 0 \\ 0 & \frac{E_2}{1-\nu^2} & 0 \\ 0 & 0 & \beta G' \end{bmatrix} \begin{Bmatrix} d\varepsilon_1 \\ d\varepsilon_2 \\ d\gamma_{12} \end{Bmatrix} \tag{4.36}$$

The cracked shear constant, β, was proposed by Lin [39], to help estimate the effective shear modulus after cracking. It depends on the effect of dowel action and aggregate interlock and has a recommended range of

$$0.0 < \beta < 1.0$$

It should be noted, however, that there have been cases of numerical instability when $\beta = 0$. After concrete is cracked in one direction, the formation of a new tensile crack is restricted to a direction orthogonal to the first crack. When cracks in both orthogonal directions occur, the effective shear modulus is the only non-zero term in the material matrix.

$$\begin{Bmatrix} d\sigma_1 \\ d\sigma_2 \\ d\tau_{12} \end{Bmatrix} = \begin{bmatrix} 0 & 0 & 0 \\ 0 & 0 & 0 \\ 0 & 0 & \beta G' \end{bmatrix} \begin{Bmatrix} d\varepsilon_1 \\ d\varepsilon_2 \\ d\gamma_{12} \end{Bmatrix} \tag{4.37}$$

When a reinforced concrete member under uniaxial tension reaches the peak tensile strength, primary cracks are formed at finite intervals as shown in Fig. 4.6. At these cracks, the stress in the concrete declines to zero, and the total load is carried across the crack by the steel reinforcement. The bond forces at the contact surface induce tension stresses into the concrete between the cracks. Between cracks the concrete remains bonded to the steel bar and contributes to the overall stiffness of the system. This stiffness effect, often called *tension stiffening*, may be quite significant for finite element modelling and can be accounted for by assuming a gradual loss of tensile strength in concrete. Scanlon [47] and Lin [39] advanced this line of approach, but in different ways.

Two tension stiffening options are provided in the computer program used. A method suggested by Gilbert and Warner [25], and the linear unloading curve of Lin [39]. The Gilbert-Warner method is simpler and computationally more efficient. The tensile strength of concrete between cracks is ignored. Instead, this additional stress is conveniently lumped at the level of the steel and an increased steel modulus is used.

With Lin's model, the tensile modulus of the concrete is set to zero once there is tensile crack formation. The steel and concrete stresses obtained from Lin's model are estimates of the average stresses in the concrete and the steel, as shown in Fig. 4.6.

4.2.5 Concrete Strain Softening

Experimental results indicate that concrete is a strain-softening material when loaded beyond the maximum compressive stress level due to material degradation. This gives a negative tangent modulus, which is likely to cause numerical instabilities when used in the constitutive equation (4.5). To circumvent this problem, the following technique developed by Kabir [35] is used.

When a calculated principal stress σ_i^n exceeds the value of σ_{ic}, yielding is assumed to have occurred. The stress drops to σ_i^n and the elastic moduli are set to zero for the next load iteration. At the stress level $\sigma_i^{n'}$, an unloading of σ_{ol} occurs, which is the unbalanced stress. This is redistributed in the next load iteration. The process is continued until crushing occurs at ε_u. The use of the zero modulus in place of the negative value is to facilitate the numerical solution of the finite element equilibrium equations.

The constitutive relationship for the finite element formulation after yielding is.

$$d\sigma = 0d\varepsilon \tag{4.38}$$

Lin [39] used the unconstrained flow rule and the normality flow rule separately with a Von Mises yield criterion to investigate the behaviour of reinforced concrete slabs and shells and concluded that the yield criterion was independent on the type of flow used. Subsequently, the simpler to formulate "unconstrained flow rule" is assumed for the unloading branch of this model.

4.2.6 Stress Reversal

Unloading can result from the time-dependent effects of creep and shrinkage or applied load history. Darwin and Pecknold [17] developed a constitutive model which included loading, unloading and reloading curves for use in the analysis of structures subjected to cyclic loading. A simple loading and unloading curve based on the Darwin model is illustrated in Fig. 4.8 and assumes that all unloading take place with an initial tangent modulus E_o. The model has four distinct parts which are described below.

1. AB – compressive loading before yield is restricted along the path AB. Based on the initial assumption, any unloading in zone AB should have a slope E_o. This means that unloading from H should occur along HP. Further unloading from P will occurs along PQ.

2. BCD - compressive unloading after yield at M occurs along MN with a slope E_o. The strain increment determines whether unloading path BC or MN will be followed at point M.

3. AF – Tensile loading before cracking takes place along AF with a slope of E_o. Any unloading before F is reached will happen along FA.

4. FG – tensile unloading after initial cracking occurs along FG or FH depending on the tension stiffening model[1] being used. For the gradually unloading model of Lin, unloading takes place along FG with the tensile stress reducing to zero at and beyond G. At G reloading will occur along GA and then AB. For the increased steel modulus model, the stress in concrete drops to zero from F to E and any reloading takes place along HA and then AB.

4.3 Reinforcing Steel Model

A simple bilinear constitutive model (see Fig. 4.9) is used to represent reinforcing steel behaviour. The model may be perfectly elasto-plastic or exhibit strain-hardening with Bauschinger[2] type effect.

The basic parameters needed to define the various material states are:

- initial modulus of elasticity, E_s
- strain-hardening modulus, E_{sh}
- steel yield stress, f_y and
- ultimate strain, ε_{us}.

Figure (4.9) illustrates the reinforcement model for which, the following four different material states are defined.

[1] Discussed under section 4.2.4

[2] Refers to one particular type of *directional anisotropy* induced by plastic deformation. That is, an initial plastic deformation of one sign reduces the resistance of the material with respect to a subsequent plastic deformation of the opposite sign (page 352 of [14]).

1. AB, AF – An initial linear elastic portion representing loading in primary tension or compression and with a constant slope E_s.

2. BD – At the point B, steel attains its yield stress value f_y and initial yielding begins. Loading after yielding occurs along BD with a reduced slope E_{sh}.

3. CH – unloading is assumed to occur along a path parallel to the primary curve. At a point C for example, unloading will take place along CH with a slope E_s, and continue along HFG with a slope E_{sh}.

4. FG – Stress reversal along AB continues to D after which loading initiates along FG with a slope E_{sh}.

Failure is assumed to have occurred when the total strain in steel exceeds E_{us}. If *1* is an axis parallel to the steel's longitudinal axis and *2*, an axis perpendicular to it, then the incremental stress-strain relationship is given by:

$$\begin{Bmatrix} d\sigma_1 \\ d\sigma_2 \\ d\tau_{12} \end{Bmatrix} = \frac{1}{1-\nu^2} \begin{bmatrix} E_s & 0 & 0 \\ 0 & 0 & 0 \\ 0 & 0 & 0 \end{bmatrix} \begin{Bmatrix} d\varepsilon_1 \\ d\varepsilon_2 \\ d\gamma_{12} \end{Bmatrix} \tag{4.39}$$

In the strain-hardening region, E_s in the elasticity matrix of Eq. (4.39) is replaced by E_{sh}. For perfectly elasto-plastic steel, E_{sh} is taken as zero.

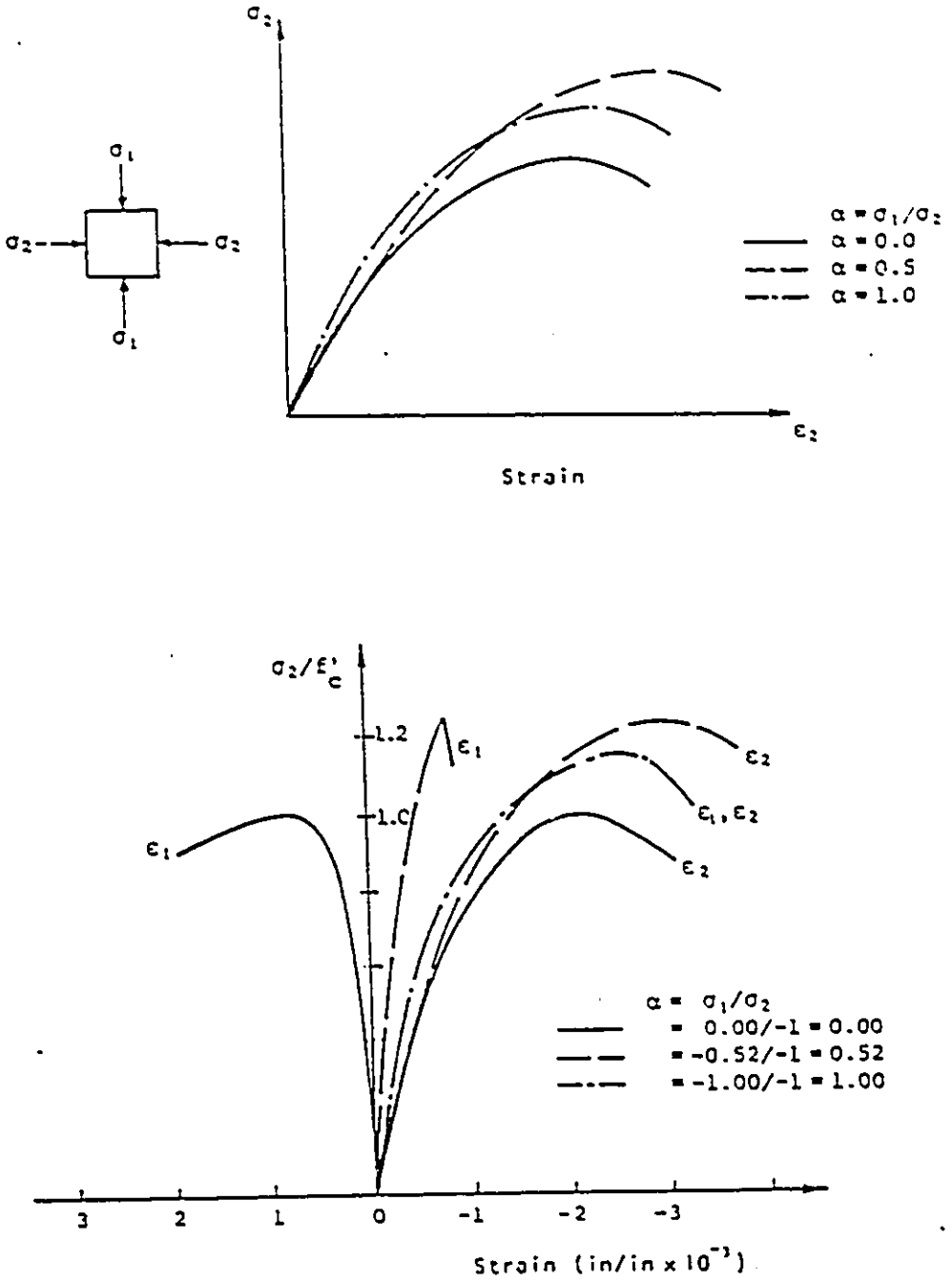

Figure 4.1: Concrete Under Biaxial Compression [74]

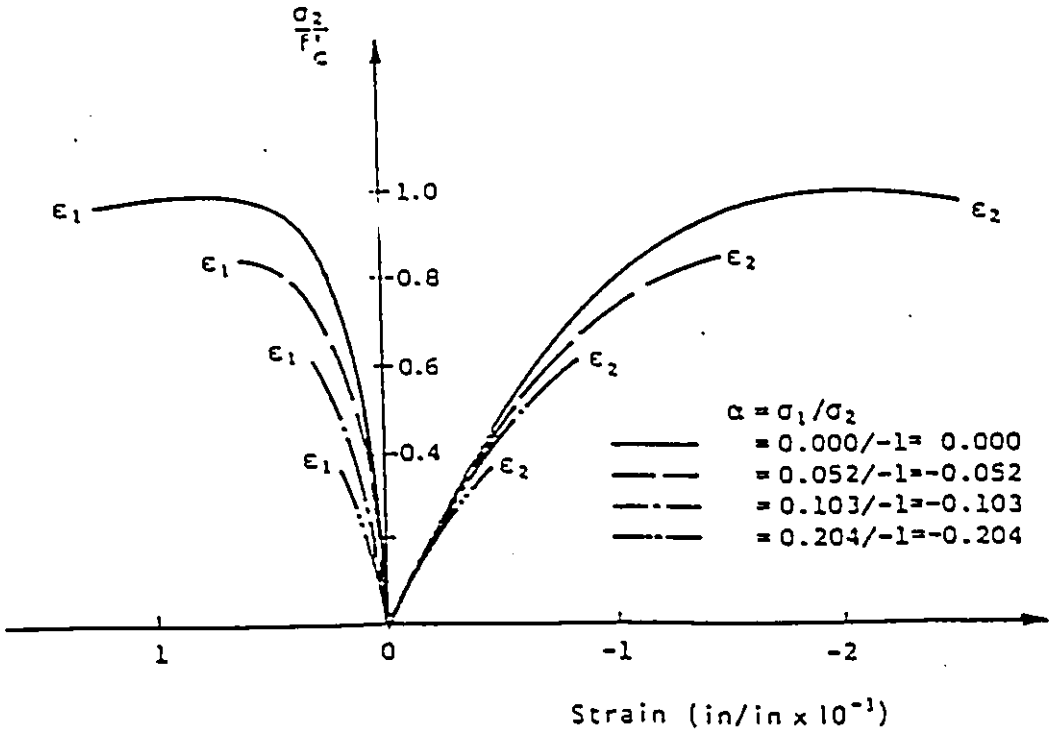

Figure 4.2: Concrete Under Combined Tension and Compression [74]

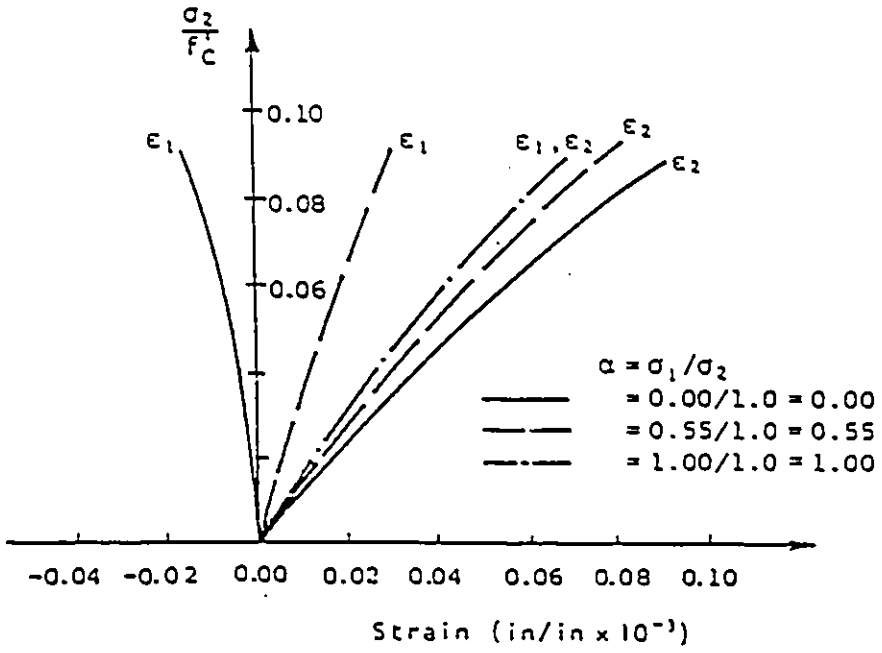

Figure 4.3: Concrete Under Biaxial Tension [74]

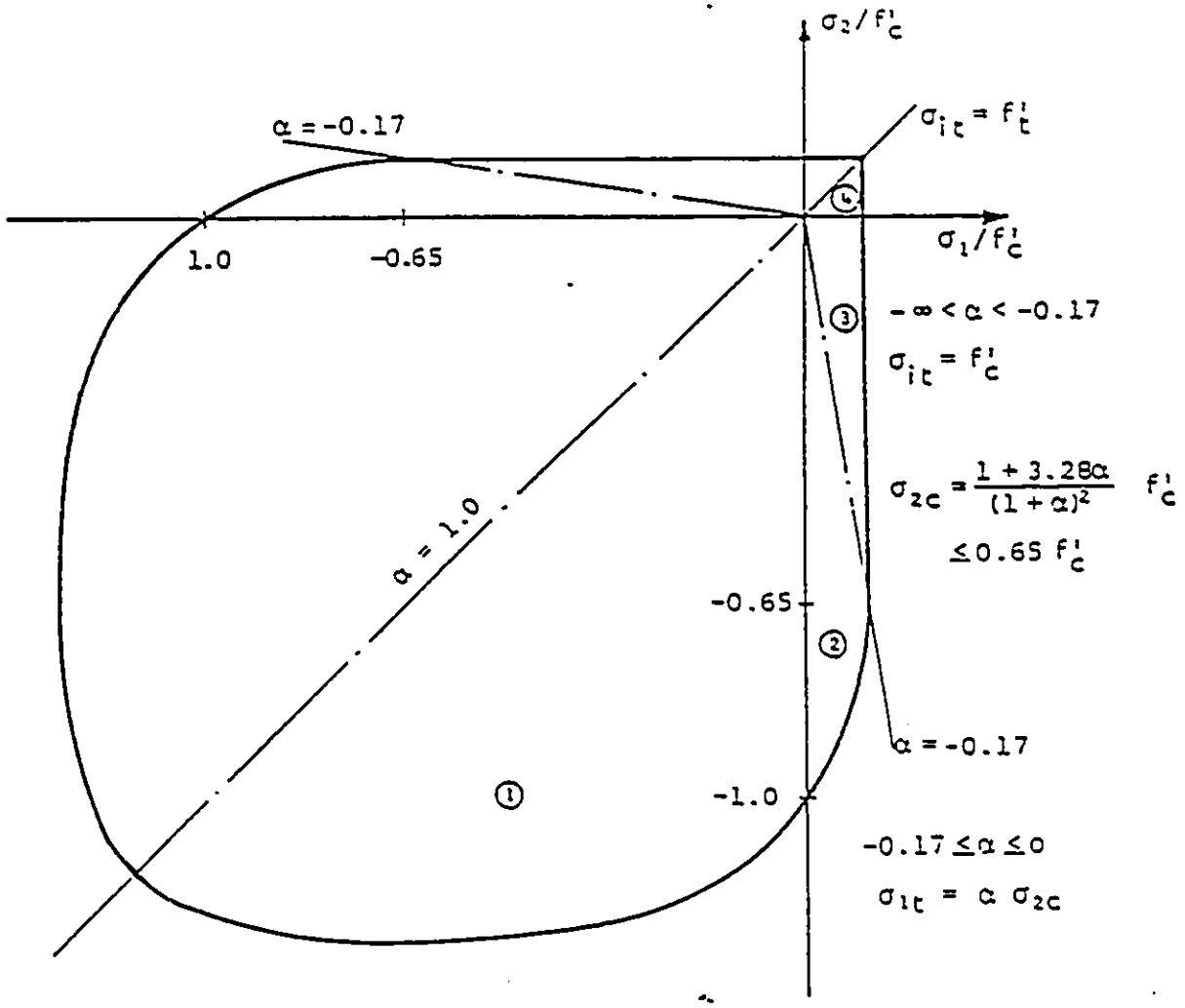

$$\sigma_{2c} = \frac{1 + 3.65\alpha}{(1+\alpha)^2} f'_c$$

$$\sigma_{1c} = \alpha\, \sigma_{2c}$$

$$\alpha = \sigma_1 / \sigma_2$$

Compression = -
Tension = +

Figure 4.4: Biaxial Strength Envelope [74]

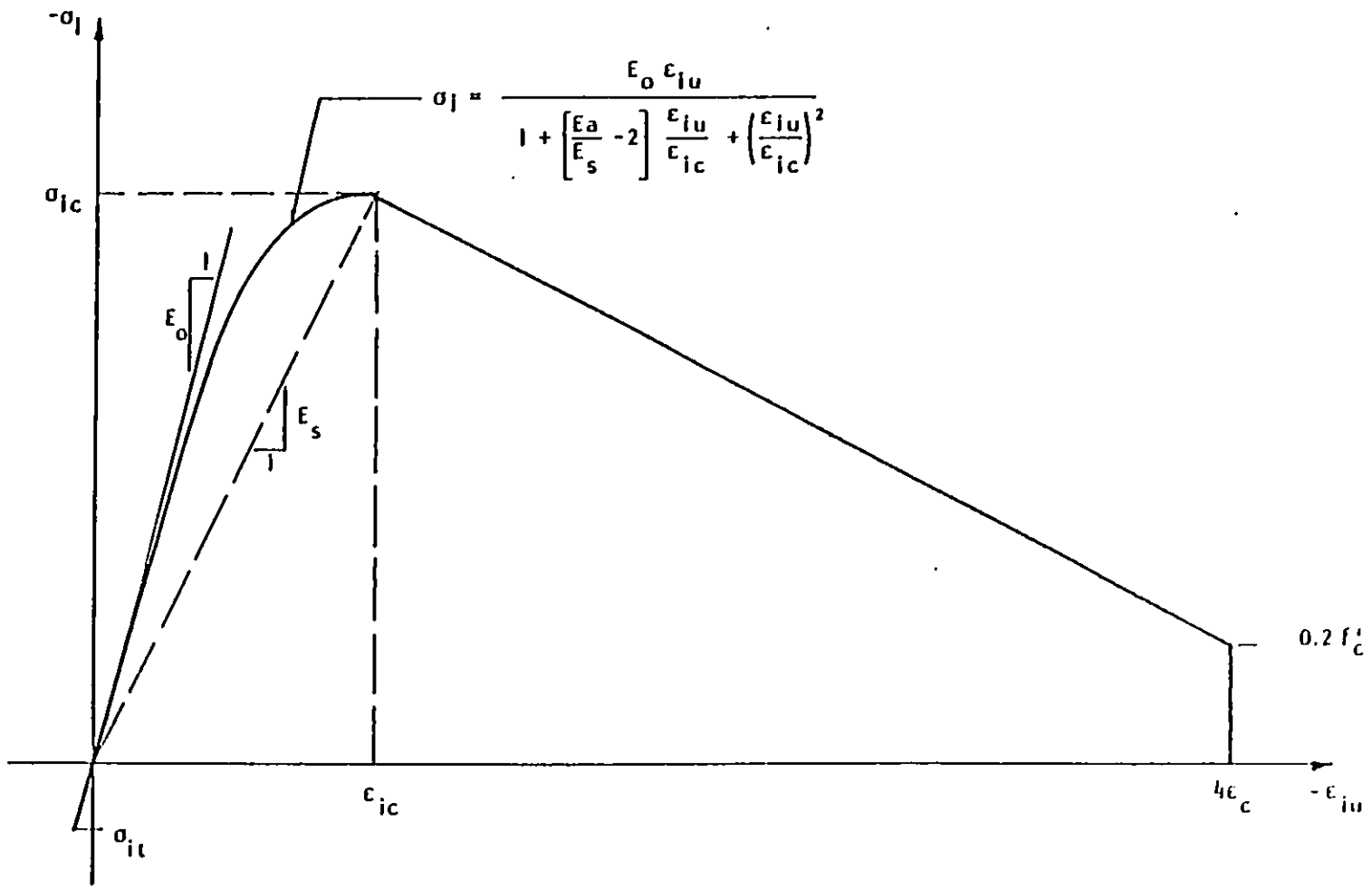

Figure 4.5: Equivalent Uniaxial Stress-Strain Curve

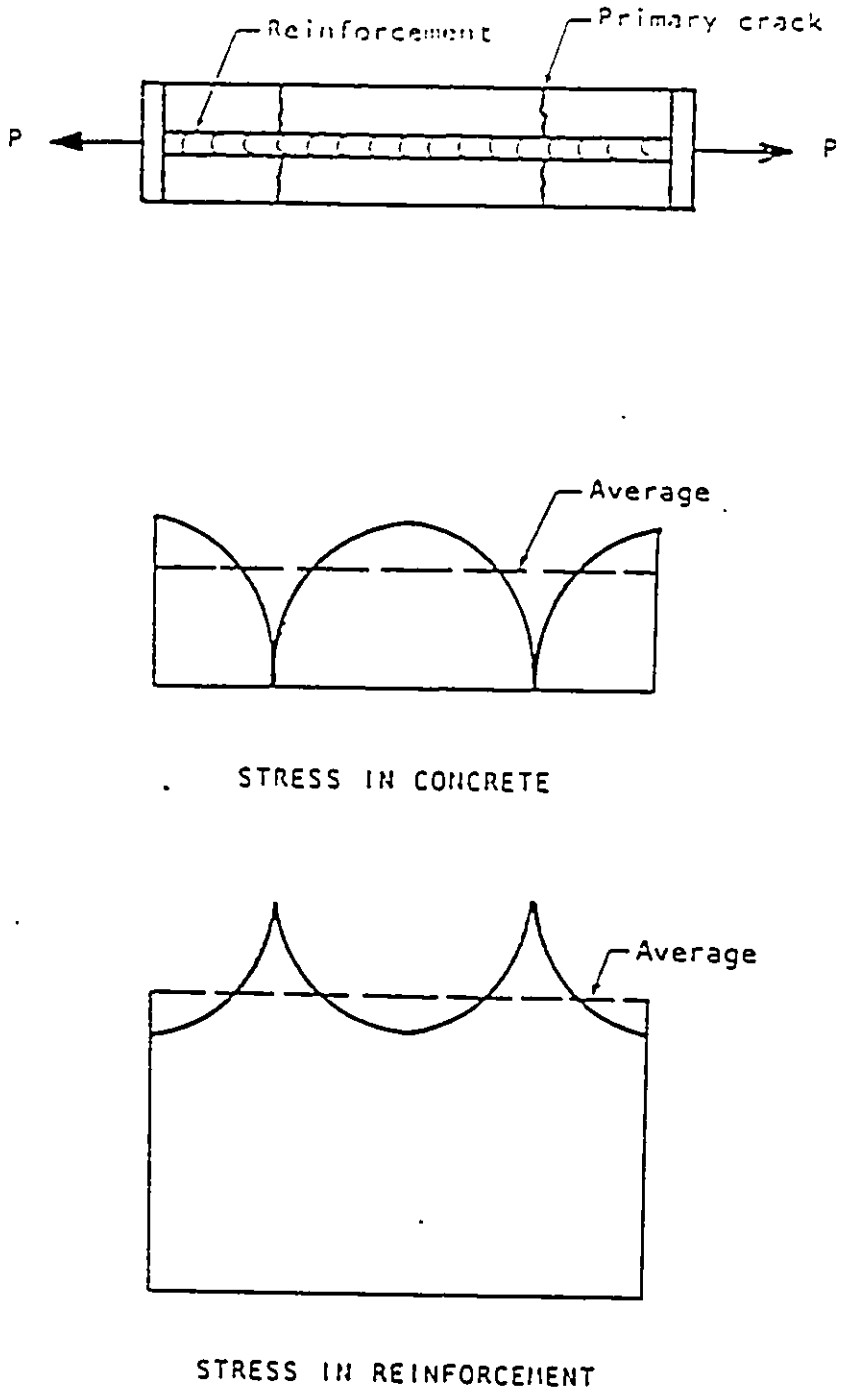

Figure 4.6: Stress Distribution in a Cracked Reinforced Concrete Element

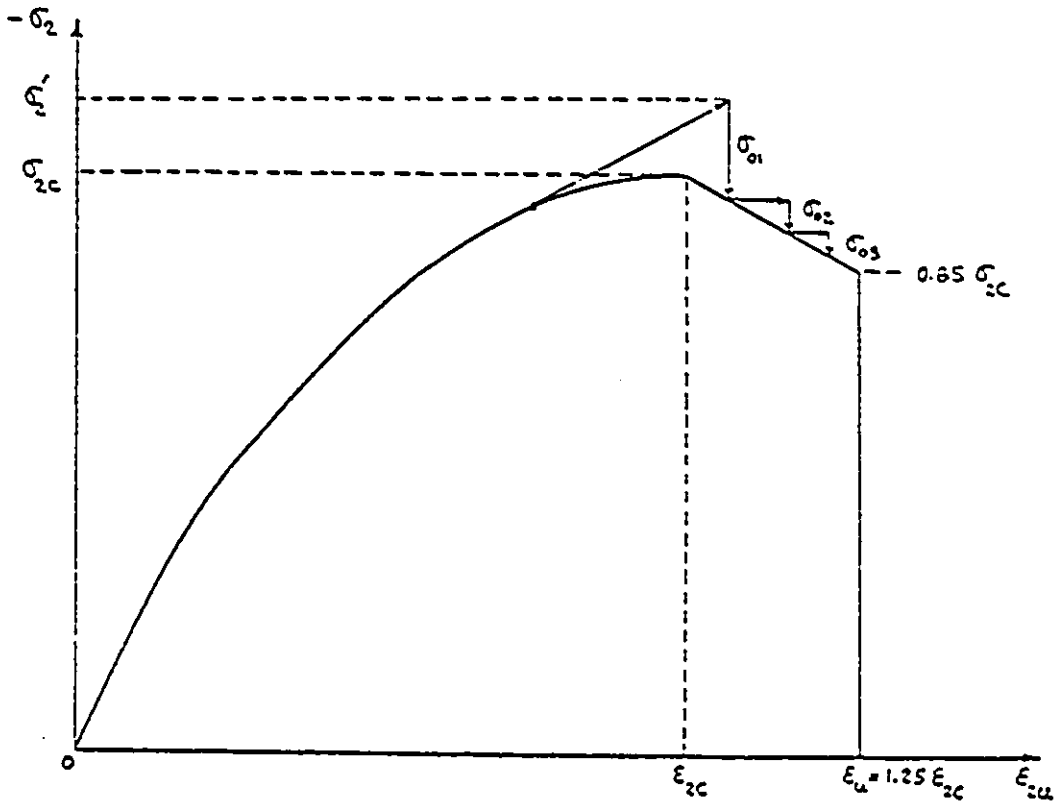

Figure 4.7: Unbalanced Stresses Due to Strain Softening

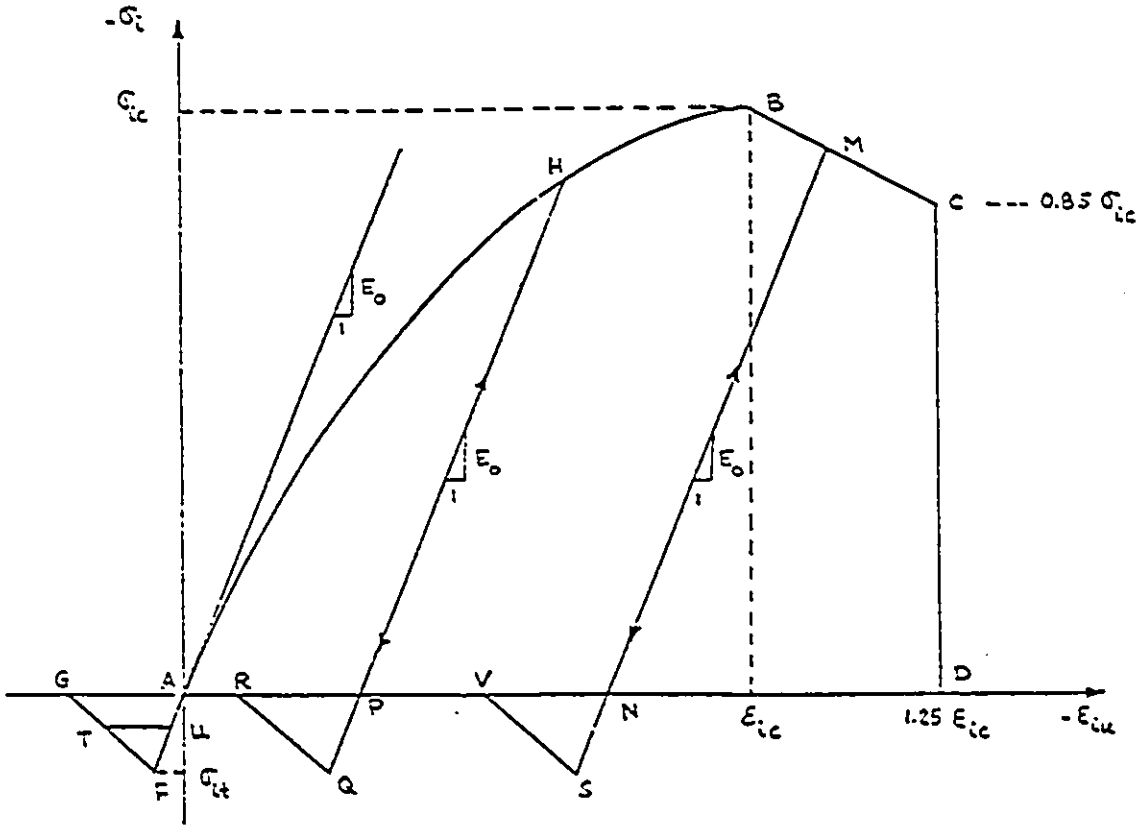

Figure 4.8: Load Reversal Model for Concrete

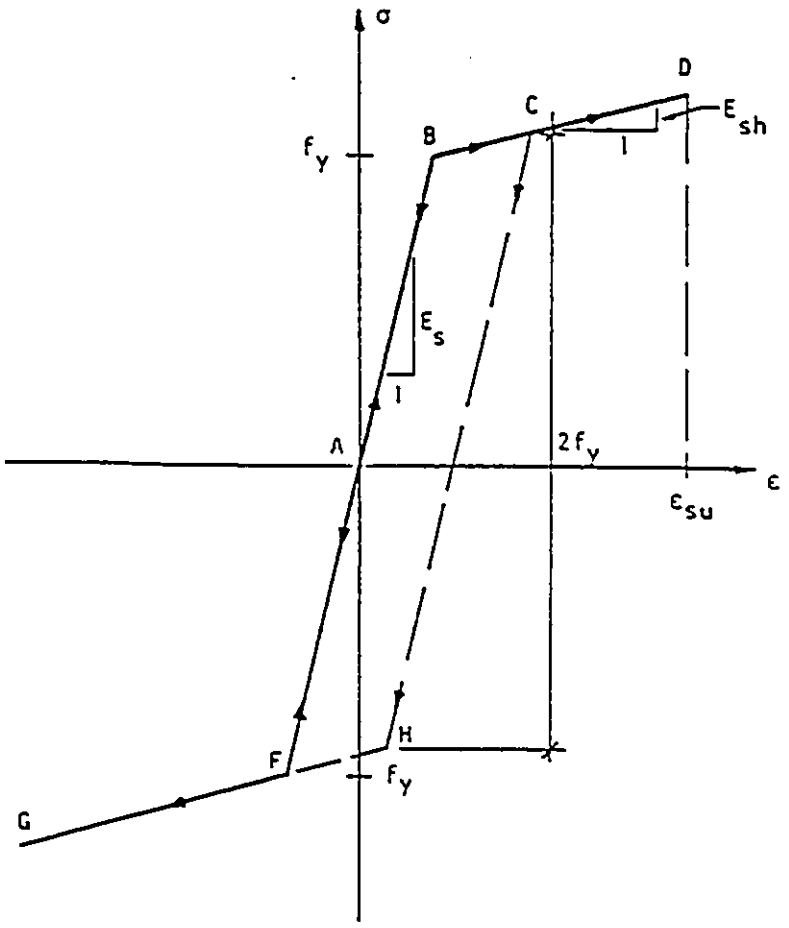

Figure 4.9: Reinforcing Steel Model for Present Study

Chapter 5

TIME DEPENDENT CONCRETE PROPERTIES

5.1 General Remarks

A significant complication in the analysis of the time-dependent effects of concrete is that the relationship between total stress and total strain is not a linear function of time. In predicting the time-dependent behaviour of concrete it is assumed that the total strain in concrete is the sum of the elastic, creep, and shrinkage strains [36].

$$\varepsilon_T(t) = \varepsilon_e(t) + \varepsilon_s(t) + \varepsilon_c(t) \tag{5.1}$$

where $\varepsilon_T(t)$ = total strain in concrete,

$\varepsilon_e(t)$ = elastic strain,

$\varepsilon_s(t)$ = shrinkage strain, and $\varepsilon_c(t)$ = creep strain.

In this chapter, the time-dependent properties of shrinkage, and creep, and the

constitutive relations used to model them are discussed.

5.2 Shrinkage Strain

Shrinkage is a concrete deformation phenomena which is defined as the time dependent volume change occurring independent of applied loads.

5.2.1 Mechanism and Influencing Factors

Shrinkage is attributed to two main factors:

1. loss of water on drying from concrete to the surrounding unsaturated enviroment (*drying shrinkage*)
2. volumetric change due to carbonation (*carbonation shrinkage*).

With *drying shrinkage*, free water held in the capillaries is first lost causing practically no shrinkage. Upon further drying, some absorbed water is lost thereby initiating shrinkage. The process of moisture diffusion from the interior of concrete to the surface is slow and complex. The surface dries more quickly than the interior causing non-uniform shrinkage distribution through the volume. For slabs and panels, however, the assumption of uniform shrinkage distribution is generally considered an adequate approximation.

Carbonation shrinkage is caused by a reaction between calcium hydroxide, a hydrated cement mineral, and atmospheric carbon dioxide in the presence of water.

The major factors influencing the shrinkage of concrete are aggregate content, water-cement ratio, member size and ambient relative humidity. Shrinkage increases with an increase in water content, while it decreases with any increase in relative humidity, aggregate content and specimen size.

5.2.2 ACI Shrinkage Model [3]

ACI Committee 209 recommends the use of the following equation for the computation of shrinkage strain:

$$\varepsilon_{sh}(t) = K_s K_h K_H \frac{(t-t_o)^e}{f+(t-t_o)^e} \varepsilon_{shu} \tag{5.2}$$

where,

$\varepsilon_{sh}(t)$ = shrinkage strain at time t,

$\varepsilon_{shu}(t)$ = ultimate shrinkage strain,

t_o = time from which shrinkage starts (i.e drying commenced),

t = time at observation,

f, e = constants determined from experiments,

K_s = slump correction factor,

K_h = member size correction factor,

K_H = correction factor for relative humidity.

Normal ranges of constants e, f and ε_{shu} using normal or light weight concrete are:

$$e = 0.9 - 1.10$$

$$f = 20 - 130$$

$$\varepsilon_{shu} = 415 \times 10^{-6} - 1070 \times 10^{-6}$$

Standard relations for the prediction of shrinkage strains using appropriate constants are:

- For concrete moist cured for 7 days

$$\varepsilon_{sh}(t) = K_s K_h K_H \frac{(t-7)}{35+(t-7)} \times 800 \times 10^{-6} \tag{5.3}$$

- For concrete steam cured for 3 days

$$\varepsilon_{sh}(t) = K_s K_h K_H \frac{(t-3)}{55+(t-3)} \times 730 \times 10^{-6} \tag{5.4}$$

The correction factors which take into account variations in slump, relative humidity, cement content and specimen size are

$$K_s = 0.89 + 0.041s$$

$$K_H = 1.4 - 0.01H, \quad for \ 40 \leq H \leq 80$$

$$K_H = 3.0 - 0.03H, \quad for \ 80 \leq H \leq 100$$

where, s is slump in inches, and H, the ambient humidity.

5.2.3 CEB-FIP Shrinkage Model [13]

According to CEB-FIP 1990, shrinkage strains developed for a particular concrete specimen should be calculated by

$$\epsilon_{cs} = \epsilon_{cso}\beta_s(t - t_s) \tag{5.5}$$

where,

ϵ_{cso} = notional shrinkage coefficient,

β_s = coefficient describing the development of shrinkage with time,

t = age of concrete in days,

t_s = age of concrete at the beginning of shrinkage.

The notional shrinkage coefficient is expressed as:

$$\epsilon_{cso} = \epsilon_s(f_{cm})\beta_{RH} \tag{5.6}$$

with,

$$\epsilon_s(f_{cm}) = [250 + \epsilon_{sc}(75 - f_{cm})] \times 10^{-6} \tag{5.7}$$

where,

f_{cm} = 28-day compressive strength of concrete (N/mm^2),

β_{sc} = coefficient dependent on concrete type and is equal to:

- *3* for normal or slowly hardening cement,
- *5* for rapid hardening cement,
- *9* for rapid hardening high strength cement, and

For $40\% < RH < 99\%$

$$\beta_{RH} = -1.55\beta_{SRH}$$

where,

$$\beta_{SRH} = 1 - (\frac{RH}{100})^3$$

and for $RH \geq 99\%$

$$\beta_{RH} = 0.25$$

RH is relative humidity in %.

The development of shrinkage with time is given by the following equation.

$$\beta_s\{t - t_s\} = (\frac{t - t_s}{0.035h_o^2 + t - t_s})^{0.5} \tag{5.8}$$

where, h_o = nominal size of the member in mm. and is equal to

$$h_o = \frac{2A_c}{\mu}$$

A_c being cross-sectional area, and

μ - perimeter of the member in contact with the atmosphere.

5.2.4 Gardner-Zhao Shrinkage Model [24]

ACI-209 and CEB use a Ross type equation to relate shrinkage at a given time to a hypothetical ultimate shrinkage. However, experimental evidence does not support this conclusion. Gardner and Zhao on the basis of experimental data review, proposed that the shrinkage strain, $\Psi(t)$ should be calculated using the following equation:

$$\Psi(t) = \epsilon_{shu} \times \beta_h \times \beta_t \tag{5.9}$$

The variables in Eq. (5.9) are defined as follows:

$$\epsilon_{shu} = 900 * K * \left(\frac{f'_{cm28}}{f'_{cmtc}}\right)^{0.5} * \left(\frac{25}{f'_{cm28}}\right)^{0.5} * 10^{-6} \tag{5.10}$$

$$\beta(t) = \left[\frac{7.27 + In(t - t_c)}{17.18}\right] * \left(\frac{t - t_c}{t - t_c} + 0.0125 * (V/S)^2\right) \tag{5.11}$$

$$\begin{aligned} \beta_h &= 1 - h^4, \quad for \ h < 1.0 \\ &= -0.20, \quad for \ h = 1.0 \end{aligned} \tag{5.12}$$

where, $\Psi(t)$ = shrinkage strain,

f'_{cm28} = concrete mean compressive strength at 28 days,

f'_{cmtc} = concrete mean compressive strength when drying commenced,
V/S = volume to surface ratio (mm), and K = 1.0 for Type I Cement concrete. This model gives a better characterization of shrinkage deformation than the ACI model and is used in this study. According to Gardner and Zhao [24], the ACI shrinkage provision shows a systematic trend in overestimating shrinkage at early ages but underestimates it at later ages.

5.3 Creep Strain

Creep is a stress originated phenomena which is defined as the time dependent increase in strain under sustained load. There are two types of creep strains which are lumped together to give what is generally referred to as total creep. These are, *basic creep* and *drying creep*.

Basic creep is the time-dependent deformation that occurs when a loaded concrete specimen is in hygral equilibrium with its environment. Drying creep (sometimes called the Pickett effect) is the additional creep in excess of basic creep when the same concrete undergoes moisture diffusion under sustained loading. In practice, however, these distinctions are not always made. The total creep strain is generally used in the creep compliance function[1].

Generally, creep has little effect on the strength of a structure, but it causes stress redistribution in reinforced concrete members under service loads and leads to an increase in service load deflections, thereby possibly creating serviceability problems. Stress redistribution is sometimes beneficial as it tends to reduce the

[1] Discussed in section 5.4.5

maximum stresses produced. For example, stresses in concrete caused by differential settlement of structures are reduced by creep.

Creep has both recoverable and irrecoverable components. Figure 5.1 shows concrete deformation as a result of creep when concrete is subjected to a constant axial compressive stress. The instantaneous elastic strain on the application of stress is represented by ε_{inst}. If the stress is maintained at this level, creep proceeds at a decreasing rate with time. At any given time, the increase in strain above the initial elastic strain is termed the creep strain, ε_{cp}. If the sustained load is removed, an elastic strain is immediately recovered. The recovered elastic strain is slightly less than the initial elastic strain because the elastic modulus increases with time. After the instantaneous recovery, there is a gradual decrease in strain which is termed creep recovery. The exact mechanism of creep is not understood. Extensive research effort has been directed towards finding logical explanations to the observed physical phenomena and to provide a mathematical basis for the existing theories.

5.3.1 Mechanism and Influencing Factors

Several theories have been proposed in recent years to explain creep behaviour, but no single theory has been able to account for all observed trends. Some of the widely acknowledged theories are:

1. *mechanical deformation theory* - attributes concrete creep to internal stresses set up as a result of the change in the form of the capillary structure of the cement paste due to the application of load.

2. *viscous flow theory* - postulates that creep is due to the sliding of the colloidal sheets in cement gel between the layers of the absorbed water.

3. *seepage theory* - attributes creep to the expulsion and decomposition of the inter-layer water with the cement gel.

4. *plastic theory* - suggests that creep may be the result of crystalline flow (i.e the slippage along planes within the crystal lattice).

The magnitude of creep and its rate of development are influenced by a large number of factors, including: the compressive strength of the specimen at loading, age of loading, type of aggregate, ambient relative humidity, temperature, member size, concrete composition, duration of sustained loading, and stress intensity. Experimental test data often required for creep deformation analyses are not always available. However, several empirical equations for predicting creep deformations exist. Some of these expressions are presented below but details of the assumptions and methods used in their derivation are not discussed.

5.3.2 ACI Creep Expression [3]

Based on studies by Branson and Christianson [11], ACI Committee 209 proposed the following expression for predicting creep deformation under constant stress:

$$C_t = K_s K_H K_h K_t \frac{(t-\tau)^{0.60}}{10 + (t-\tau)^{0.60}} C_u \tag{5.13}$$

where,

K_s = *slump correction factor* $= 0.81 + 0.07s$

K_H = *humidity correction factor*$= 1.27 - 0.0067H$

K_h = *minimum thickness correction factor* $= 1.0 - 0.0167(sz - 6.0)$

K_t = *correction factor for age at loading* = $1.25\tau^{-0.118}$

s = slump in inches,

H = humidity in %,

sz = minimum size of member,

τ = age at loading,

t = observation time in days, and

C_u = *ultimate creep coefficient.*

The ultimate creep coefficient is the ratio of creep strain at infinite time after loading to the initial creep strain at time of loading, and is numerically equal to 2.35.

Standard conditions for which all correction factors are equal to 1.0 are

- slump = 2.7 inches
- ambient relative humidity = 40% or less
- minimum member size = 6 inches or less
- age at loading = 7 days for moist cured concrete

5.3.3 CEB-FIP Creep Expression [13]

The CEB-FIP Model Code 1990, recommends that the creep strain coefficient should be calculated using the expression:

$$\phi(t, t_o) = \phi_o \beta_c(t - t_o) \tag{5.14}$$

where,

ϕ_o = nominal creep coefficient,

β_c = coefficient describing the development of creep with time after loading.
The nominal creep coefficient is calculated as:

$$\phi_o = \phi_{RH}\beta(f_{cm})\beta(t_o) \tag{5.15}$$

with.

$$\phi_{RH} = 1 + \frac{1 - \frac{RH}{100}}{0.0Sh_o^{\frac{1}{3}}} \tag{5.16}$$

$$\beta(f_{cm}) = \frac{21.S}{3 + \sqrt{f_{cm}}} \tag{5.17}$$

$$\beta(t_o) = \frac{1}{0.1 + t_o^{0.18}} \tag{5.1S}$$

where, RH is the relative humidity, f_{cm} - the mean concrete strength and h_o, effective thickness of specimen.
The creep time function is given by:

$$\beta(t - t_o) = (\frac{t - t_o}{\beta_H + t - t_o})^{0.3} \tag{5.19}$$

with,

$$\beta_H = 1.5[1 + 0.00012(\frac{RH}{50})^{18}]h_o + 250 \ \leq 1500mm \tag{5.20}$$

5.3.4 Gardner-Zhao Creep Model [24]

The age at which concrete is loaded is known to influence the magnitude of the creep strains. Based on the analysis of the experimental results of L'Hermite et al, and Bryant and Vadhanavikkit [13], Gardner and Zhao [24] developed an expression in the form of Eq. (5.21), for predicting the creep strain coefficient.

This is adopted for the present study as it accounts for the effects of early-age loading, relative humidity and member size on creep.

$$C_t = \left[\frac{7.27 + Ln(t - t_o)}{17.18}\right] * \left[1.57 + 2.98 * \left(\frac{f'_{cm28}}{f'_{cmto}}\right) * \left(\frac{25}{f'_{cm28}}\right)^{0.5} * \left(1 - h^2\right) * \left(\frac{t - t_o}{t - t_o + 0.1 * (V/S)^2}\right)\right] \quad (5.21)$$

where,

C_t = creep coefficient,

f_{cm28} = 28-day mean concrete strength in (MPa),

f_{cmto} = mean concrete strength at the age of loading in (MPa),

t = age of concrete in days,

t_o = age of concrete at loading,

h = humidity expressed as a decimal, and

$\frac{V}{S}$ = volume/surface ratio (mm).

The data used by Gardner and Zhao to calculate the creep strain coefficient was the total load induced strains less the calculated elastic strain. It should be noted that, unlike the ACI and CEB creep equations, the Gardner-Zhao expression does not assume an ultimate creep strain.

Creep strains calculated using Eq. (5.21), and the creep equations of ACI 209-82, and CEB MC 1990 were compared with measured creep strains at an applied stress to developed strength ratio of 0.30. Both the Gardner-Zhao and the CEB Model Code expressions showed reasonable agreement with the measured values. The ACI 209-82 equation underestimated creep [24].

5.4 Mathematical Modelling of Creep Strains

The formulation of an analytical model for creep should account for any inherent accuracy limitations. For constant hygro-thermal conditions and concrete stress-strength ratios less than 45%, creep deformation is reasonably well predicted by the linear viscoelastic theory. There are two basic formulation procedures for this theory, *differential* and *integral*.

5.4.1 Differential Formulation

The differential formulation of the linear viscoelastic theory is based on a general differential equation:

$$[\frac{d^n}{dt^n} + p_1(t)\frac{d^{n-1}}{dt^{n-1}} + ... + p_n(t)]\varepsilon = [q_n(t)\frac{d^n}{dt^n} + ... + q_n(t)]\sigma \qquad (5.22)$$

where $p_n(t)$ and $q_n(t)$ are time variable properties of concrete. Difficulties associated with the determination of coefficients and its application to numerical problems have restricted the use of this method.

5.4.2 Integral Formulation

The integral formulation of the linear viscoelastic theory developed by Voleterra [55] has received wide acceptability and is used in this study. For a linear viscoelastic ageing material under uniaxial stress, the constitutive relationship is expressed as an integral in the form

$$\varepsilon_c(t) = \int_{-\alpha}^{t} \overline{C}(\tau, t-\tau)\frac{\partial\sigma(\tau)}{\partial\tau}d\tau \qquad (5.23)$$

where, $\varepsilon_c(t)$ = creep strain,

$\overline{C}(\tau, t-\tau)$ = specific compliance function, and

τ = time of initial application of load (days), and t = age of concrete.

The solution to Eq. (5.23) depends on the form of the Kernel function, $\overline{C}(\tau, t-\tau)$, generally referred to as the specific compliance function and mathematically expressed as:

$$\overline{C}(\tau, t-\tau) = \frac{1}{E(\tau)} + C(\tau, t-\tau) \tag{5.24}$$

where,

$\frac{1}{E(\tau)}$ = instantaneous compliance function, and

$C(\tau, t-\tau)$ = creep compliance function.

The creep strain can therefore be written as:

$$\varepsilon_c(t) = \int_o^t C(\tau, t-\tau)\frac{\partial\sigma(\tau)}{\partial\tau}d\tau \tag{5.25}$$

An efficient solution to Eq.(5.25) will depend on the choice of a suitable creep compliance function. The criteria for the selection of such a function should be based on the following:

1. the function should accurately fit the experimental compliance data, taking into account such factors as: age at loading, size of member, curing regime, relative humidity, and temperature variations,
2. unknown coefficients of the function should be easy to evaluate, and
3. numerical evaluation of the function should require minimum computational effort.

A number of different compliance functions have been proposed by various researchers. A few are discussed below but detailed documentation and analysis of

compliance functions can be found in Ref. [6]. A compliance function in the form

$$\overline{C}(\tau, t-\tau) = (a + \frac{b}{\tau}) \sum_{k=0}^{m} \beta_k e^{-\vartheta_k (t-\tau)} \tag{5.26}$$

was suggested by Arutyunyan, where

a, b, β_k, ϑ_k, and m are constants to be determined from experiments

$\frac{1}{E(\tau)}$ = instantaneous compliance function, and

$C(\tau, t-\tau)$ = creep compliance function.

A comparatively advanced compliance function which takes into account age, and temperature effects was proposed by Mukaddam and Bresler [41].

$$\overline{C}(\tau, t-\tau, T) = \sum_{i=1}^{m} a_i e^{\lambda_i (t-\tau)\phi(T)\overline{\phi}(\tau)} \tag{5.27}$$

where, a_i, and λ_i are constants,

$\phi(T)$ = temperature shift function,

$\overline{\phi}(\tau)$ = age shift function,

T = temperature at loading, and

τ = age of loading.

5.4.3 Creep Under Biaxial Stress

Concrete under sustained uniaxial stress induces lateral strains in the directions orthogonal to the applied stress direction. The ratio of the laterally induced creep strain to the normal creep strain is called creep Poisson's ratio and ranges between 0.16 and 0.25. If concrete is subjected to sustained biaxial stress, creep strains would be produced in the two orthogonal stress directions. The magnitude of the strain in a particular direction would be the sum of the strain in that direction due to the applied stress in that direction, and the laterally induced strain resulting from the applied stress in the other orthogonal direction.

Gopalakrishnan et al. [28] indicated that, the creep Poisson's ratio under multi-axial stress depends on the relative magnitude of the applied stress and is slightly less than the uniaxial value. For simplicity and considering the inherent uncertainties involved in experimental creep strain measurements, the creep Poisson's ratio for the biaxial stress state is assumed to be equal to the elastic Poisson's ratio. Based on the above assumption, the incremental stress-strain relationship for creep can be written as:

$$\begin{Bmatrix} \Delta\varepsilon_x^c(t) \\ \Delta\varepsilon_y^c(t) \\ \Delta\gamma_{xy}^c(t) \end{Bmatrix} = \begin{bmatrix} 1 & -\nu_c & 0 \\ -\nu_c & 1 & 0 \\ 0 & 0 & 2(1+\nu_c) \end{bmatrix} C(\tau, t-\tau, T) \begin{Bmatrix} \Delta\sigma_x(t) \\ \Delta\sigma_y(t) \\ \Delta\tau_{xy}(t) \end{Bmatrix} \tag{5.28}$$

The total creep strain vector from the initial age of loading t_i to the final observation time t_n will be:

$$\begin{Bmatrix} \Delta\varepsilon_x^c(t_n) \\ \Delta\varepsilon_y^c(t_n) \\ \Delta\gamma_{xy}^c(t_n) \end{Bmatrix} = D_o^{-1} \sum_{i=1}^{n} C(t_i, t_n - t_i, T_i) \begin{Bmatrix} \Delta\sigma_x(t_i) \\ \Delta\sigma_y(t_i) \\ \Delta\tau_{xy}(t_i) \end{Bmatrix} \tag{5.29}$$

where,

$$D_o^{-1} = \begin{bmatrix} 1 & -\nu_c & 0 \\ -\nu_c & 1 & 0 \\ 0 & 0 & 2(1+\nu_c) \end{bmatrix} \tag{5.30}$$

There are experimental indications that the creep stress-strain relationship is non-linear beyond $0.35f_c'$. To account for this behaviour, Becker and Bresler [7] proposed the use of an effective stress concept based on the following empirical equations:

$$\sigma_{eff} = \sigma \tag{5.31}$$

for,

$$\frac{\sigma}{f_c'} \leq 0.35$$

and,

$$\sigma_{eff} = 2.33\sigma - 0.465 f'_c \tag{5.32}$$

for,

$$0.35 \leq \frac{\sigma}{f'_c} \leq 1.0$$

5.4.4 Formulation of a Creep Model

The creep model used herein is based on an incremental step-by-step solution procedure in the time domain. The following are the assumptions made in the formulation process:

Assumptions

1. total strain in any direction is the algebraic sum of several strains caused by different phenomena
2. strains caused by different effects are independent and additive
3. the time-dependent structural response is the same in tension and compression for an uncracked concrete

Studies by Becker and Bresler [12], Zienkiewicz and Watson [58] indicate that certain types of mathematical approximations for the creep compliance function, $C(\tau, t-\tau, T)$, while representing the experimental data accurately, overcome the necessity of storing all the stress increments of the previous time step. One such function in the form of Dirichlets series was successfully used by Kabir [35] and is

adopted for this analysis. The function is in the form:

$$C(\tau, t-\tau, T) = \sum_{i=1}^{m} a_i(\tau)[1 - \exp^{-\lambda_i \phi(T)(t-\tau)}] \tag{5.33}$$

where,

$a_i(t)$ = scale factor dependent on age at loading τ,

λ_i = exponential constants determining the shape of the logarithmically decaying creep curve, and

$\phi(T)$ = temperature shift function.

The creep strain increment for the time interval $\Delta t_n = t_{n+1} - t_n$ is given by

$$\Delta \varepsilon_n^c = \varepsilon_{n+1}^c - \varepsilon_n^c \tag{5.34}$$

or,

$$\Delta D_o \varepsilon_n^c = D_o \varepsilon_{n+1}^c - D_o \varepsilon_n^c \tag{5.35}$$

Substituting the values of $C(\tau, t-\tau, T)$ from Eq. (5.33) into (5.29) and simplifying gives

$$\Delta D_o \varepsilon_n^c = \sum_{i=1}^{m} A_{i_n}[1 - e^{-\lambda_i \phi_n \Delta t_n}] \tag{5.36}$$

where,

$$A_{i_n} = A_{i_{n-1}} e^{-\lambda_i \phi_{n-1} \Delta t_{n-1}} + \Delta \sigma_n a_{i_n} \tag{5.37}$$

and,

$$A_{i_1} = \Delta \sigma_1 a_{i_1} \tag{5.38}$$

Thus, Eqs. (5.36), (5.37), and (5.38) are the necessary expressions for calculating the creep strain increment for any time step n, defined by the time interval $\Delta t_n = t_{n+1} - t_n$. With this formulation, knowledge of the previous stress histories for strain increment calculations is not required. The stress history is implicitly incorporated in the vector A_{i_n}, called the hidden state variables. The value of A_{i_n} is calculated

as a progressive sum by the use of Eq.(5.38) knowing the stress change $\Delta\sigma_n$ at the current time, t_n.

This approach is time efficient and considerably reduces storage capacity thereby making time-dependent analysis of reasonably large structural problems possible.

5.4.5 Creep Compliance Coefficients

The assumption of a suitable compliance function is the most important step in the formulation of a creep strain computation algorithm. Evaluation of the creep compliance coefficients is based on the assumed function:

$$C(\tau, t-\tau, T) = \sum_{i=1}^{m} a_i(\tau)[1 - \exp^{-\lambda_i(t-\tau)}] \tag{5.39}$$

The input data required for the compliance function are values of total creep strain, $C(\tau, t, T)$ for a set of loading ages, τ and the observation times t. These may be obtained by performing an experimental creep data analysis, or adopting an empirical creep equation. In order to make the best fit approximation of the creep strain data with the assumed compliance function, the following procedure is followed:

1. Choose the parameters m and λ_i, for $i = 1, m$ on a trial basis.

2. Select a particular age at loading, τ_o and concrete temperature T_o.

3. Various times $t_j, j = 1, 2, ..., n$ are chosen such that $t_j \geq \tau_o$, where t_j is the time in days when concrete was cast.

4. Calculate the values of $C(\tau_o, t_j - \tau_o, T_o)$ at the points $j = 1, 2, ..., n$.

5. Set up the following simultaneous equations

$$\begin{bmatrix} 1-e^{\lambda_1(t_1-\tau_o)} & 1-e^{\lambda_2(t_1-\tau_o)} & \ldots\ldots & 1-e^{\lambda_m(t_1-\tau_o)} \\ & & & \\ & & & \\ & & & \\ 1-e^{\lambda_1(t_n-\tau_o)} & 1-e^{\lambda_2(t_n-\tau_o)} & \ldots\ldots & 1-e^{\lambda_m(t_n-\tau_o)} \end{bmatrix} \begin{Bmatrix} a_1(\tau_o) \\ a_2(\tau_o) \\ \cdot \\ \cdot \\ \cdot \\ a_m(\tau_o) \end{Bmatrix} = \begin{Bmatrix} C(\tau_o, t_1-\tau_o, T_o) \\ C(\tau_o, t_2-\tau_o, T_o) \\ \cdot \\ \cdot \\ \cdot \\ C(\tau_o, t_n-\tau_o, T_o) \end{Bmatrix} \tag{5.40}$$

or,

$$\underline{A}_{n\times m}\underline{a}_{m\times 1} = \underline{B}_{n\times 1 \; n>m} \tag{5.41}$$

The least square method is applied to solve the over-determinate systems of Eq. (5.41) for values of $\underline{a}$

$$\underline{A}^T_{m\times n}\,\underline{A}_{n\times m}\,\underline{a}_{m\times 1} = \underline{A}^T_{m\times n}\underline{B}_{n\times 1}$$

$$(\underline{A}^T\underline{A})_{m\times m}\,\underline{a}_{m\times 1} = (\underline{A}^T\underline{B})_{m\times 1}$$

$$\underline{a}_{m\times 1} = (\underline{A}^T\underline{A})^{-1}_{m\times m}\,(\underline{A}^T\underline{B})_{m\times 1}$$

6. Choose a different m and λ_i and repeat steps 2 to 5.

7. Optimize the m's and λ's according to the following criteria:

- minimization of square errors,
- all computed $a_i(\tau)$ values should satisfy Eq.(5.41) for the period of analysis with a deviation of 5% or less.

8. Choose a different age at loading, τ_1 and repeat steps 3 to 5 to determine a new set of $a(\tau_1)$. The process is continued to give sets of $a_i(\tau)$ for different ages. Values for in-between ages are determined by linear interpolation.

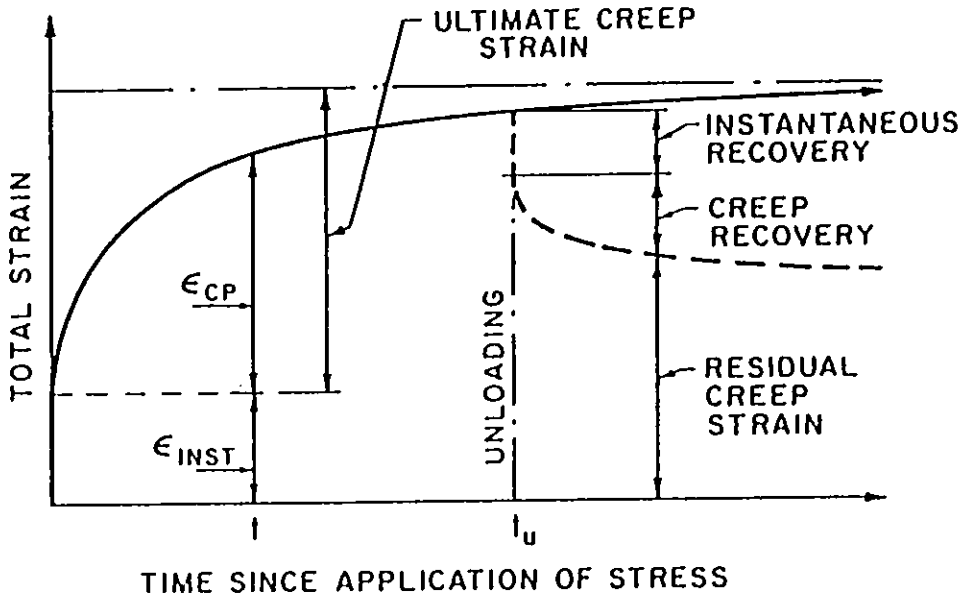

Figure 5.1: A Typical Creep Curve for Concrete in Uniaxial Compression

Chapter 6

PRESENTATION AND DISCUSSION OF RESULTS

6.1 Verification of TIDARCS

Prior to producing results it was necessary to verify the adequacy of the computer program used. This was done by a comparative assessment of computed deflections using TIDARCS and experimentally measured results reported in literature.

Three experimental slabs and a reinforced concrete beam were analyzed;

- to check the validity of the material models and to test their ability to reflect reality with reasonable accuracy,
- to check how well the finite element used in the study predicts experimental behaviour,

- to test the creep and shrinkage models used in the study, and
- to demonstrate the applicability of the analytical procedure to a variety of structures subjected to different load histories.

The first example considered was a rectangular square slab tested by McNeice [33]. The slab was analyzed for an instantaneous and a step-like load history. The second example involved a flat plate model tested by Fu [19] at the University of Ottawa. The slab was analyzed for both instantaneous and sustained load deflections. In the third example, a reinforced concrete flat plate model tested by Shao [49] was analyzed for instantaneous deflections. The fourth example involved a reinforced concrete beam tested by Branson [10].

6.1.1 McNeice Slab [33]

The McNeice slab was 0.91 m square, simply supported at the four corners, and isotropically reinforced. It had a thickness of 44.45 mm and was subjected to a concentrated load at mid-span. The finite element mesh and the material properties used are shown in Fig. 6.1. Due to the symmetrical nature of the slab, only a quarter portion was modelled for the analysis. The concentrated load was applied in four equal load increments of 4.45 kN. A displacement tolerance of 0.025 mm was set for convergence and the stiffness matrix was reformed after each iteration.

The two tension stiffness models discussed under section 4.2.4 were separately introduced in the analysis. This allowed the models to be compared as to which best represented the experimental behaviour. The load deflection curve of the slab is presented in Fig. 6.2 together with the experimental results of McNeice. The model with increased steel modulus showed a better agreement with the

The model with increased steel modulus showed a better agreement with the experimental curve.

6.1.2 Fu's Flat Plate Model 3 [19]

An analytical investigation was carried into one of three reinforced concrete flat plate models constructed and tested by Fu [19]. The 63.5 mm thick slab had a square profile with a clear span of 1.96 m and was supported by four 203 mm square columns. The slab was designed in accordance with the empirical method of the ACI code.

The aim was to investigate experimentally the effects of early-age construction loads, and the time-dependent effects of creep and shrinkage on slab deflection. The slab was cured for 10 days before the formwork was stripped allowing the slab to deflect under its own weight. A superimposed dead load was applied to the slab at 28 days giving it a total sustained load of 1.5 times the design dead load.

The material properties of the slab were as follows:

- 28-day compressive strength = 34.1 MPa
- Steel yield strength = 417 MPa
- Modulus of elasticity of steel = 200 GPa
- Diameter of reinforcing steel = 5 mm

The response of the test structure to load was evaluated through short and longterm deflection measurements as summarized in Table 6.1. The two sets of results show that the experimental and analytical deflections compared favourably.

6.1.3 Shao's Flat Plate [49]

An experimental flat plate model tested by Shao [49] at the University of Ottawa was analyzed for instantaneous deflections. The 140 mm thick slab was designed in accordance with the provisions of the ACI 318-89 Building Code [1]. The slab spanned two bays in both directions of the x - y coordinate system with a center to center span of 2.74 m.

The slab had a 28-day compressive strength of 19.5 MPa and an average elastic modulus of 20.9 GPa. Deformed #10 bars with yield strength of 400 MPa were used to reinforce the slab. The amount of reinforcement was calculated and distributed in such a way that the slab had enough strength to ensure punching shear failure. A uniformly distributed load of 12.4 kN/m^2 not including the self-weight of the slab was applied to the structure.

Immediate deflections, measured at the center points of the slab panels were compared with calculated values from TIDARCS. An average instantaneous deflection of 2.04 mm was experimentally observed for values ranging from 1.66 mm to 2.39 mm while a calculated average of 1.70 mm was realized using TIDARCS.

6.1.4 Branson's Continuous Beam LB-3

Branson reported the results of a study conducted for the Alabama Highway Department into the time-dependent deflections of a series of reinforced concrete beams. The purpose of the study was to consolidate information on deflections and to study the complex deformational behaviour of reinforced concrete beams as influenced by the interrelated effects of cracking, shrinkage, and creep.

The experiment measured the instantaneous and time-dependent deflections for a continuous reinforced concrete beam. The 217 mm thick beam had two spans, each 2.74 m long. It had a 28-day compressive strength of 35.4 MPa, modulus of elasticity of 30338 MPa, and a steel yield strength of 358.5 MPa. The beam was loaded 28 days after casting with the beam dead load and a uniformly distributed superimposed load. The ratio of the superimposed load to the slab dead load was 5.50. The specimen had an average ambient relative humidity of 59% and a temperature of 29°*C*.

A comprehensive schedule of deflection and strain measurements were maintained throughout the test period. An observed instantaneous deflection of 1.42 mm and a longterm (80 days) deflection of 2.95 mm were reported. The analytical investigation using *TIDARCS* produced an instantaneous deflection of 1.27 mm and 80 days longterm deflection was 2.77 mm.

6.2 Computer Simulation

6.2.1 General Remarks

In general, deflection serviceability requirements are satisfied by ensuring that the thickness of the slab is such that it satisfies a specified span/thicknes ratio. However, there is no guarantee that the ACI-CSA requirements are appropriate for modern construction methods which impose high early age construction loads on the slabs. The availability of complicated sophisticated finite element analysis programs do not meet the needs of designers.

The objective of this thesis is to derive an easy to use method to determine the

necessary minimum thickness for flat slabs, constructed with various construction cycles, to satisfy the appropriate deflection limit. The approach used was to choose a construction load, in terms of slab self weight, to be applied at a given age, and calculate the long term deflections for an assumed slab thickness.

The serviceability limit chosen was an exterior panel interior column line deflection of span/240. If the calculated column line deflection did not equal span/240 the slab thickness was changed and the calculations repeated until the calculated deflection matched the target deflection.

6.2.2 Loading History

In the shore-reshore construction process, the greater the number of forms used, the greater the construction loads applied to the slabs [21]. The use of one level of forms and multiple levels of reshores is considered the most efficient. To determine the construction loads imposed on the formwork and on the individual slabs, one level of forms and three levels of reshores (1+3) were used. Five different construction cycles were considered for the simulation process. Slabs were loaded 3, 4, 7, 14, and 28 days after casting.

The distribution of loads between the various slabs in the system was determined using the procedure suggested by Grundy and Kabaila [30], and later extended by Agarwal and Gardner [5]. A significant assumption made in the application of the Grundy-Kabaila method is that all slabs have equal stiffnesses.

Using Agarwal and Gardner the construction load is 1.25D, assuming the formwork weighs 0.1D and no construction live load, the total unfactored construction load is 1.35D.

Assuming the slab is put to service at 28 days, it is subjected to its own self weight plus some fraction of the live load. For a slab designed for a live-load to dead-load ratio of 0.5 the sustained load was chosen to be self weight plus 50% of the live load plus, superimposed dead load of 0.1D to total 1.35D. In determining the load history, slabs were assumed to support construction loads, dead load and service live loads (occupancy loads). The live load component was expressed as a ratio of the slab dead load. Because of computational problems in unloading the slabs the simplified load history was used (see Fig. 6.3).

For a given slab thickness, an increase in design live load would be expected to produce an increase in live load deflection and an increase in incremental deflection. Instead, slabs with the lowest ratio produced larger incremental deflections. This was verified from preliminary investigations conducted into the effect of live-load to dead-load ratios on slab deflections (see Table 6.2). The explanation is that any increase in live load was offset by the corresponding increase in steel reinforcement thereby restraining further increases in incremental deflections.

6.2.3 Permissible Deflection Limit

ACI 318-89 and CSA A23.3-84M specify maximum deflections permitted under various circumstances as fractions of span length. Specified limits are provided for live-load deflections and incremental deflections occuring after installation of nonstructural partitions. Neither code, however, contains specified limits on total deflection.

Total deflections can be reduced by introducing camber in the slabs during construction. Camber will not reduce the incremental deflection, but will reduce visual and alignment problems. A further complication is that exterior panels experience

larger deflections than interior panels and hence all serviceability criteria, incremental deflection and camber, are determined by the exterior panel. Camber was assumed to be equal to the instantaneous deflection of the exterior mid-panel. In this study, serviceability was defined as an exterior panel, column line incremental deflection equal to or greater than clear span/240. This is intended to represent the deflection which can be tolerated by nonstructural installations; partitions, doors, etc.

6.2.4 Slab Details

Because of the large number of possible parameters and the objective of deriving an easy to use equation the present investigation was conducted within the scope of a parametric study. A total of 169 analyses were carried out for various combinations of slab dimensions, material properties, and construction schedules. The study was restricted to reinforced concrete flat plates and flat slabs with drop panels. The slabs were designed in accordance with the Direct Design Method of the ACI Building Code [1].

The slab layout spanned three bays in both directions of the cartesian coordinate system as illustrated in Fig. 6.4. Due to symmetry, only a quarter of the slab system was modelled for the analysis. One mesh layout was used throughout the study. The mesh was selected based on a preliminary mesh refinement analysis for a converged solution. The layout has the general configuration of the mesh shown in Fig. 6.5 with given dimensions adjusted to suit the column and middle strips for each slab.

Catastrophic failure of flat slabs is usually caused by punching shear. The punching shear capacity available is dependent upon the shear perimeter, developed concrete

strength, reinforcement ratio and the assumed relationship between shear strength and concrete strength. To avoid possible punching failure, larger column sizes were used for slabs with longer spans, and without drop panels.

For each slab layout a 10% increase in thickness was applied for exterior panels as required by the code. For slabs with drop panels, the codes specified minimum drop panel thickness of 1.25 times the slab thickness was used.

All the slabs were reinforced with steel of yield strength 60,000 psi (417 MPa), but required steel areas were not matched with available sizes of reinforcing bars. Instead, the computed areas per unit width were specified as input for the computer analyses. Nine reinforcing steel layer systems (see Fig. 6.6) were used. Reinforcement details for some selected slabs are given in Appendix B and the reinforcements for slabs SS-A26 and SS-B22 are given in Table 6.3. In calculating the effective depths, a clear concrete cover of 20 mm (0.8 in) was assumed. The analyses were carried out for a duration of 5000 days, a period for which the solution converged within the time domain. A characteristic concrete strength of 3000 psi (20 MPa) was specified for most slabs. Two series of slabs were analyzed with compressive strengths of 24.0 MPa (3500 psi) and 27.5 MPa (4000 psi) to investigate the effect of concrete strength on slab deflection.

Details of the slabs analyzed are presented in Appendix A.

6.3 Presentation of Results

Before the revised concrete parameters of Gardner and Zhao were incorporated in the computer program, a preliminary investigation was carried out to deter-

mine the effect of live-load to dead-load ratio on calculated deflections using the shrinkage and creep equations of ACI-209. Table 6.2 shows the results of the preliminary investigation and the quantity of information available. As stated, the control criterion was chosen to be the incremental column line deflection of the exterior panel (Node 17). It can be seen that the assumption by Boussouf [9] that deflections are inversely proportional to h^3 is questionable. Secondly, it is easily observed that the slabs designed for live load to dead load ratio of 0.5 have greater instantaneous, incremental and total deflections than slabs designed for load ratios of 1.0 and 1.5.

Table 6.4 illustrates the re-iterative procedure used to determine the required slab thickness to satisfy the exterior panel column line criteria. A complete set of the re-iterative results for all slabs is given in Appendix E.

To check if the pattern of result conform to those expected, Table 6.5 shows that the long-term to short-term deflection ratios range from a high of 7.02 to a low of 2.61. These ratios are similar to field measured values reported by Scanlon [47] and Sbarounis [46].

Tables 6.5 to 6.10 summarize the deflection results taken from the tables in Appendix E.

The following definitions pertain to all the tables of results.

1. The incremental deflection Δ_{incr} is the difference between the total deflection, Δ_{tot} and the instantaneous deflection Δ_{inst}.

2. Deflection at Node 7 (refer to Fig. 6.5) is the mid-panel deflection of the interior panel.

3. Deflection at Node 31 is the mid-panel deflection of the exterior panel.

4. Deflections at Nodes 17 and 45 are the deflections along the column lines of the exterior panel in the E-W direction.

5. Deflection at Node 33 is the deflection of the longer span along the column line of the exterior panel.

6. In applying the deflection limit $l/240$, the span l was taken as the distance between the column faces when considerng mid-span deflections along the column centerlines.

6.4 Discussion of Results

Figure 6.7 shows the thicknesses required to satisfy a serviceability limit of $l/240$ on the interior column line of the exterior panel for square slabs. It can be observed that the age of loading (construction cycle) and the span have significant effects on the required slab thickness. The current ACI 318-89 and CSA A23.3-M84 requirements do not give consistent serviceability.

As the required slab thickness is highly dependent upon construction load a review of the form of the span-thickness equation is warranted. The general deflection equation is

$$\delta = \frac{wl^4}{KEI}$$

where K is a constant.

For the given permissible deflection limit used,

$$\delta < \frac{l}{240}$$

and

$$I = h^3/12$$

Therefore,

$$l/240 < \frac{wl^4}{KEh^3/12}$$

But

$$w(load) = D(1.4 + 1.7L/D)$$

where

$$D = \rho h$$

Thus,

$$l/240 < \frac{\rho h(1.4 + 1.7L/D)l^4}{KEh^3/12}$$

If all the constants are put together the expression becomes

$$Const < l^3/h^2$$

Assuming $h = kl$, where k is a constant,

$$Const < l^3/(kl)^2$$

This implies that

$$Const < l^{1.5}$$

For a given thickness which is itself a constant, we can write

$$Const = kh < l^{1.5}$$

which implies

$$Const < l^{1.5}/h$$

Thus the minimum thickness is proportional to the span to the 3/2 power.

Using the above logic as a base and the results of the computer analysis the following best fit expression was derived.

$$h_{min} \geq \frac{l^{1.42}}{K} * \beta(\frac{1.2}{\beta} - 0.2) * t^{-0.20} * \frac{30}{f_{ck} + 8} \qquad (6.1)$$

where,

h = the minimum thickness required for an exterior panel (m),

β = ratio of the longer span to the shorter span,

t = age of concrete at the time of loading in days,

f_{ck} = characteristic strength of concrete (MPa),

l = clear span between column faces for column strip deflections. Using the square panels experimental results the constant K was determined to be 41.77 with a coefficient of variation of 4.4%. Figure 6.8 shows the fit of the equation with the data from Table 6.5.

The variation of the constant with specified concrete strength is shown in Fig. 6.9 for all square slabs loaded at 3 days. The table shows that the required slab thickness reduces with increased concrete mean strength. Using a strength correction factor of the inverse of the concrete mean strength is easy and the agreement is shown in Fig. 6.9.

Rectangular panels are not as sensitive to deflection problems as square slabs. A linear reduction factor, originally proposed by Scanlon, was used to modify the equation. Comparison of the constant of the equation with the rectangular slab data is shown in Fig. 6.8. The agreement becomes more conservative with panel aspect ratios other than unity. It can be noted that the data for different ages of loading is taken into account.

As stated previously camber equal to the 28-day deflection should be provided. The calculated instantaneous deflections for the square slabs are shown in Table

6.11 and illustrated in Fig. 6.13. It is not surprising that larger span slabs have larger deflections than shorter span slabs: but it is surprising that slabs loaded at early ages have smaller deflections. This is because slabs loaded at early ages require larger thicknesses to satisfy the serviceability requirement.

The simplest camber requirement would be a simple fraction of span, perhaps, $l/500$. A more exact expression would include span and age of loading. An appropriate equation would be

$$camber = 0.35\, l_n^{1.5}\, t_o^{0.2} \qquad (mm) \tag{6.2}$$

An alternative formulation for exterior panel camber is

$$camber = \frac{l_n^{2.75}}{80\, h} \qquad (mm) \tag{6.3}$$

where,

camber = the 28-day mid-panel deflection of the exterior slab,

l = the clear span of the diagonals between opposite column corners (mm),

t_o = the age of concrete at the time of loading (days), and

h = slab thickness

The column line camber should be the mid-panel camber multiplied by the cosine of the angle between the diagonal and the column line.

For a square slab,

$$\begin{aligned} column\ \ line\ \ camber &= mid-panel\ \ camber \times cos45^o \\ &= 0.71 \times mid-panel\ \ camber \end{aligned} \tag{6.4}$$

The various camber requirements are compared in Fig. 6.14.

Table 6.8 shows the effect of drop panels on slab deflections. The use of code recommended minimum drop panel thickness of 1.25 times the slab thickness reduces

the thickness required to satisfy the serviceability criterion by approximately 10%.

6.4.1 Summary

For design purposes it would be preferable to ensure that the minimum thickness equation should be conservative. Consequently it is recommended that, for design, equation 6.1 should be changed to

$$h_{min} \geq \frac{l^{1.42}}{40} * \beta(\frac{1.1}{\beta} - 0.1) * t^{-0.20} * \frac{30}{f_{ck} + 8} \tag{6.5}$$

For interior panels the thickness given by Eq. (6.1) can be reduced by 15%.

For slab with drop panels, the minimum thickness can be reduced by 10% as in the present code.

Camber should be provided and a reasonable mid-panel camber would be longer-span/500. The column line camber would be the mid-panel camber multiplied by the cosine of the angle between the diagonal and the column line.

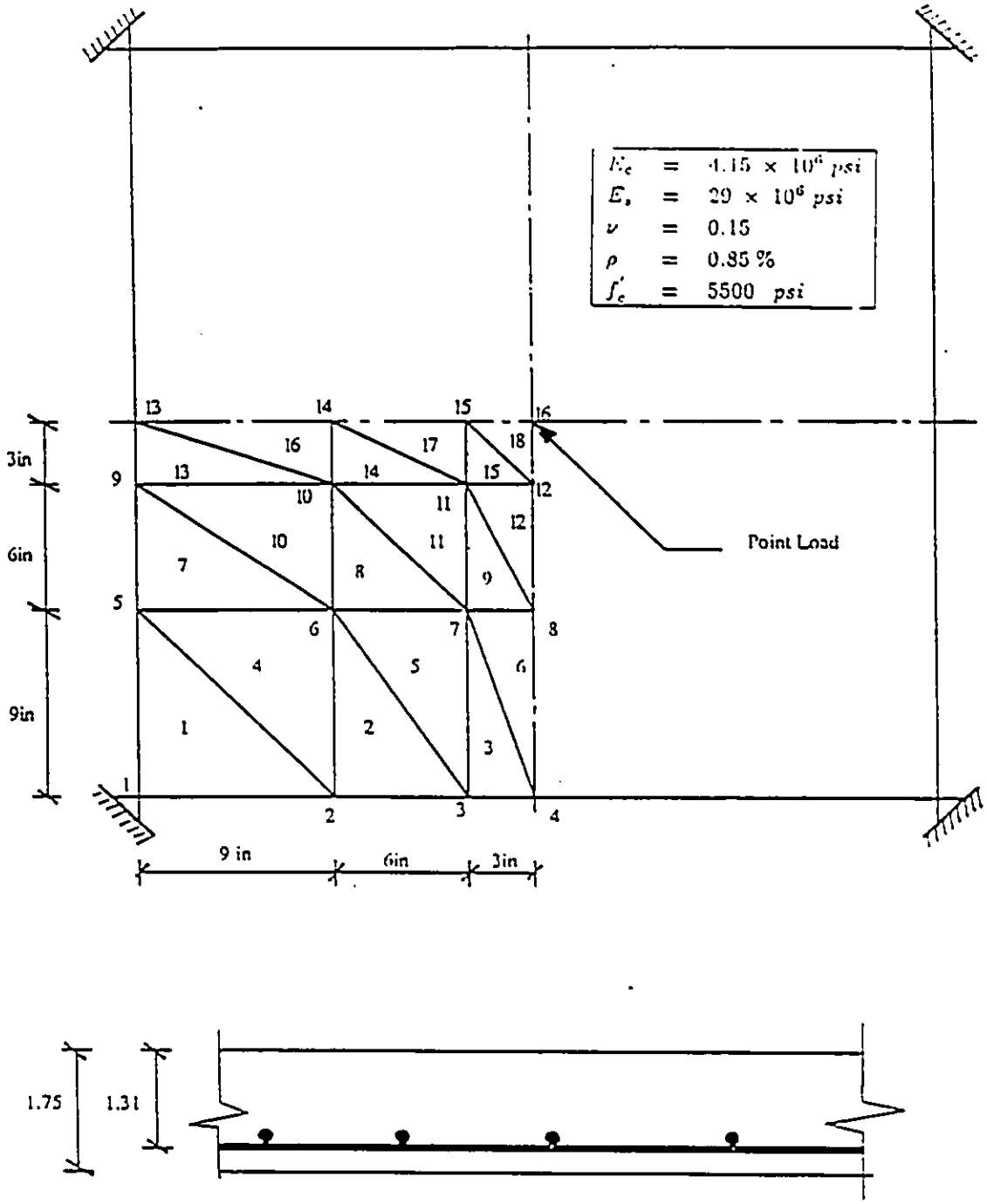

Figure 6.1: McNeice Slab: Details and Material Properties

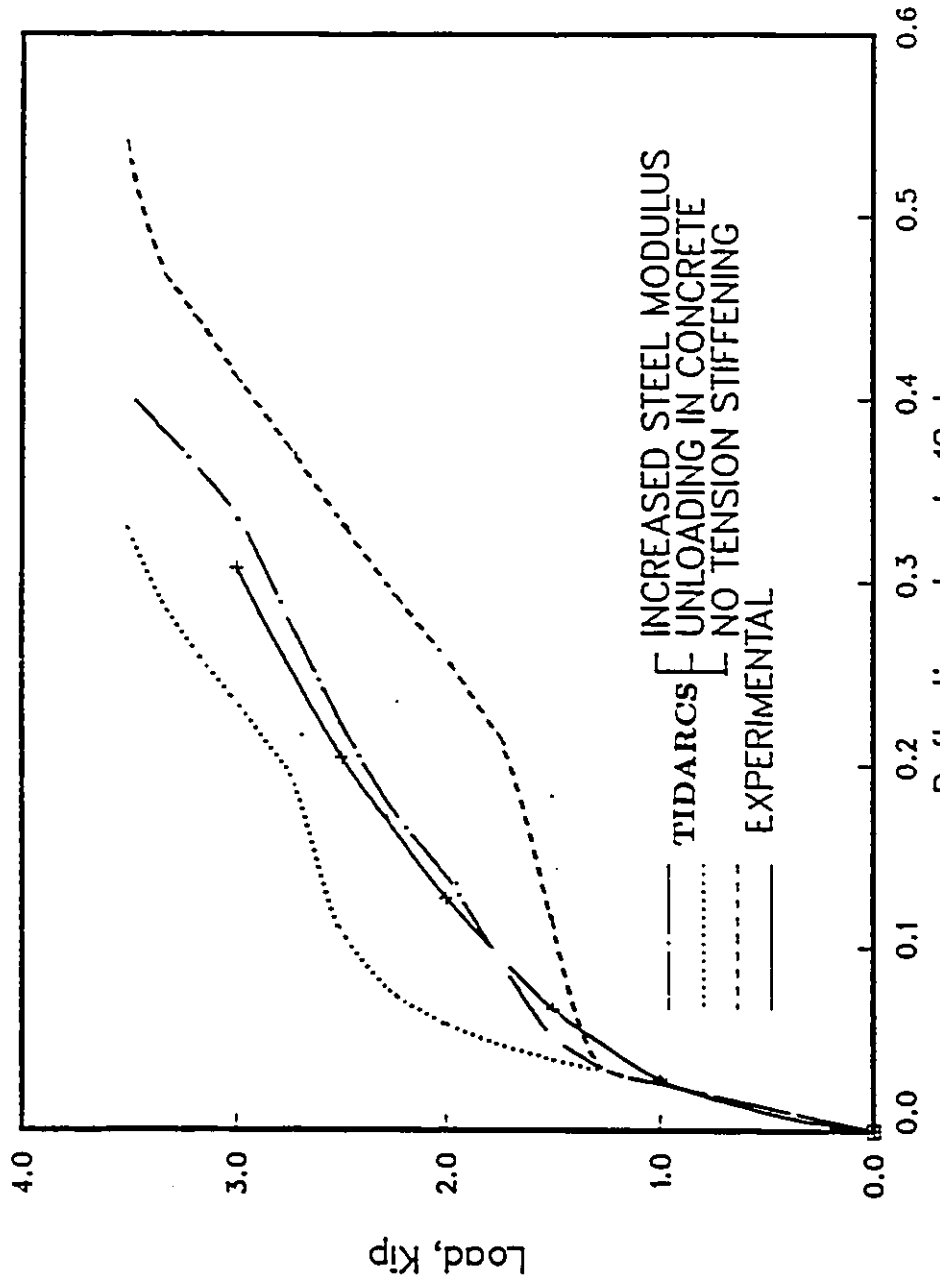

Figure 6.2: Load-Deflection Plot for McNeice Slab

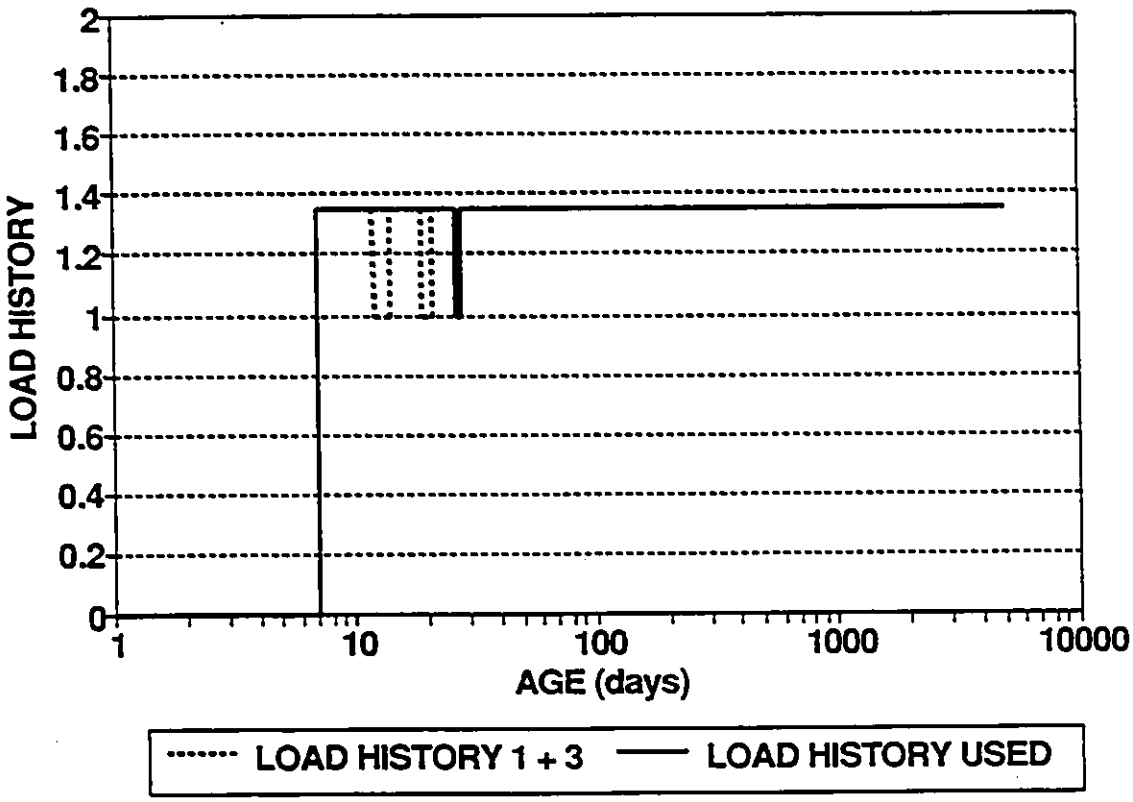

Figure 6.3: Assumed Load History for Present Analysis

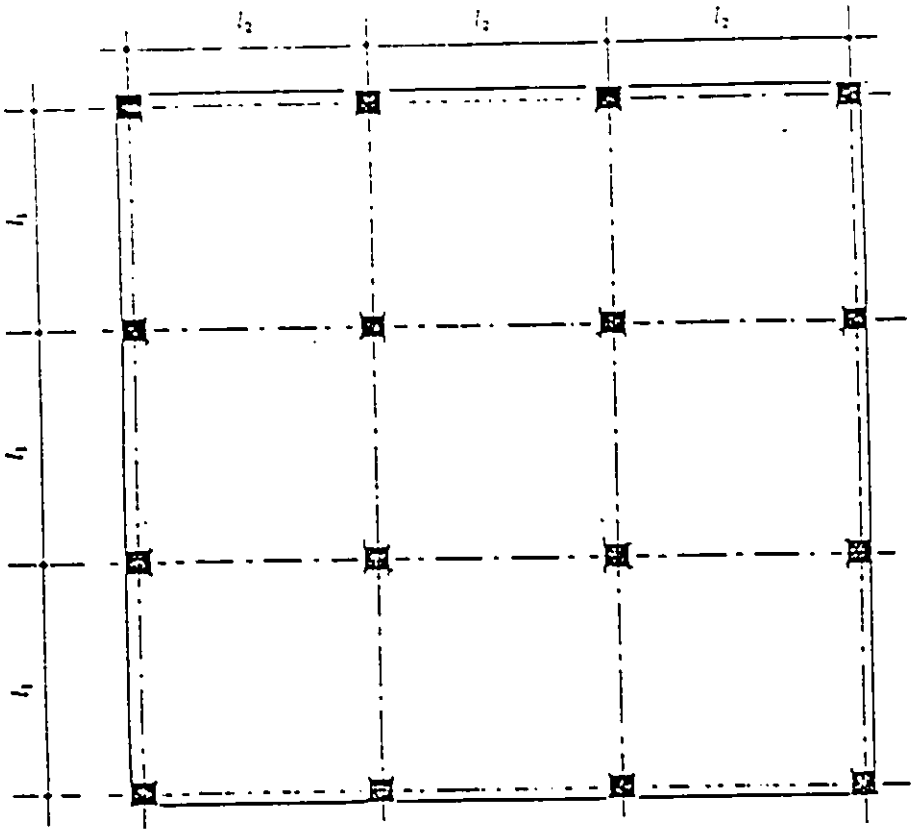

Figure 6.6: Slab Layout for Present Analysis

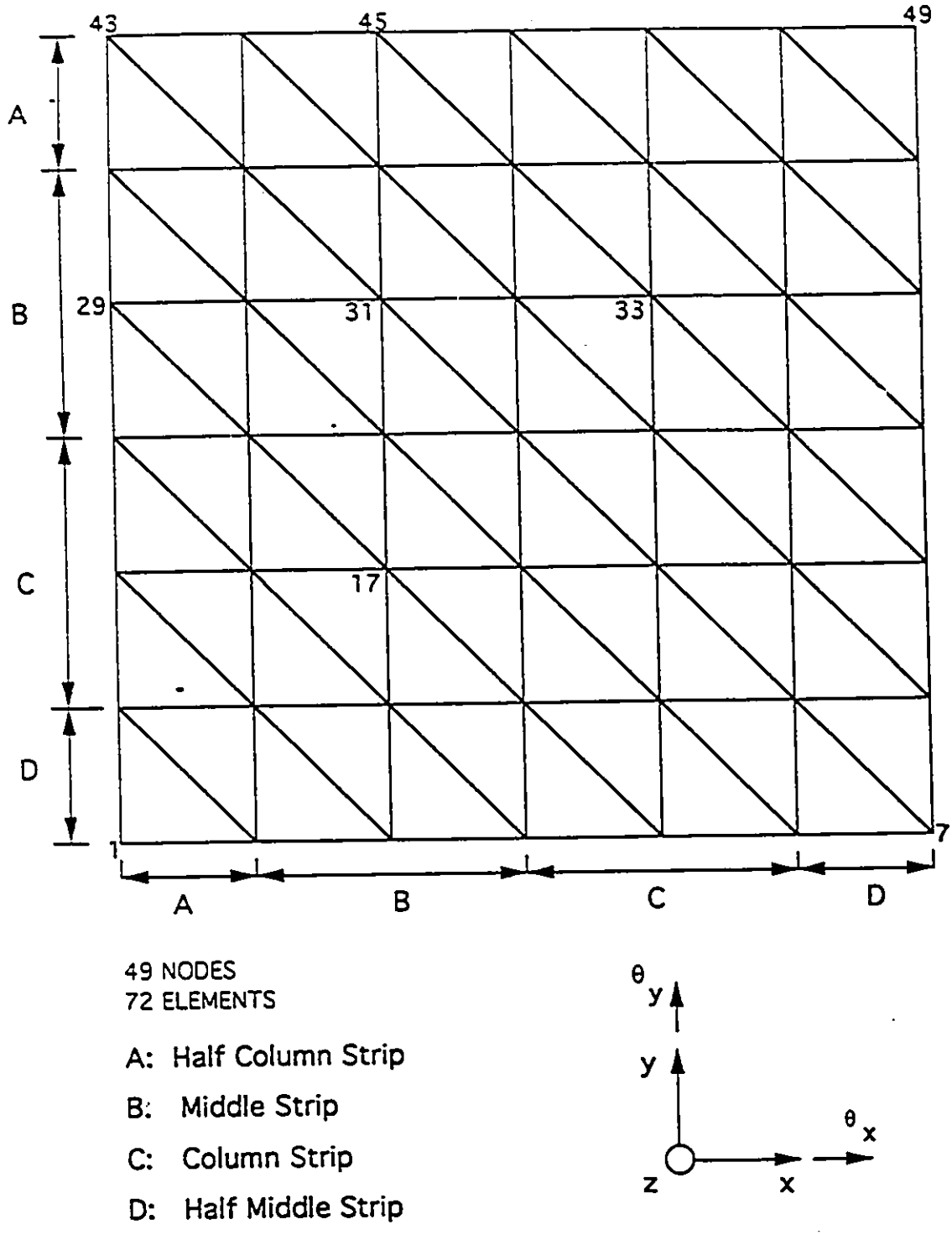

Figure 6.7: Finite Element Mesh Used in Present Analysis

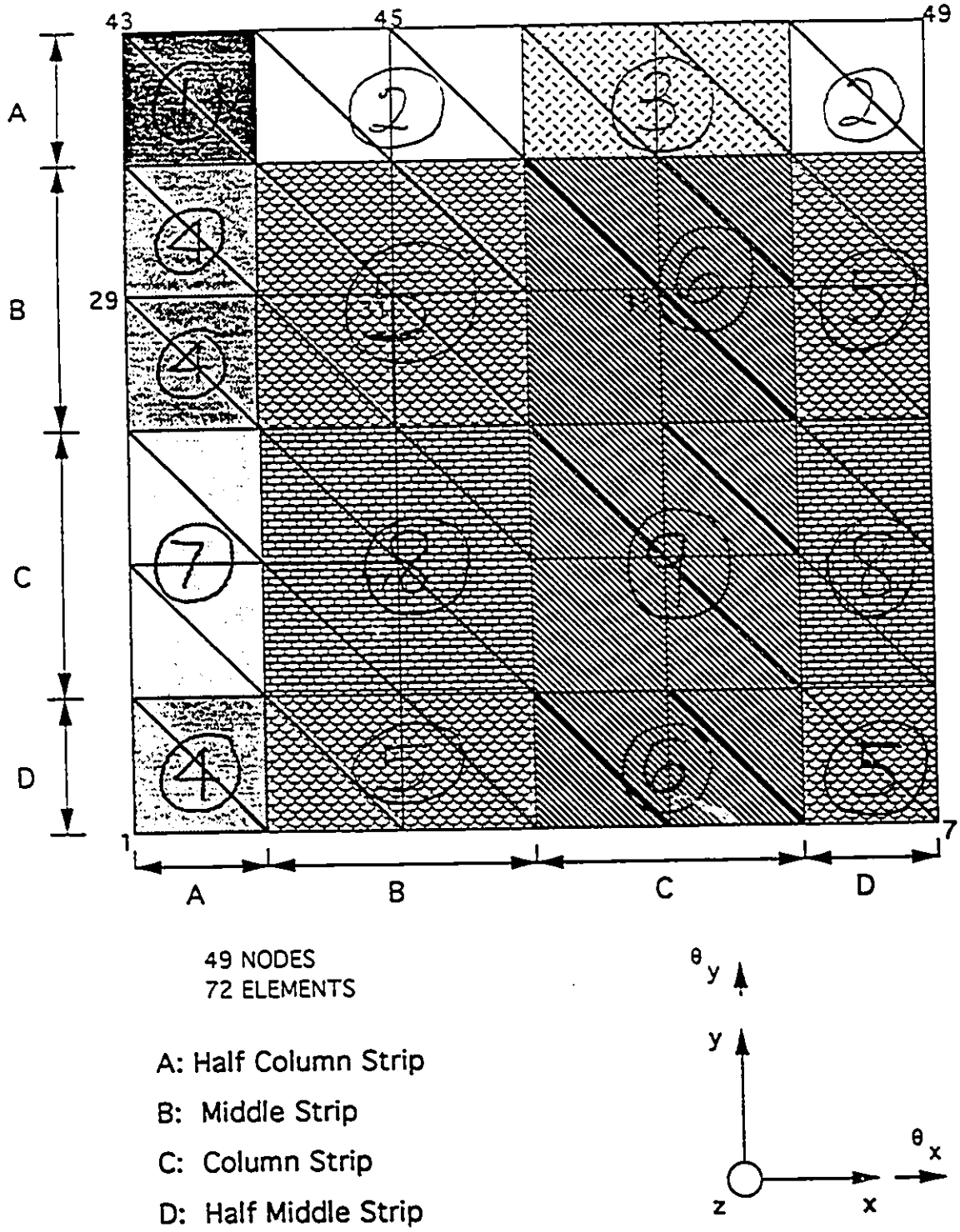

Figure 6.8: Reinforcing Steel Layer System

Table 6.1: Observed and Computed Deflections for Fu's Slab 3

	Observed Deflections (0.01 mm)	Calculated Deflections (0.01 mm)
At 28 days (due to loading)	212	213
Total defl. at 28 days	345	377
Total defl. at 60 days	460	504
Total defl. at 120 days	600	595
Total defl. at 240days	760	673
Total defl. at 483days	848	759

Table 6.2: Deflections for Square Slabs Using ACI-209 Recommendation

Slab ID	Clear span (ins)	Slab Thickness (ins)	Live-Load to Dead-Load Ratio	Computed Deflections (ins)											
				Mid-panel Deflections						Deflections Along Column Lines					
				Interior (Node 7)			Exterior (Node 31)			Node 17			Node 45		
				Δ_{tot}	Δ_{inst}	Δ_{incr}	Δ_{tot}	Δ_{inst}	Δ_{incr}	Δ_{tot}	Δ_{inst}	Δ_{incr}	Δ_{tot}	Δ_{inst}	Δ_{incr}
ACI-S1	210	6.00	0.50	1.735	0.563	1.172	2.473	0.861	1.612	1.592	0.572	1.020	1.269	0.409	0.860
ACI-S2	210	6.00	1.00	1.380	0.414	0.966	1.693	0.616	1.077	1.077	0.412	0.665	0.818	0.289	0.529
ACI-S3	210	6.00	1.50	1.189	0.371	0.818	1.490	0.540	0.950	0.927	0.370	0.557	0.741	0.262	0.479
ACI-S4	210	8.00	0.50	1.244	0.428	0.816	1.417	0.554	0.863	0.893	0.364	0.529	0.679	0.261	0.418
ACI-S5	210	8.00	1.00	0.980	0.253	0.727	1.131	0.379	0.752	0.689	0.252	0.437	0.510	0.175	0.335
ACI-S6	210	8.00	1.50	0.805	0.166	0.639	0.971	0.321	0.650	0.557	0.202	0.355	0.431	0.146	0.285

Table 6.3: Reinforcement Detail (Square Slabs)

Slab ID	Steel System Number	Reinforcement Areas (in^2/in)			
		Top X-Direction	Top Y-Direction	Bottom X-Direction	Bottom Y-Direction
SS-A26	1	0.02420	0.02420	0.01360	0.01360
	2	0.01360	0.01360	0.02904	0.01360
	3	0.04887	0.02420	0.01360	0.01360
	4	0.01360	0.01360	0.01360	0.02904
	5	-	-	0.01936	0.01936
	6	0.01629	0.01360	0.01360	0.02904
	7	0.02420	0.04887	0.01360	0.01360
	8	0.01360	0.01629	0.02904	0.01360
	9	0.04887	0.04887	0.01360	0.01360
SS-B22	1	0.03874	0.03874	0.02560	0.02560
	2	0.02560	0.02560	0.04648	0.02560
	3	0.07822	0.03874	0.02560	0.02560
	4	0.02560	0.02560	0.02560	0.04648
	5	-	-	0.03099	0.03099
	6	0.02607	0.02560	0.02560	0.04648
	7	0.03874	0.07822	0.02560	0.02560
	8	0.02560	0.02607	0.04648	0.02560
	9	0.07822	0.07822	0.02560	0.02560

Table 6.4: Computed Deflections for Square Slabs Loaded at 7 days

Slab ID	Clear span (ins)	Slab Thickness (ins)	Computed Deflections (ins)												Perm. Defl. (l/240) (ins)
			Mid-panel Deflections						Deflections Along Column Lines						
			Interior (Node 7)			Exterior (Node 31)			Node 17			Node 45			
			Δ_{tot}	Δ_{inst}	Δ_{incr}	Δ_{tot}	Δ_{inst}	Δ_{incr}	Δ_{tot}	Δ_{inst}	Δ_{incr}	Δ_{tot}	Δ_{inst}	Δ_{incr}	
SS-A11	210	6.00	1.150	0.244	0.906	3.062	0.603	2.459	1.838	0.372	1.466	1.415	0.280	1.135	0.875
SS-A12	210	6.60	0.844	0.175	0.669	2.295	0.435	1.860	1.310	0.255	1.055	1.050	0.206	0.844	0.875
SS-A13	210	7.00	0.781	0.157	0.624	1.447	0.272	1.175	0.890	0.175	0.715	0.602	0.120	0.482	0.875
SS-A14	210	6.80	0.855	0.174	0.681	1.677	0.313	1.364	1.053	0.203	*0.850*	0.712	0.141	0.571	0.875
SS-B8	314	9.0	2.789	0.486	2.303	5.413	0.906	4.507	3.559	0.643	2.916	2.902	0.494	2.408	1.310
SS-B9	314	10.0	2.183	0.356	1.827	4.669	0.777	3.892	2.848	0.495	2.353	2.183	0.377	1.806	1.310
SS-B10	314	12.0	1.364	0.230	1.134	3.152	0.548	2.604	1.876	0.356	1.520	1.475	0.256	1.219	1.310
SS-B11	314	12.9	1.139	0.190	0.949	2.757	0.487	2.270	1.620	0.310	*1.310*	1.256	0.226	1.030	1.310
SS-C10	432	16.0	2.011	0.423	1.588	4.906	1.109	3.797	2.992	0.725	2.267	2.347	0.537	1.811	1.800
SS-C11	432	17.8	1.573	0.262	1.311	4.222	0.825	3.397	2.552	0.548	2.004	1.925	0.360	1.565	1.800
SS-C12	432	18.5	1.407	0.231	1.176	3.841	0.773	3.068	2.366	0.515	1.851	1.775	0.378	1.397	1.800
SS-C13	432	18.7	1.302	0.212	1.089	3.773	0.762	3.011	2.325	0.507	*1.818*	1.742	0.373	1.369	1.800

Table 6.5: Computed Deflection Ratios for Node 17

Slab ID	Clear Span (ins)	Age at Loading (Days)	Computed Deflections (ins)			Long-term to Short-term Defl. Ratio
			Total	Immediate	Long-term	
SS-A5	210	3	1.027	0.128	0.899	7.02
SS-A10	210	4	1.036	0.159	0.877	5.52
SS-A14	210	7	1.053	0.203	0.850	4.19
SS-A17	210	14	1.103	0.225	0.878	3.47
SS-A20	210	28	1.084	0.233	0.851	3.65
SS-B3	314	3	0.759	0.220	1.300	5.91
SS-B7	314	4	0.762	0.248	1.286	5.19
SS-B11	314	7	0.949	0.310	1.310	4.23
SS-B15	314	14	0.967	0.355	1.322	3.72
SS-B18	314	28	1.066	0.392	1.282	3.27
SS-C4	432	3	0.911	0.417	1.803	4.32
SS-C9	432	4	1.012	0.440	1.770	4.02
SS-C13	432	7	1.089	0.507	1.818	3.59
SS-C17	432	14	1.084	0.521	1.787	3.42
SS-C20	432	28	1.274	0.681	1.779	2.61

Table 6.6: Summary of Incremental Deflections

Slab ID	Clear Span (ins)	Age at Loading (Days)	Thickness Required	Incremental Deflections (ins) (28 - 5000 days)			Span Thickness Ratio
				Node 7	Node 17	Node 31	
SS-A3	210	3	8.50	0.590	0.899	1.442	24.71
SS-A10	210	4	7.70	0.669	0.877	1.430	27.27
SS-A14	210	7	6.80	0.681	0.850	1.364	30.88
SS-A17	210	14	5.90	0.710	0.878	1.413	35.59
SS-A20	210	28	5.50	0.759	0.851	1.392	38.18
SS-B3	314	3	16.00	0.759	1.300	2.237	19.63
SS-B7	314	4	14.80	0.762	1.286	2.210	21.22
SS-B11	314	7	12.90	0.949	1.310	2.270	24.34
SS-B15	314	14	11.50	0.967	1.322	2.263	27.30
SS-B18	314	28	10.30	1.066	1.282	2.248	30.89
SS-C4	432	3	22.7	0.911	1.803	2.973	19.03
SS-C9	432	4	21.3	1.012	1.770	2.884	20.28
SS-C13	432	7	18.7	1.089	1.818	3.011	23.10
SS-C17	432	14	17.2	1.084	1.787	2.950	25.12
SS-C20	432	28	15.0	1.274	1.779	2.952	28.80

Table 6.7: Effects of Panel Aspect Ratio on Defections

Slab ID	Clear Spans ins		Slab Aspect Ratio	Age at Loading (days)	Required Slab Thickness	Mid-panel Incremental Deflections (ins)	
	l_{xn}	l_{yn}				Node 7	Node 31
SS-A10	236.00	236.00	1.0	4	7.70	0.669	1.430
RS-A6	157.33	236.00	1.5	4	6.70	0.598	0.913
RS-A21	118.00	236.00	2.0	4	6.20	0.690	0.882
SS-B7	354.00	354.00	1.0	4	14.80	0.762	2.210
RS-B5	236.00	354.00	1.5	4	13.20	0.571	1.289
RS-B17	177.00	354.00	2.0	4	11.60	0.733	1.312
SS-C9	472.00	472.00	1.0	4	21.30	1.012	2.884
RS-C2	314.67	472.00	1.5	4	18.30	0.820	1.904
RS-C13	236.00	472.00	2.0	4	17.50	0.971	1.772
SS-A14	236.00	236.00	1.0	7	6.80	0.681	1.364
RS-A10	157.33	236.00	1.5	7	5.80	0.601	0.926
RS-A24	118.00	236.00	2.0	7	5.40	0.681	0.854
SS-B11	354.00	354.00	1.0	7	12.90	0.949	2.270
RS-B9	236.00	354.00	1.5	7	11.70	0.587	1.299
RS-B22	177.00	354.00	2.0	7	11.20	0.746	1.252
SS-C13	472.00	472.00	1.0	7	18.70	1.089	3.011
RS-C6	314.67	472.00	1.5	7	16.40	0.889	1.881
RS-C18	236.00	472.00	2.0	7	16.50	1.057	1.786

Table 6.8: Effects of Panel Aspect Ratio on Defections (cont'd)

Slab ID	Clear Spans ins		Slab Aspect Ratio	Age at Loading (days)	Required Slab Thickness	Mid-panel Incremental Deflections (ins)	
	l_{xn}	l_{yn}				Node 7	Node 31
SS-A17	236.00	236.00	1.0	14	5.90	0.710	1.413
RS-A13	157.33	236.00	1.5	14	5.20	0.610	0.882
RS-A26	118.00	236.00	2.0	14	4.70	0.710	0.891
SS-B15	354.00	354.00	1.0	14	11.50	0.967	2.263
RS-B12	236.00	354.00	1.5	14	10.30	0.656	1.357
RS-B25	177.00	354.00	2.0	14	9.90	0.721	1.266
SS-C17	472.00	472.00	1.0	14	17.20	1.084	2.950
RS-C8	314.67	472.00	1.5	14	14.80	0.971	1.901
RS-C21	236.00	472.00	2.0	14	14.20	1.072	1.783
SS-A20	236.00	236.00	1.0	28	5.50	0.759	1.392
RS-A17	157.33	236.00	1.5	28	4.80	0.649	0.922
RS-A30	118.00	236.00	2.0	28	4.50	0.705	0.846
SS-B18	354.00	354.00	1.0	28	10.30	1.066	2.248
RS-B14	236.00	354.00	1.5	28	9.60	0.682	1.384
RS-B27	177.00	354.00	2.0	28	9.20	0.755	1.290
SS-C20	472.00	472.00	1.0	28	15.00	1.274	2.952
RS-C11	314.67	472.00	1.5	28	13.70	1.098	1.918
RS-C25	236.00	472.00	2.0	28	13.10	1.139	1.804

Table 6.9: Effect of Compressive Strength on Required Slab Thickness

Slab ID	Clear Span (ins)	f'_c (MPa)	Required Thickness (ins)	Incremental Deflections (ins)		
				Node 7	Node 17	Node 31
SS-A5	210	3000	8.50	0.590	0.899	1.442
SS-A23	210	3500	7.60	0.586	0.843	1.308
SS-A27	210	4000	7.00	0.570	0.825	1.279
SS-B3	314	3000	16.00	0.759	1.300	2.237
SS-B20	314	3500	13.80	0.873	1.315	2.147
SS-B22	314	4000	12.80	0.902	1.296	2.076

Table 6.10: Effect of Drop Panels on Slab Deflections

Slab ID	Use of Drop Panel	Clear Span (ins)	Age at Loading (days)	Required Thickness (ins)	Incremental Deflections (ins)		
					Node 7	Node 17	Node 31
SS-A14	No	210	7	6.80	0.681	0.850	1.364
DP-A4	Yes	216	7	5.70	0.741	0.871	1.435
SS-B11	No	314	7	12.90	0.949	1.310	2.270
DP-B4	Yes	324	7	10.90	0.947	1.262	2.214
SS-C13	No	432	7	18.70	1.089	1.818	3.011
DP-C4	Yes	442	7	15.70	1.303	1.810	3.105

Table 6.11: Deflections of Node 31

Slab ID	Clear Span (ins)	Age at Loading (Days)	Thickness Required	Computed Deflections (ins)			Span Thickness Ratio
				Total	Camber	Incremental	
SS-A5	210	3	8.50	1.644	0.202	1.442	24.71
SS-A10	210	4	7.70	1.679	0.249	1.430	27.27
SS-A14	210	7	6.80	1.677	0.313	1.364	30.88
SS-A17	210	14	5.90	1.685	0.310	1.375	35.59
SS-A20	210	28	5.50	1.699	0.307	1.392	38.18
SS-B3	314	3	16.00	2.583	0.346	2.237	19.63
SS-B7	314	4	14.80	2.599	0.389	2.210	21.22
SS-B11	314	7	12.90	2.757	0.487	2.270	24.34
SS-B15	314	14	11.50	2.814	0.551	2.263	27.30
SS-B18	314	28	10.30	2.809	0.561	2.248	30.89
SS-C4	432	3	22.7	3.596	0.623	2.973	19.03
SS-C9	432	4	21.3	3.541	0.657	2.884	20.28
SS-C13	432	7	18.7	3.773	0.762	3.011	23.10
SS-C17	432	14	17.2	3.716	0.766	2.950	25.12
SS-C20	432	28	15.0	3.892	0.940	2.952	28.80

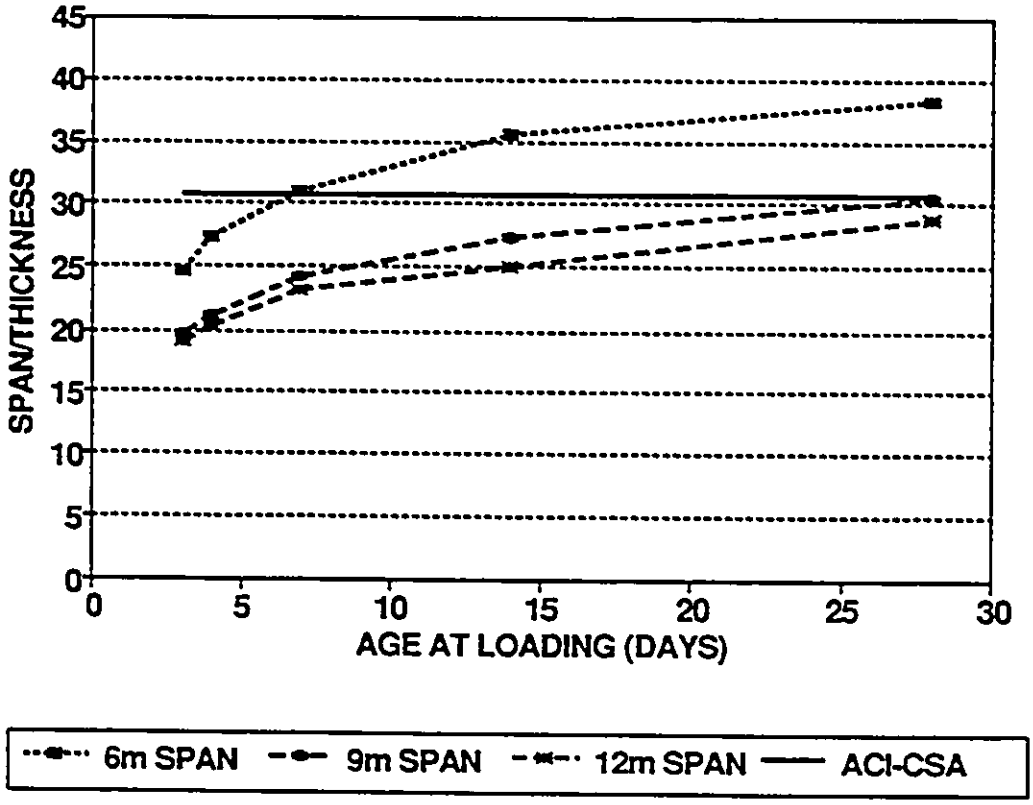

Figure 6.7: Required Span-Thickness Ratio for Serviceability

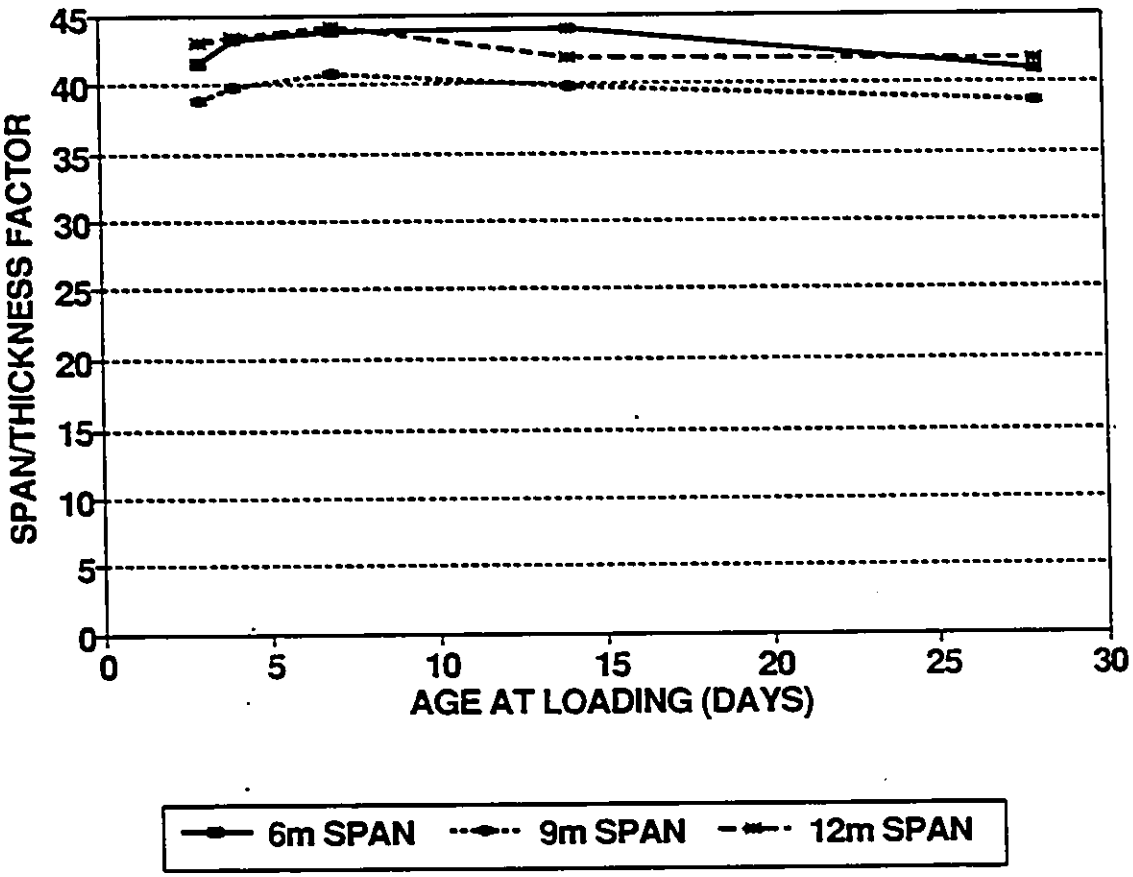

Figure 6.8: Constant for Eq. (6.1) to Ensure Serviceability

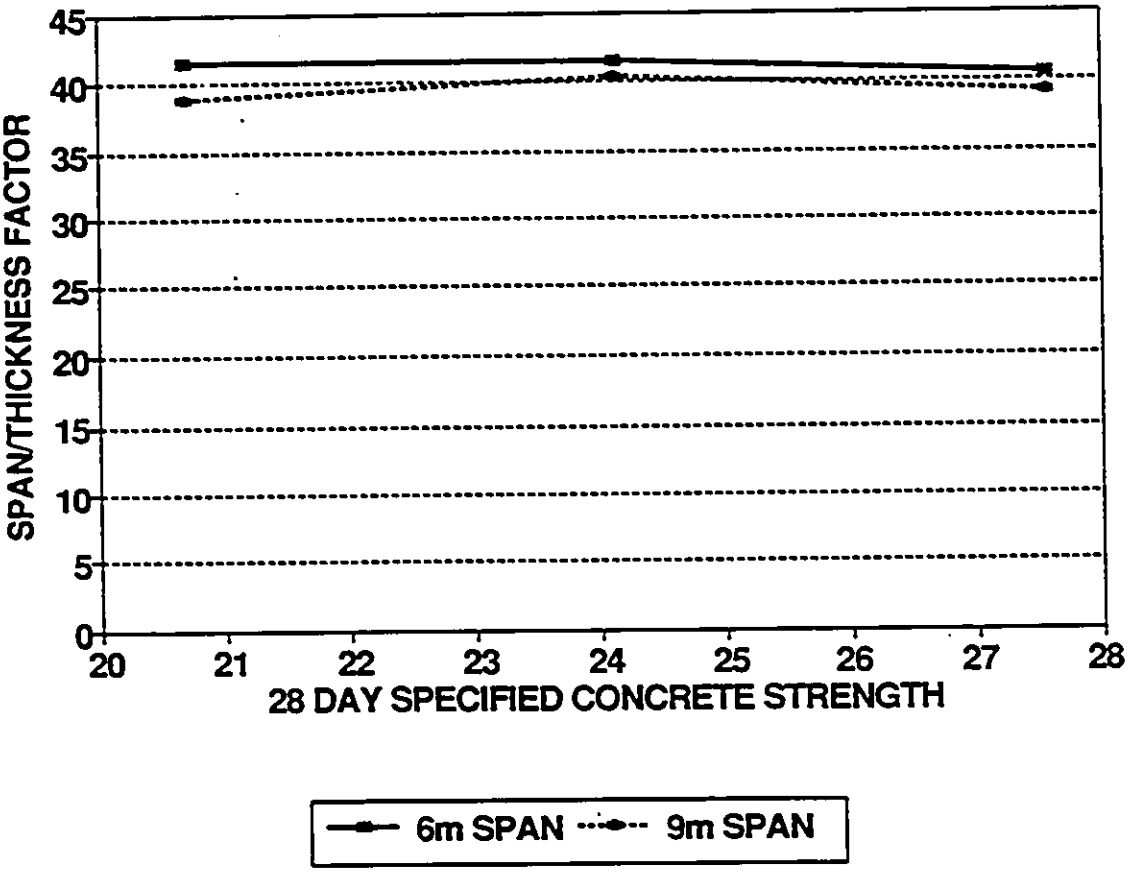

Figure 6.9: Effect of Concrete Specified Strength on Eq. (6.1)

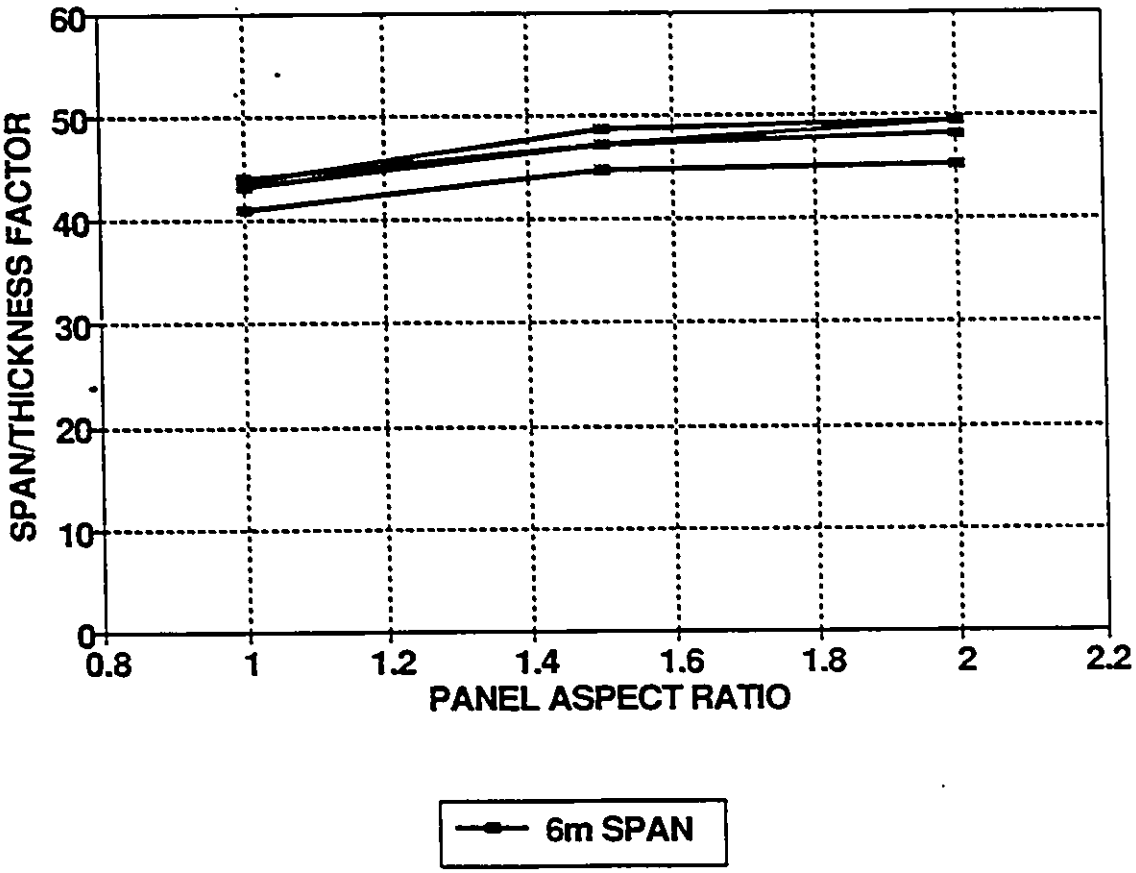

Figure 6.10: Effect of Panel Aspect Ratio on Eq. 6.1 (6 m Span Slab)

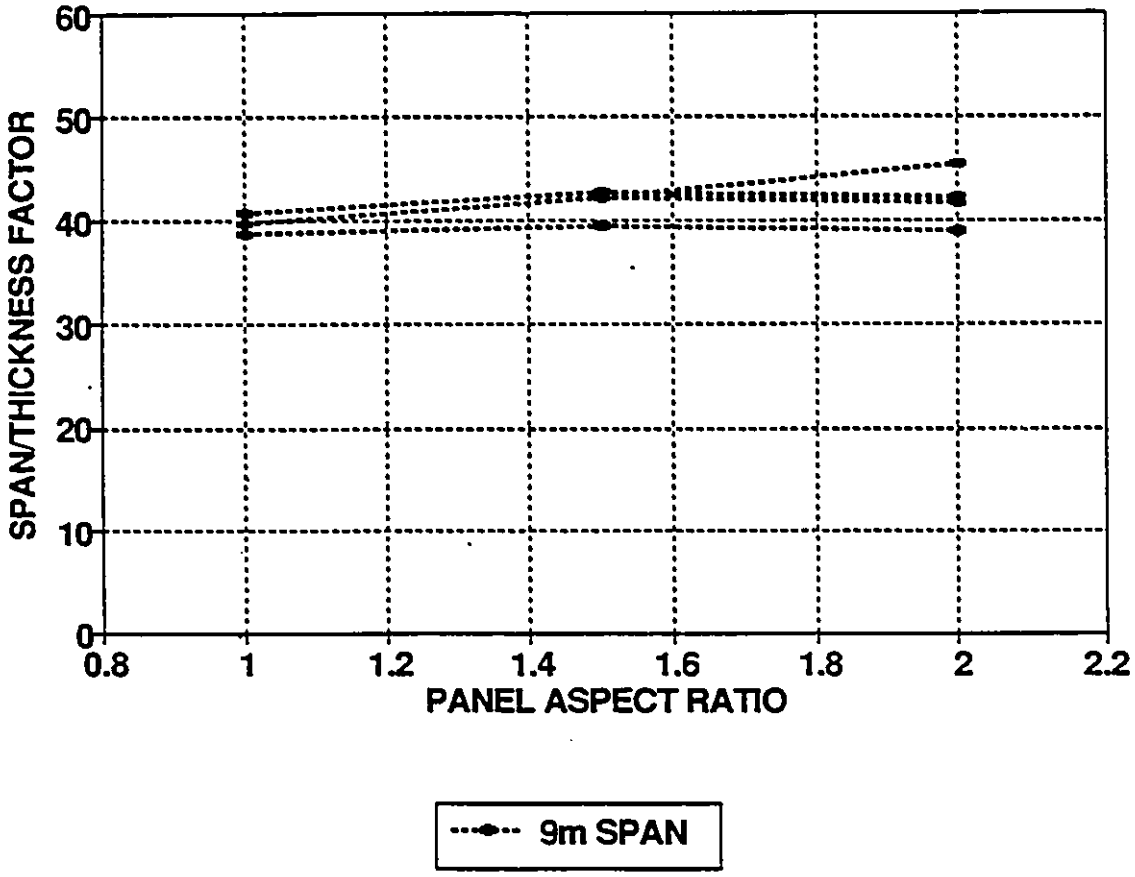

Figure 6.11: Effect of Panel Aspect Ratio on Eq. 6.1 (9 m Span Slab)

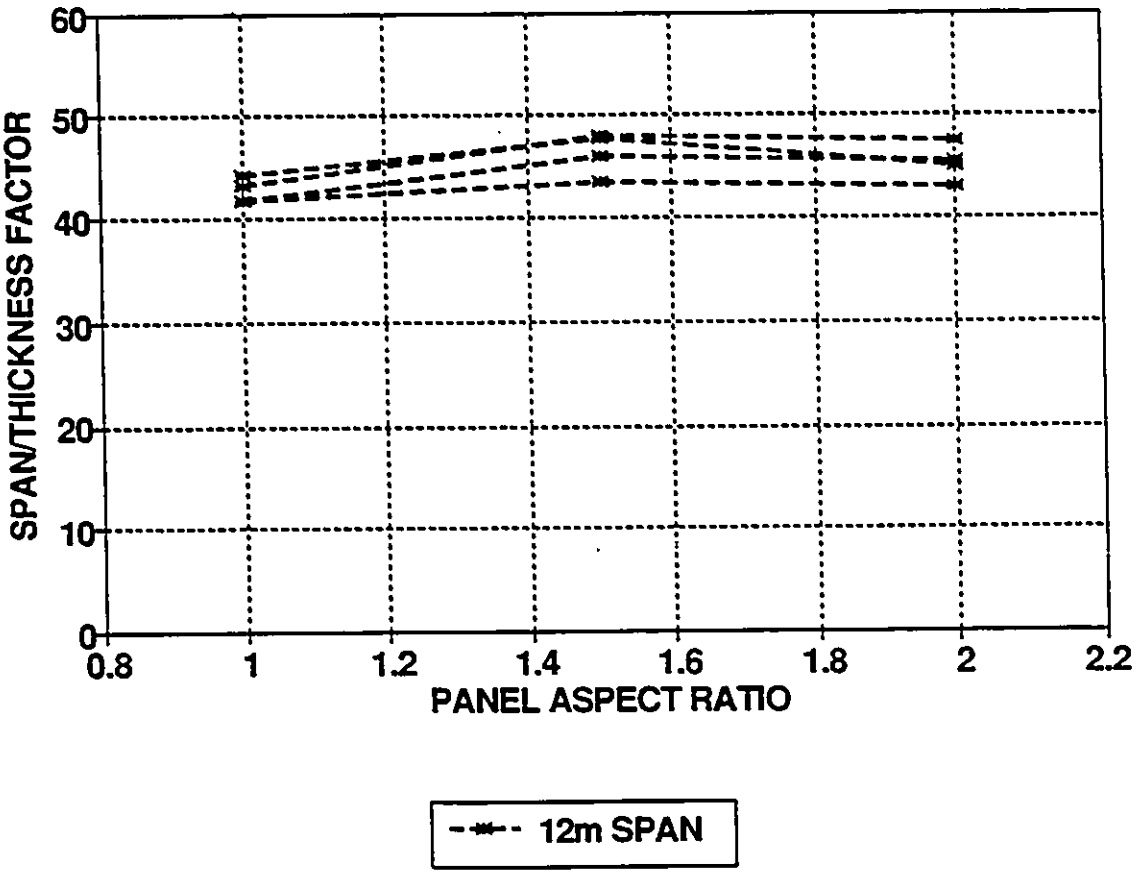

Figure 6.12: Effect of Panel Aspect Ratio on Eq. 6.1 (12 m Span Slab)

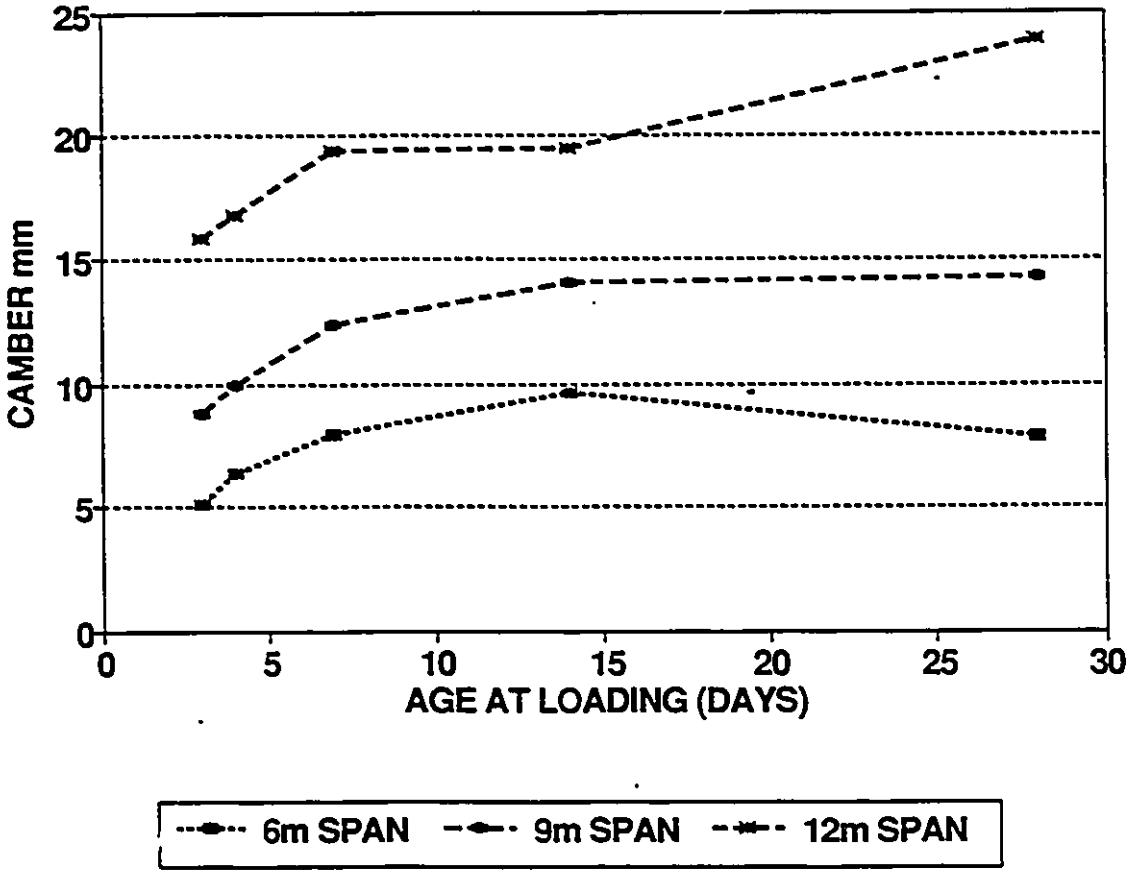

Figure 6.13: Recommended Camber for Slabs Meeting Serviceability Requirements

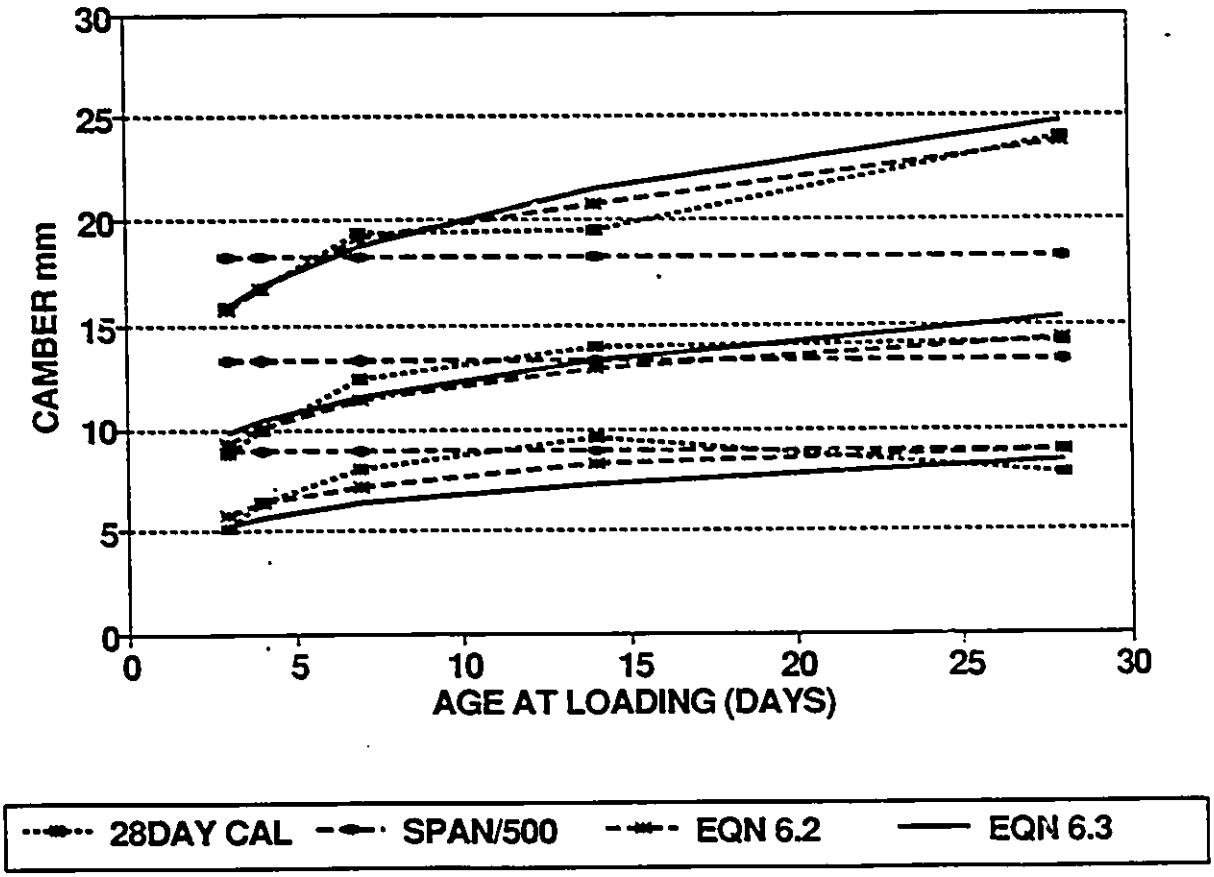

Figure 6.14: Expressions to Calculate Recommended Camber

Chapter 7

CONCLUSIONS AND RECOMMENDATIONS

7.1 General Remarks

Most cases of deflection damage occur as a result of exceeding the permissible deflection of slabs supporting non-structural elements. This creates serviceability problems such as cracking of partitions, jamming of doors and windows, and an uneven placement of furniture. In some cases, the visual impact of cracks and sagging floors may cause concern for the safety of the structure even though the structure may have adequate strength.

Serviceability problems in smaller span slabs may be noticeable earlier than in larger span slabs. This may be because the absolute magnitude of deflection is of lesser concern than the magnitude relative to the span of the slab.

The ACI Building Code [1] and the Canadian Standard [15], give the maximum deflections permitted under various circumstances as fractions of span length. The maximum permissible deflections are, however, based on live-load deflections and deflections occuring after the installation of non-structural partitions. Regrettably, there is no limit placed on total deflection.

The present study presents an alternative span-thickness criterion for the control of excessive slab deflections based on formwork precambering. Undesirable slab deflections can be significantly reduced by an appropriately chosen camber in the formwork. The idea is to use a prescribed camber to offset the immediate deflections. An equation is recommended for the estimation of the amount of camber needed for any given span. The equation was developed using the immediate deflections generated from the computer simulations.

7.2 Conclusions

The following are the conclusions drawn from the study based on the results of the computer experiments:

1. The age at which load is applied to a slab has a significant effect on the overall performance of the structure. Slabs loaded at early ages produced high longterm deflections.

2. The tensile strength of concrete is an important factor in the service load behaviour of concrete slabs. Slab deflections increase as the tensile strength of concrete decreases.

3. Construction loads are of great importance in the longterm behaviour of reinforced concrete slabs. Construction overloads produce extensive cracking and higher immediate and longterm deflections.

4. The time-dependent effects of creep and shrinkage are interactive in nature and contribute significantly to the longterm deflection of slabs.

5. Mid-panel deflections are greater for corner slabs than the interior or the column line mid-span deflections.

6. The total longterm deflections ranged from 2.6 to 7.0 times the immediate deflections.

7. Deflection multipliers are dependent on the age at loading of concrete. The deflection multipliers recommended by the current ACI the Canadian codes do not consider age of loading in predicting longterm deflections.

8. The characteristic strength of the concrete affects both the immediate and longterm deflections of slabs. Use of higher strength concrete leads to reduction in slab deflections.

9. Use of drop panels contributes to reducing net total deflections and helps prevent the likelihood of early-age punching shear failures.

10. Sensitivity of slab deflections to live-load to dead-load ratios (L/D) is not significant. However, slabs designed using high L/D ratios resulted in slightly lower longterm deflections as the increase in reinforcement tends to offset further deflection increases.

11. Rectangular slabs with larger panel aspect ratios are less likely to have deflection problems than those with lower aspect ratios. Square slabs are the most critical group.

12. Exterior panel deflections were approximately 2 to 3 times the interior panel deflection. The present codes requirement of increasing the minimum thickness for exterior panels by 10% should be revised. A 15 % increase would be appropriate.

13. A realistic minimum thickness criterion should reflect factors influencing slab deflections such as, age at loading, characteristic concrete strength, panel aspect ratio, construction rate and the time-dependent behaviour of concrete. The current ACI and CSA equations lack the necessary correction factors and should be revised.

7.3 Recommendations

1. Based on the results of an extensive computer-based computations the following limitation is proposed as an alternative to the code's minimum thickness criterion for flat plates and flat slabs with an appropriately chosen camber

$$h_{min} \geq \frac{l^{1.42}}{40} * \beta(\frac{1.1}{\beta} - 0.1) * t^{-0.20} * \frac{30}{f_{ck28} + 8} \qquad (7.1)$$

where,

h = the minimum thickness required for an exterior panel slab (m),

l = clear span of the longer side of the panel (m),

β = ratio of the longer span to the shorter span,

t = age of concrete at the time of loading in days, and

f_{ck28} = characteristic strength of concrete at 28 days (MPa).

2. Use of Eq. (7.1) is subject to the use of an appropriately chosen camber. The amount of mid-panel camber required should be estimated using one of the following equations.

- The simplest camber requirement should be

$$camber = l/500 \tag{7.2}$$

- A more exact expression would be

$$camber = 0.35\, l^{1.5}\, t_o^{0.2} \qquad (mm) \tag{7.3}$$

or,

$$camber = \frac{l^{2.75}}{80\, h} \qquad (mm) \tag{7.4}$$

where,

camber = the 28-day mid-panel deflection of the exterior slab,

l = the clear span of the diagonals between opposite column corners (mm),

t_o = the age of concrete at the time of loading (days), and

h = slab thickness (mm)

The column line camber should be the mid-panel camber multiplied by the cosine of the angle between the diagonal and the column line.

3. In the absence a camber the minimum thickness of Eq. (7.1) should be increased by 10%.

4. The minimum thickness required by the Eq. (7.1) can be reduced by 15% for interior panel slabs.

5. For flat slabs with drop panels, Eq. (7.1) can be decreased by 10% if the thickness of the drop panel is greater than or equal to 1.25 times the slab thickness.

6. A limit of $l/200$ should be imposed on net total deflection.

7. Further studies may be carried out into other types of slabs for a unified format to be established in sizing members.

REFERENCES

[1] ACI Committee 318, *Building Code Requirements for Reinforced Concrete (ACI 318-89),* American Concrete Institute, Detroit, 1989.

[2] ACI Committee 435, *Observed Deflections of Reinforced Concrete Slab Systems, and Causes of Large Deflections,* Deflections of Concrete Structures, SP-S6, American Concrete Institute, Detroit, 1984, pp. 15-61.

[3] ACI Committee 209, *Prediction of Creep, Shrinkage, and Temperature Effects in Concrete Structures,* (ACI 209R-82), American Concrete Institute, Detroit, 1982, 108 pp.

[4] ACI Committee 435, *Allowable Deflections,* ACI Journal, Proceedings V. 65, June 1986 pp. 433-444.

[5] Agarwal, R.K., and Gardner, N.J., *Form and Shore Requirements for Multi-storey Flat Slab Type Building,* ACI Journal, Proceedings V. 71, No. 11, November 1974, pp. 559-569.

[6] Bazant, Z.P., *Mathematical Modelling of Creep and Shrinkage of Concrete,* Wiley and Sons, New York, 1988.

[7] Becker, J., and Bresler, B., *FIRES-RC, A Computer Program for the Fire Response of Structures - Reinforced Concrete Frames*, Report No. UCB FRG 74-3, Division of Structural Engineering and Structural Mechanics, University of California, Berkeley, July 1974.

[8] Beton-Kalender 1991 Teil 2, *Eurocode No. 2, Design of Concrete Structures*, December 1989.

[9] Boussouf, A-H., *Long-Term Deflection Analysis of Reinforced Concrete Flat Plates Under Construction Loads*, M.A.Sc. Thesis, Department of Civil Engineering, University of Ottawa, Ottawa, Ontario, Canada, March 1990.

[10] Branson, D.E., *Design Procedures for Computing Deflection*, ACI Journal, Proceedings V. 65, No. 9, September 1968, pp. 730-742.

[11] Branson, D.E., and Christianson, M.L., *Concrete Properties Related to Design Strength and Elastic Properties - Creep and Shrinkage*, Designing for Effects of Creep, Shrinkage, and Temperature in Concrete Structures, SP-27, American Concrete Institute, Detroit, 1971, pp. 257-277.

[12] Bryant, A.H., and Vadhanavikkit, C., *Creep, Shrinkage-Size, and Age at Loading Effects*, ACI Material Journal, March-April 1987.

[13] CEB-FIP Model Code for Concrete Structures 1990, *Evaluation of the Time-Dependent Behaviour of Concrete*, Bulletin d'Information No. 199, Comite Euro du Beton / Federation Internationale de la Precontrainte, Laussanne, 1991, 201 pp.

[14] Chen, W.F., *Plasticity in Reinforced Concrete*, McGraw-Hill Inc., New York, 1982.

[15] *Code for the Design of Concrete Structures for Buildings*, (CSA A23.3-M84), Canadian Standards Association, Rexdale, 1984.

[16] C.S.I.R.O., *Experimental Lightweight Flat Plate Structure* Mechanics and Physics Section of the Division of Building Research, Commonwealth Scientific and Industrial Research Organization Construction Review,
Part 1 : *Measurements and Observations During Erection*, vol. 34, No. 1, January 1961, pp. 21-32
Part 2 : *Deformations Due to Self Weigth*, vol. 34, No. 3, March 1961, pp. 25-32,
Part 3 : *Long-Term Deformations*, vol. 34, No. 4, April 1961, pp. 21-26.

[17] Darwin, D. and Pecknold, D.A., *Inelastic Model for Cyclic Biaxial Loading of Reinforced Concrete*, SRS No. 409, University of Illinois at Urbana-Champaign, Illinois, July 1974.

[18] Darwin, D., and Pecknold, D.A., *Nonlinear Biaxial Stress-Strain Law for Concrete*, Journal of the Engineering Mechanics Division, ASCE, vol. 103, No. EM2, April 1977, pp. 229-241.

[19] Fu, H.C., *Effects of High Construction Loads on the Short-Term and Long-Term Deflection of Slabs*, Ph.D Thesis, Department of Civil Engineering, University of Ottawa, Ottawa, Ontario, Canada, 1985.

[20] Fu, H.C., and Gardner, N.J., *Effects of Construction Loads on the Long Term Behaviour of Slab Structures*, Concrete at Early Ages, SP-95, American Concrete Institute, Detroit, 1986, pp. 173-200.

[21] Gardner, N.J., *Control of Construction Loads on Multifloor Buildings*, Canadian Journal of Civil Engineering, V. 6, 1979, pp. 253-259.

[22] Gardner, N.J., *Shoring, Reshoring and Safety,* Concrete International, April 1985.

[23] Gardner, N.J., and Fu H.C., *Effects of High Construction Loads on the Long-Term Deflections of Flat Slabs,* ACI Structural Journal, vol. 84, No. 4, July-August 1987, pp. 349-360.

[24] Gardner, N.J., and Zhao, J-W., *Shrinkage and Creep Revisited,* ACI Materials Journal, May-June 1993.

[25] Gilbert, R.I.,and Warner, R.F., *Tension Stiffening in Reinforced Concrete Slabs,* ASCE, V. 104, December 1978, pp. 1885-1900.

[26] Gilbert, R.I., *Computer Experiments with Reinforced Concrete Slabs,* UNICIV Report No. R-195, School of Civil Engineering, University of New South Wales, Sydney, March 1980, 64 pp.

[27] Gilbert, R.I., *Deflection Control of Slabs Using Allowable Span-to-Depth Ratios,* ACI Journal, Proceedings V. 75, No. 1, January-Feburary 1985, pp. 559-569.

[28] Gopalakrishnan, K.S., Neville, A.M., and Ghali, A., *Creep Poisson's Ratio for Concrete Under Multiaxial Compression,* ACI Journal, V. 66, No. 12, December 1969.

[29] Graham, C.J., and Scanlon, A., *Long Time Multipliers for Estimating Two-Way Slab Deflections,* ACI Journal, Proceedings V. 83, No. 6, November-December 1986, pp. 899-908.

[30] Grundy, P., and Kabaila, A., *Construction Loads on Slabs with Shored Formwork in Multi-storey Buildings,* ACI Journal, Proceedings V. 60, No. 12, December 1963, pp. 1729-1738.

[31] Heiman, J.L., and Taylor, P.J., *Long-Term Deflections of a Reinforced Concrete Flat Plate*, Architectural Science Review, Sydney, vol. 15, No. 2, June 1972, pp. 25-29.

[32] Hognestad, E., *A Study of Combined Bending and Axial Load in Reinforced Concrete Members*, Bulletin Series No. 399, Bulletin No. 1, Engineering Experiment Station, University of Illinois, 1951.

[33] Jofriet, J.C., and McNeice, G.M., *Finite Element Analysis of Reinforced Concrete Slabs*, Proceedings, ASCE, V. 97, ST3, March 1971, pp. 785-806.

[34] Jokinen, E.P., and Scanlon, A., *Field Measured Two-way Slab Deflections*, Canadian Journal of Civil Engineering, V. 14, No. 6, December 1987, pp. 807-819.

[35] Kabir, A.F., *Nonlinear Analysis of Reinforced Concrete Slabs and Shells for Time Dependent Effects*, Ph.D Dissertation, Division of Structural Engineering and Structural Mechanics, University of California, Berkeley, June 1977.

[36] Ketchum, M.A., *Redistribution of Stresses in Segmentally Erected Prestressed Concrete Bridges*, Ph.D Dissertation, Division of Structural Engineering and Structural Mechanics, University of California, Berkeley, June 1986.

[37] Kupfer, H.B., Hilsdrof, H.K., and Rusch, H., *Behaviour of Concrete Under Biaxial Stress*, ACI Journal, V. 66, No. 8, August 1969, pp. 656-666.

[38] Kupfer, H.B., and Gerstle, K.H., *Behaviour of Concrete Under Biaxial Stresses*, Journal of the Engineering Mechanics Division, ASCE, V. 99, No. EM4, August 1973.

[39] Lin, C.S., *Nonlinear Analysis of Reinforced Concrete Slabs and Shells*, Ph.D Dissertation, Division of Structural Engineering and Structural Mechanics, University of California, Berkeley, September 1972.

[40] Mayer, H., and Rusch, H., *Building Damage Caused by Deflection of Reinforced Concrete Building Components*. Technical Translation 1412 by J.H. Rainer, National Research Council, Ottawa, Canada, 1970.

[41] Mukhaddam, M.A., and Bresler, B., *Behaviour of Concrete under Variable Temperature and Loading,* ACI Seminar on Concrete for Nuclear Reactors, ACI Special Publication SP-34, 1972.

[42] Rangan, B.V., *Prediction of Long Term Deflections of Flat Plates and Slabs,* ACI Journal, Proceedings V. 73, No. 4, April 1976, pp. 686-690.

[43] Razzaque, A., *Program for Triangular Bending Elements with Derivative Smoothing*, Int. J. Num. Meth. Eng., V. 6, 1973, pp. 333-343.

[44] Ross, A.D., *Creep of Concrete Under Variable Stress,* ACI Journal, V. 64, No. 9, March 1958.

[45] Sbarounis, J.A., *Multi-storey Flat Plate Buildings - Construction Loads and Immediate Deflections,* Concrete International, V. 6, No. 2, February 1984, pp. 70-77.

[46] Sbarounis, J.A., *Multi-storey Flat Plate Building - Effect of Construction Loads on Longterm Deflections,* Concrete International: Design and Construction, V. 6, No. 4, April 1984, pp. 62-70.

[47] Scanlon, A., *Time Dependent Deflections of Reinforced Concrete Slabs, Ph.D Thesis,* Department of Civil Engineering, University of Alberta, Edmonton, Alberta, Canada, Structural Engineering Report, No. 38, December, 1971.

[48] Scanlon, Andrew, and Thompson, David P., *Evaluation of ACI-318 Requirements for Control of Two-Way Slab Deflections,* ACI Structural Journal, V. 87, No. 6, November-December 1990, pp. 657-661.

[49] Shao, X.Y., *Punching Shear Strength of Reinforced Concrete Slab*, M.A.Sc. Thesis, Department of Civil Engineering, University of Ottawa, Ottawa, Ontario, Canada, 1993.

[50] Taylor, P.J., *Long Term Deflection Calculation Methods for Flat Plates*, Constructional Review, Technical Supplement, Sydney, V. 43, No. 2, May 1970, pp. 68-74.

[51] Taylor, P.J., *Initial and Long-Term Deflections of a Reinforced Concrete Flat Plate Structure*, Paper No. 2794, Conference on the Deformation of Concrete and Concrete Structures, The Institution of Engineers Australia, Brisbane, September 1969, Civil Engineering Transactions, The Institution of Engineers Australia, vol. CE12, No. 1, April 1970, pp. 16-22.

[52] Taylor, P.J., and Heiman, J.L., *A Long-Term Investigation of Deflections of a Flat-Slab Structure*, Proceedings, Fourth Australian Building Research Congress, Sydney, August 1970, pp. 27-31.

[53] Thompson, David P., and Scanlon, Andrew, *Minimum Thickness Requirements for Control of Two-Way Slab Deflections*, ACI Structural Journal, V. 85, No. 1, January-February 1988, pp. 12-22.

[54] Van Greunen, J., *Time Dependent Analysis of Reinforced and Prestressed Concrete Slabs and Panels*, Ph.D Dissertation, Division of Structural Engineering and Structural Mechanics, University of California, Berkeley, UC-SESM Report No. 79-3, October 1979.

[55] Volterra, V., *Sur les Equations Integro-Differentielles et Leurs Applications*, Acta Mathematica, Stockholm, 1912.

[56] Wilson, E.L., *Solid SAP - A Static Analysis Program for Three Dimensional Solid Structures*, UC-SESM Report No. 71-19, University of California, Berkeley, March 1972.

[57] Zienkiewicz, O.C., *The Finite Element Method in Engineering Science*, McGraw-Hill Publishing Co., Ltd., London, 1988.

[58] Zienkiewicz, O.C., and Watson, M., *Some Creep Effects in Stress Analysis with Particular Reference to Concrete Pressure Vessels*, Nuclear Engineering and Design, No. 4, 1966.

SUGGESTED BIBLIOGRAPHY

[59] ACI Committee 435, *Deflections of Reinforced Concrete Flexural Members*, ACI Journal, Proceedings V. 63, No. 6, June 1966, pp. 637-674.

[60] ACI Committee 209, *Prediction of Creep, Shrinkage, and Temperature Effects in Concrete Structures*, SP-27, American Concrete Institute, Detroit, 1971, pp. 51-93.

[61] ACI Committee 435, *Deflection of Two-Way Reinforced Concrete Floor Systems*, State-of-the-Art Report, ACI 435.6R-74 (Reapproved 1989), American Concrete Institute, Detroit, 1974.

[62] ACI Committee 209, *Designing for Creep and Shrinkage in Concrete Structures*, SP-76, American Concrete Institute, Detroit, 1971, pp. 193-300.

[63] Arutyunyan, A., *Some Problems in the Theory of Creep in Concrete Structures*, Pergammon Press, New York, 1966.

[64] Bell, J.C., *A Complete Analysis of Reinforced Concrete Slabs*, Ph.D Dissertation, Department of Civil Engineering, University of Canterbury, Christchurch, New Zealand, 1970.

[65] Bergan, P.G., *Nonlinear Analysis of Plates Considering Geometric and Material Effects*, Ph.D Dissertation, UC-SESM Report No. 71-7, University of California, Berkeley, April, 1971.

[66] Beresford, F.D., *Experimental Lightweight Flat Plate Structure, Part V - Deformations under Lateral Load*, Constructional Review (Sydney), vol. 35, No. 2, December 1962, pp. 17-23.

[67] Beresford, F.D., and Blakey, F.A., *Experimental Lightweight Flat Plate Structure, Part VII - A Test to Destruction*, Constructional Review (Sydney), vol. 36, No. 6, June 1963, pp. 18-26.

[68] Beresford, F. D., *An Analytical Examination of Propped Floors in Multi-storey Flat Plate Construction*, Constructional Review, North Sydney, V. 37, No. 11, November 1964, pp. 16-20.

[69] Beresford, F. D., *Shoring and Reshoring of Floors in Multi-storey Buildings*, Symposium on Formwork, Concrete Institute of Australia, North Sydney, April 1971, 14 pp.

[70] Blakey, F.A., *Deformations of an Experimental Lightweight Flat Plate Structure*, Civil Engineering Transactions (Sydney), Institution of Engineers Australia, vol. CE3, No. 1, March 1961, pp. 18-22.

[71] Blakey, F.A., *Australian Experiments with Flat Plates*, ACI Journal, Proceedings vol. 60, No. 4, April 1963, pp. 515-525.

[72] Blakey, F.A. *The Deflection of Flat Plate Structures*, Civil Engineering and Public Works Review, vol. 58, September 1963, pp. 1133-1136.

[73] Blakey, F. A., and Beresford, F. D., *Stripping of Formwork for Concrete in Buildings in Relation to Structural Design*, Civil Engineering Transactions, Institution of Engineers Australia, V. CE7, No. 2, October 1965, pp. 92-96.

[74] Branson, D.E., *Design Procedures for Computing Deflection*, ACI Journal, Proceedings V. 65, No. 9, September 1968, pp. 730-742.

[75] Bryant, A.H., *Creep and Shrinkage of a Bridge-Building Concrete*, ACI Journal, Proceedings V. 76, No. 3, March 1979, pp. 387-403.

[76] Byfors, J., *Plain Concrete at Early Ages*, Swedish Cement and Concretes Research Institute, Fo.3, No. 80, 1980, 566 pp.

[77] Committee 25 of the Council on Tall Buildings and Urban Habitat, *Creep, Shrinkage, and Temperature Effects*, Chapter CB-10, Monograph on Planning and Design of Tall Buildings, vol. CB, American Society of Civil Engineers, New York, 1978, pp. 425-500.

[78] *Draft for Australian Standard for Concrete Structures, (AS 1480)*, Standards Association of Australia, Sydney, Australia, 1985.

[79] *Experimental Flat Plate Structure of Expanded Shale Concrete*, Constructional Review (Sydney), vol. 33, No. 2, February 1960, pp. 22-29.

[80] *Experimental Lightweight Flat Plate Structure, Part I - Measurements and Observations During Construction*, Constructional Review (Sydney), vol. 34, No. 1, January 1961, pp. 21-32.

[S1] *Experimental Lightweight Flat Plate Structure. Part II - Deformations due to Self Weight*, Constructional Review (Sydney), vol. 34, No 3, March 1961, pp. 25-33.

[S2] *Experimental Lightweight Flat Plate Structure. Part III - Long-Term Deformations*, Constructional Review (Sydney), vol. 34, No. 4, April 1961, pp. 21-26.

[S3] *Experimental Lightweight Flat Plate Structures, Part IV - Design and Erection of Structures with Concrete Columns*, Constructional Review (Sydney), vol. 35, No. 1, January 1962, pp. 29-33.

[S4] Ferguson, P.M., *Reinforced Concrete Fundamentals*, 4th Edition, John Wiley and Sons, New York, 1979.

[S5] Fintel, M., Ghosh, S.K., and Iyenger, H., *Column Shortening in Tall Structures - Prediction and Compensation,* Publication EB108, Portland Cement Association, Skokie, Illinois, 1985.

[S6] Franklin, H.A., *Nonlinear Analysis of Reinforced Concrete Frames and Panels*, Ph.D Dissertation, Division of Structural Engineering and Structural Mechanics, University of California, Berkeley, March 1970.

[S7] Gardner, N.J., and Ofosu-Asamoah, K., *Proposed Code Provisions for Slab Span Thickness Limitations Including Early-Age Construction Loads*, Paper Presented at ACI Spring Convention in Washington D.C., March 1992.

[S8] Gardner, N.J., and Poon, S.M., *Time and Temperature Effects on Tensile, Bond, and Compressive Strength*, ACI Journal, Proceedings V. 73, No. 7, July 1976, pp. 405-409.

[89] Gardner, N.J., Sau, P.L., and Cheung, M.S., *Strength Development and Durability of Concretes Cast and Cured at* 0^0 *C*, ACI Materials Journal, November-December 1988, pp. 529-536.

[90] Griffiths, D.V., and Smith, I.M., *Numerical Methods for Engineers, A Programming Approach*, University of Manchester, Blackwell Scientific Publications, Inc., 1991.

[91] Hand, F.R., Pecknold, D.A., and Schnobrich, W.C., *Nonlinear Layered Analysis of Reinforced Concrete Plates and Shells,* Proceedings, ASCE, V. 99 ST7, July 1973, pp. 1491-1505.

[92] Heiman, J.L., *Long-Term Deformations in the Tower Building, Australia Square, Sydney,* ACI Journal, Proceedings, vol. 70, No. 4, April 1973, pp. 279-284.

[93] Heiman, J.L., *A Comparison of Measured and Calculated Deflections of Flexural Members in Four Reinforced Concrete Buildings,* Deflections of Concrete Structures, SP-43, American Concrete Institute, Detroit, 1974, pp. 515-545.

[94] Irons, B., and Ahmad, S., *Techniques of Finite Elements,* Ellis Horwood Limited, Wiley and Sons, New York, U.S.A., 1980.

[95] Kripanarayanan, K.M., and Branson, D.E., *Short Time Deflections of Flat Plates, Flat Slabs, and Two-Way Slabs,* ACI Journal, Proceedings V. 73, No. 12, December 1976, pp. 686-690.

[96] Lasisi, M. Y., and Ng, S. F., *Construction Loads Imposed on High-Rise Floor Slabs,* Concrete International, V. 1, No. 2, February 1979, pp. 24-29.

[97] Lewis, R.K., *Experimental Lightweight Flat Plate Structure. Part VI - Design and Erection of a Post-tensioned Flat Plate*, Constructional Review (Sydney), vol. 36, No. 3, March 1963, pp. 21-24.

[98] Marosszeky, M., *Construction Loads in Multi-storey Structures*, Civil Engineering Transactions, Institution of Engineers Australia, V. CE14, No. 1, April 1972, pp. 91-93.

[99] Metz, G.A., *Instantaneous and Time-Dependent Deflections of Simple and Continuous Reinforced Concrete Beams, PART-II*, Alabama Highway Research Report No.7, Dept. of Civil Engineering, Auburn University, June 1965.

[100] Mufti, A.A., et al., *A Study of the Behaviour of Reinforced Concrete Elements using Finite Elements*, Structural Concrete Series No. 70-5, McGill University, Montreal, Canada, September 1970.

[101] Mufti, A.A., Mirza, M.S., McCutcheon, J.O., and Houde, J., and Spokowski, R.W., *A Finite Element Study of Reinforced Concrete Structures*, Structural Concrete Series No. 71-8, McGill University Montreal, Canada, October 1971.

[102] Mukaddam, M., *Creep Analysis of Concrete at Elevated Temperatures*, ACI Journal, V. 71, No. 2, February 1974.

[103] Murray, D.W., *Large Deflection Analysis of Plates*, Ph.D Dissertation, Report No. 67-44, Department of Civil Engineering, University of California, Berkeley, September 1967.

[104] Nielsen, K. E. C., *Loads on Reinforced Concrete Floor Slabs and Their Deformations During Construction*, Proceedings No. 15, Swedish Cement and Concrete Research Institute, Stockholm, 1952, 113 pp.

[105] Nilson, A.H., and Walters, D.B. Jr., *Deflection of Two-Way Floor Systems by the Equivalent Frame Method*, ACI Journal, Proceedings V. 72, No. 5, May 1975, pp 210-218.

[106] Pfeifer, D. W., and Hognestad, E., *Incremental Loading of Reinforced Lightweight Concrete Columns*, Lightweight Concrete, Special Publication SP-29, 1971, pp. 35-45.

[107] Rajagopal, K.R., *Nonlinear Analysis of Reinforced Concrete Beams, Beam-Columns and Slabs by Finite Elements*, Ph.D Dissertation, Iowa State University, Ames, Iowa, 1976.

[108] *Reinforced Concrete Floor Slabs - Research and Design*, American Society of Civil Engineers, The Reinforced Concrete Research Council, Bulletin No. 20, New York, 1969.

[109] RILEM Commission 42-CEA, *Properties of Set Concrete at Early Ages: State-of-the-Art Report*, Materials and Structures, V. 14, No. 84, November-December 1981, pp. 399-450.

[110] Russell, H. G., and Corley, W. G., *Time-Dependent Behavior of Columns in Water Tower Place*, Research and Development Bulletin RD 052.01B, Portland Cement Association, Skokie, Illinois, 1977.

[111] Scanlon, A., and Murray, D.W., *Time Dependent Reinforced Concrete Deflections*, Proceedings, ASCE, V. 100, ST9, September 1974, pp. 1911-1924.

[112] Scanlon, A., and Murray, D.W., *Practical Calculation of Two-Way Slab Deflections*, Concrete International: Design and Construction, V. 4, No. 11, November 1982, pp. 43-50.

[113] Scanlon, A., and Thompson, D.P., *Evolution of Minimum Thickness Requirements for Control of Deflections*, Proceedings, Centennial Conference, Canadian Society of Civil Engineering, Montreal, May 1987.

[114] Scordelis, A.C., *Finite Element Analysis of Reinforced Concrete Structures*, Proceedings of the Speciality Conference on Finite Element Methods in Civil Engineering, Montreal, Canada, June 1972.

[115] Selna, L.G., *Time Dependent Behaviour of Reinforced Concrete Structures*, SESM Report No. 67-19, University of California, Berkeley, August 1967.

[116] Tam, Stephen K.S., and Scanlon, Andrew, *Deflection of Two-Way Slabs Subjected to Restrained Volume Change and Transverse Loads*, ACI Journal, Proceedings V.83, No.5, September-October 1986, pp. 737-744.

[117] Taylor, P.J., *Effects of Formwork Stripping Time on Deflection of Flat Slabs and Plates*, Australian Civil Engineering and Construction, Melbourne, V. 8, No. 2, February 1967, pp. 31-35.

[118] Taylor, P.J., *Initial Deflection Calculation Methods for a Reinforced Concrete Flat Plate*, Constructional Review,.Sydney, V. 43, No. 1, February 1970, pp. 66-71.

[119] Taylor, P.J., *The Initial and Long-Term Deflections of Reinforced Concrete Flat Slabs and Plates*, ME Thesis, University of New South Wales, Kensington, 1971, 179 pp.

[120] Taylor, P.J., and Heiman, J.L., *A Long-Term Deflection of Reinforced Concrete Flat Slabs and Plates*, ACI Journal, V. 74, No. 11, November 1977, pp. 556-561.

[121] Troxell, G.E., Raphael, J.M., and Davis, R.E., *Long-Time Creep and Shrinkage Tests of Plain and Reinforced Concrete*, Proceedings, ASTM, V. 58, 1958.

[122] Vanderbilt, M.D., Sozen, M.A., and Seiss, C.P., *Deflections of Multiple-Panel Reinforced Concrete Floor Slabs,* Proceedings, ASCE Structural Division, V. 91, No. ST4, August 1965, pp. 77-101.

[123] Wheen, R. J., *Invention to Control Construction Floor Loads in Tall Concrete Buildings*, Concrete International, V. 4, No. 5, May 1982, pp. 56-62.

[124] Yamamoto, T., *Longterm Deflections of Reinforced Concrete Slabs Subjected to Overloading at an Early Age*, International Conference on Concrete at Early Ages, RILEM, Ecole Nationale des et Chausses, Paris, April 1982, vol. 1, pp. 103-108.

[125] Yang, T.Y., *Finite Element Structural Analysis*, Prentice-Hall Inc., Englewood Cliffs, N.J., 1986.

[126] Zhao, J-W., *Mechanical Properties of Concrete at Early Ages*, M.A.Sc. Thesis, Department of Civil Engineering, University of Ottawa, Ottawa, Ontario, Canada, March 1990.

Appendix A

SLAB DETAILS

Table A.1: Slab Details (Square Panels)

Slab ID	Span Lengths (ins)		Slab Thickness (ins)	Age of Loading (days)	28-Day Compressive Strength (psi)	Drop Panel Included
	l_x	l_y				
SS-A1	236.0	236.0	7.0	3	3000	No
SS-A2	236.0	236.0	8.4	3	3000	No
SS-A3	236.0	236.0	8.6	3	3000	No
SS-A4	236.0	236.0	8.2	3	3000	No
SS-A5	236.0	236.0	8.5	3	3000	No
SS-A6	236.0	236.0	7.0	4	3000	No
SS-A7	236.0	236.0	8.0	4	3000	No
SS-A8	236.0	236.0	7.6	4	3000	No
SS-A9	236.0	236.0	7.8	4	3000	No
SS-A10	236.0	236.0	7.7	4	3000	No
SS-A11	236.0	236.0	6.0	7	3000	No
SS-A12	236.0	236.0	6.6	7	3000	No
SS-A13	236.0	236.0	7.0	7	3000	No
SS-A14	236.0	236.0	6.8	7	3000	No
SS-A15	236.0	236.0	6.0	14	3000	No
SS-A16	236.0	236.0	5.8	14	3000	No
SS-A17	236.0	236.0	5.9	14	3000	No
SS-A18	236.0	236.0	5.4	28	3000	No

Table A.2: Slab Details (Square Panels)

Slab ID	Span Lengths (ins)		Slab Thickness (ins)	Age of Loading (days)	28-Day Compressive Strength (psi)	Drop Panel Included
	l_x	l_y				
SS-A19	236.0	236.0	5.6	28	3000	No
SS-A20	236.0	236.0	5.5	28	3000	No
SS-A21	236.0	236.0	7.8	3	3500	No
SS-A22	236.0	236.0	7.4	3	3500	No
SS-A23	236.0	236.0	7.6	3	3500	No
SS-A24	236.0	236.0	7.5	3	4000	No
SS-A25	236.0	236.0	6.6	3	4000	No
SS-A26	236.0	236.0	6.8	3	4000	No
SS-A27	236.0	236.0	7.0	3	4000	No
SS-B1	354.0	354.0	13.4	3	3000	No
SS-B2	354.0	354.0	15.8	3	3000	No
SS-B3	354.0	354.0	16.0	3	3000	No
SS-B4	354.0	354.0	13.0	4	3000	No
SS-B5	354.0	354.0	14.6	4	3000	No
SS-B6	354.0	354.0	14.7	4	3000	No
SS-B7	354.0	354.0	14.8	4	3000	No
SS-B8	354.0	354.0	9.0	7	3000	No
SS-B9	354.0	354.0	10.0	7	3000	No

Table A.3: Slab Details (Square Panels)

Slab ID	Span Lengths (ins)		Slab Thickness (ins)	Age of Loading (days)	28-Day Compressive Strength (psi)	Drop Panel Included
	l_x	l_y				
SS-B10	354.0	354.0	12.0	7	3000	No
SS-B11	354.0	354.0	12.9	7	3000	No
SS-B12	354.0	354.0	12.0	14	3000	No
SS-B13	354.0	354.0	11.6	14	3000	No
SS-B14	354.0	354.0	11.4	14	3000	No
SS-B15	354.0	354.0	11.5	14	3000	No
SS-B16	354.0	354.0	10.0	28	4000	No
SS-B17	354.0	354.0	10.4	28	4000	No
SS-B18	354.0	354.0	10.3	28	4000	No
SS-B19	354.0	354.0	14.4	3	3500	No
SS-B20	354.0	354.0	13.8	3	3500	No
SS-B21	354.0	354.0	14.0	3	4000	No
SS-B22	354.0	354.0	12.8	3	4000	No
SS-C1	472.0	472.0	21.6	3	3000	No
SS-C2	472.0	472.0	22.3	3	3000	No
SS-C3	472.0	472.0	22.5	3	3000	No
SS-C4	472.0	472.0	22.7	3	3000	No

Table A.4: Slab Details (Square Panels)

Slab ID	Span Lengths (ins)		Slab Thickness (ins)	Age of Loading (days)	28-Day Compressive Strength (psi)	Drop Panel Included
	l_x	l_y				
SS-C5	472.0	472.0	19.0	4	3000	No
SS-C6	472.0	472.0	21.0	4	3000	No
SS-C7	472.0	472.0	21.8	4	3000	No
SS-C8	472.0	472.0	21.2	4	3000	No
SS-C9	472.0	472.0	21.3	4	3000	No
SS-C10	472.0	472.0	16.0	7	3000	No
SS-C11	472.0	472.0	17.8	7	3000	No
SS-C12	472.0	472.0	18.5	7	3000	No
SS-C13	472.0	472.0	18.7	7	3000	No
SS-C14	472.0	472.0	18.0	14	3000	No
SS-C15	472.0	472.0	17.4	14	3000	No
SS-C16	472.0	472.0	17.1	14	3000	No
SS-C17	472.0	472.0	17.2	14	3000	No
SS-C18	472.0	472.0	15.7	28	3000	No
SS-C19	472.0	472.0	15.5	28	3000	No
SS-C20	472.0	472.0	15.0	28	3000	No

Table A.5: Slab Details (Square Panels)

Slab ID	Span Lengths (ins) l_{xn}	Span Lengths (ins) l_{yn}	Slab Thickness (ins)	Age of Loading (days)	28-Day Compressive Strength (psi)	Drop Panel Included
DP-A1	236.0	236.0	6.4	7	3000	No
DP-A2	236.0	236.0	5.6	7	3000	No
DP-A3	236.0	236.0	5.8	7	3000	Yes
DP-A4	236.0	236.0	5.7	7	3000	Yes
DP-B1	354.0	354.0	12.6	7	3000	Yes
DP-B2	354.0	354.0	10.7	7	3000	Yes
DP-B3	354.0	354.0	10.8	7	3000	Yes
DP-B4	354.0	354.0	10.9	7	3000	Yes
DP-C1	472.0	472.0	18.0	7	3000	Yes
DP-C2	472.0	472.0	16.8	7	3000	Yes
DP-C3	472.0	472.0	15.6	7	3000	Yes
DP-C4	472.0	472.0	15.7	7	3000	Yes
ACI-S1	236.0	236.0	17.2	7	3000	No
ACI-S2	236.0	236.0	15.7	7	3000	No
ACI-S3	236.0	236.0	15.5	7	3000	No
ACI-S4	354.0	354.0	15.0	7	3000	No
ACI-S5	354.0	354.0	15.5	7	3000	No
ACI-S6	354.0	354.0	15.0	7	3000	No

Table A.6: Slab Details (Rectangular Panels)

Slab ID	Span Lengths (ins) l_x	Span Lengths (ins) l_y	Slab Thickness (ins)	Age of Loading (days)	28-Day Compressive Strength (psi)	Panel Aspect Ratio
RS-A1	157.3	236.0	6.2	4	3000	1.5
RS-A2	157.3	236.0	6.4	4	3000	1.5
RS-A3	157.3	236.0	6.6	4	3000	1.5
RS-A4	157.3	236.0	7.0	4	3000	1.5
RS-A5	157.3	236.0	6.8	4	3000	1.5
RS-A6	157.3	236.0	6.7	4	3000	1.5
RS-A7	157.3	236.0	7.0	7	3000	1.5
RS-A8	157.3	236.0	6.4	7	3000	1.5
RS-A9	157.3	236.0	6.0	7	3000	1.5
RS-A10	157.3	236.0	5.8	7	3000	1.5
RS-A11	157.3	236.0	5.4	14	3000	1.5
RS-A12	157.3	236.0	5.0	14	3000	1.5
RS-A13	157.3	236.0	5.2	14	3000	1.5
RS-A14	157.3	236.0	5.4	28	3000	1.5
RS-A15	157.3	236.0	4.7	28	3000	1.5
RS-A16	157.3	236.0	4.8	28	3000	1.5

Table A.7: Slab Details (Rectangular Panels)

Slab ID	Span Lengths (ins)		Slab Thickness (ins)	Age of Loading (days)	28-Day Compressive Strength (psi)	Panel Aspect Ratio
	l_x	l_y				
RS-A17	118.0	236.0	6.0	4	3000	2.0
RS-A18	118.0	236.0	6.6	4	3000	2.0
RS-A19	118.0	236.0	6.4	4	3000	2.0
RS-A20	118.0	236.0	6.2	4	3000	2.0
RS-A21	118.0	236.0	7.0	7	3000	2.0
RS-A22	118.0	236.0	5.6	7	3000	2.0
RS-A23	118.0	236.0	5.4	7	3000	2.0
RS-A24	118.0	236.0	5.0	14	3000	2.0
RS-A25	118.0	236.0	4.8	14	3000	2.0
RS-A26	118.0	236.0	4.7	14	3000	2.0
RS-A27	118.0	236.0	5.2	28	3000	2.0
RS-A28	118.0	236.0	4.6	28	3000	2.0
RS-A29	118.0	236.0	4.4	28	3000	2.0
RS-A30	118.0	236.0	4.5	28	3000	2.0
RS-B1	157.3	236.0	12.0	4	3000	1.5
RS-B2	157.3	236.0	12.6	4	3000	1.5

Table A.8: Slab Details (Rectangular Panels)

Slab ID	Span Lengths (ins)		Slab Thickness (ins)	Age of Loading (days)	28-Day Compressive Strength (psi)	Panel Aspect Ratio
	l_x	l_y				
RS-B3	236.0	354.0	12.8	4	3000	1.5
RS-B4	236.0	354.0	13.0	4	3000	1.5
RS-B5	236.0	354.0	13.2	4	3000	1.5
RS-B6	236.0	354.0	10.0	7	3000	1.5
RS-B7	236.0	354.0	11.0	7	3000	1.5
RS-B8	236.0	354.0	11.6	7	3000	1.5
RS-B9	236.0	354.0	11.7	7	3000	1.5
RS-B10	236.0	354.0	10.7	14	3000	1.5
RS-B11	236.0	354.0	10.2	14	3000	1.5
RS-B12	236.0	354.0	10.3	14	3000	1.5
RS-B13	236.0	354.0	9.0	28	3000	1.5
RS-B14	236.0	354.0	9.6	28	3000	1.5
RS-B15	177.0	354.0	12.0	4	3000	2.0
RS-B16	177.0	354.0	11.5	4	3000	2.0
RS-B17	177.0	354.0	11.6	4	3000	2.0
RS-B18	177.0	354.0	10.0	7	3000	2.0

Table A.9: Slab Details (Rectangular Panels)

Slab ID	Span Lengths (ins)		Slab Thickness (ins)	Age of Loading (days)	28-Day Compressive Strength (psi)	Panel Aspect Ratio
	l_x	l_y				
RS-B19	177.0	354.0	10.6	7	3000	2.0
RS-B20	177.0	354.0	11.0	7	3000	2.0
RS-B21	177.0	354.0	11.1	7	3000	2.0
RS-B22	177.0	354.0	11.2	7	3000	2.0
RS-B23	177.0	354.0	10.2	14	3000	2.0
RS-B24	177.0	354.0	9.6	14	3000	2.0
RS-B25	177.0	354.0	9.9	14	3000	2.0
RS-B26	177.0	354.0	9.0	28	3000	2.0
RS-B27	177.0	354.0	9.2	28	3000	2.0
RS-C1	314.7	472.0	18.0	4	3000	1.5
RS-C2	314.7	472.0	18.3	4	3000	1.5
RS-C3	314.7	472.0	15.0	7	3000	1.5
RS-C4	314.7	472.0	16.2	7	3000	1.5
RS-C5	314.7	472.0	16.3	7	3000	1.5
RS-C6	314.7	472.0	16.4	7	3000	1.5
RS-C7	314.7	472.0	15.2	14	3000	1.5
RS-C8	314.7	472.0	14.8	14	3000	1.5

Table A.10: Slab Details (Rectangular Panels)

Slab ID	Span Lengths (ins)		Slab Thickness (ins)	Age of Loading (days)	28-Day Compressive Strength (psi)	Panel Aspect Ratio
	l_x	l_y				
RS-C9	314.7	472.0	13.0	28	3000	1.5
RS-C10	314.7	472.0	13.6	28	3000	1.5
RS-C11	314.7	472.0	13.7	28	3000	1.5
RS-C12	236.0	472.0	17.6	4	3000	2.0
RS-C13	236.0	472.0	17.5	4	3000	2.0
RS-C14	236.0	472.0	15.0	7	3000	2.0
RS-C15	236.0	472.0	15.4	7	3000	2.0
RS-C16	236.0	472.0	16.2	7	3000	2.0
RS-C17	236.0	472.0	16.3	7	3000	2.0
RS-C18	236.0	472.0	16.5	7	3000	2.0
RS-C19	236.0	472.0	14.8	14	3000	2.0
RS-C20	236.0	472.0	14.0	14	3000	2.0
RS-C21	236.0	472.0	14.2	14	3000	2.0
RS-C22	236.0	472.0	14.0	28	3000	2.0
RS-C23	236.0	472.0	13.2	28	3000	2.0
RS-C24	236.0	472.0	13.0	28	3000	2.0
RS-C25	236.0	472.0	13.1	28	3000	2.0

Appendix B

REINFORCEMENT DETAILS

Table B.1: Reinforcement Detail (Square Slabs)

Slab ID	Steel System Number	Reinforcement Areas (in^2/in)			
		Top X-Direction	Top Y-Direction	Bottom X-Direction	Bottom Y-Direction
SS-A26	1	0.02420	0.02420	0.01360	0.01360
	2	0.01360	0.01360	0.02904	0.01360
	3	0.04887	0.02420	0.01360	0.01360
	4	0.01360	0.01360	0.01360	0.02904
	5	-	-	0.01936	0.01936
	6	0.01629	0.01360	0.01360	0.02904
	7	0.02420	0.04887	0.01360	0.01360
	8	0.01360	0.01629	0.02904	0.01360
	9	0.04887	0.04887	0.01360	0.01360
SS-B22	1	0.03874	0.03874	0.02560	0.02560
	2	0.02560	0.02560	0.04648	0.02560
	3	0.07822	0.03874	0.02560	0.02560
	4	0.02560	0.02560	0.02560	0.04648
	5	-	-	0.03099	0.03099
	6	0.02607	0.02560	0.02560	0.04648
	7	0.03874	0.07822	0.02560	0.02560
	8	0.02560	0.02607	0.04648	0.02560
	9	0.07822	0.07822	0.02560	0.02560

Table B.2: Reinforcement Detail (Rectangular Slabs)

Slab ID	Steel System Number	Reinforcement Areas (in^2/in)			
		Top X-Direction	Top Y-Direction	Bottom X-Direction	Bottom Y-Direction
RS-A17	1	0.01951	0.03326	0.00960	0.00960
	2	0.00960	0.00960	0.02341	0.00960
	3	0.03940	0.03326	0.00960	0.00960
	4	0.00960	0.00960	0.00960	0.03991
	5	-	-	0.00960	0.01330
	6	0.00960	0.00960	0.00960	0.03991
	7	0.01951	0.06716	0.00960	0.00960
	8	0.00960	0.01119	0.02341	0.00960
	9	0.03940	0.06716	0.00960	0.00960
RS-B14	1	0.02569	0.04396	0.01920	0.01920
	2	0.01920	0.01920	0.03083	0.01920
	3	0.05188	0.04396	0.01920	0.01920
	4	0.01920	0.01920	0.01920	0.05275
	5	-	-	0.01920	0.01920
	6	0.01920	0.01920	0.01920	0.05275
	7	0.02569	0.08877	0.01920	0.01920
	8	0.01920	0.01920	0.03083	0.01920
	9	0.05188	0.08877	0.01920	0.01920

Table B.3: Reinforcement Detail (Slabs with Drop Panel)

Slab ID	Steel System Number	Reinforcement Areas (in^2/in)			
		Top X-Direction	Top Y-Direction	Bottom X-Direction	Bottom Y-Direction
DP-A4	1	0.01617	0.01617	0.01140	0.01140
	2	0.01140	0.01140	0.03535	0.01140
	3	0.03265	0.01617	0.01140	0.01140
	4	0.01140	0.01140	0.01140	0.03535
	5	-	-	0.02356	0.02356
	6	0.01983	0.01140	0.01140	0.03535
	7	0.01617	0.03265	0.01140	0.01140
	8	0.01140	0.01983	0.03535	0.01140
	9	0.03265	0.03265	0.01140	0.01140
DP-B4	1	0.02521	0.02521	0.02180	0.02180
	2	0.02180	0.02180	0.05065	0.02180
	3	0.05065	0.02521	0.02180	0.02180
	4	0.02180	0.02180	0.02180	0.05065
	5	-	-	0.03377	0.03377
	6	0.02841	0.02180	0.02180	0.05065
	7	0.02521	0.05091	0.02180	0.02180
	8	0.02180	0.02841	0.05065	0.02180
	9	0.05091	0.05091	0.02180	0.02180

Appendix C

SAMPLE INPUT FILE

Data file for slab SS-A27 loaded at 3 days

```
 49    2    3    1                1    1    1
  2
  1.        10.      .003        .003
1000.     10000.      .5          .5
  3.        28.     5000.
  1         1         1          1
  2         1         1          1      59.0
  3         1         1          1     118.0
  4         1         1          1     177.0
  5         1         1          1     236.0
  6         1         1          1     295.0
  7    1    1         1     1    1     354.0
  8                                     0.0       59.0
  9                                    59.0       59.0
 10                                   118.0       59.0
 11                                   177.0       59.0
 12                                   236.0       59.0
 13                                   295.0       59.0
 14    1                         1    354.0       59.0
 15              1                     0.0      118.0
 16                                   59.0      118.0
 17                                  118.0      118.0
 18                                  177.0      118.0
 19              1                   236.0      118.0
 20                                  295.0      118.0
 21    1                         1    354.0      118.0
 22                                    0.0      177.0
 23                                   59.0      177.0
 24                                  118.0      177.0
 25                                  177.0      177.0
 26                                  236.0      177.0
 27                                  295.0      177.0
 28    1                         1    354.0      177.0
 29                                    0.0      236.0
 30                                   59.0      236.0
 31                                  118.0      236.0
 32                                  177.0      236.0
 33                                  236.0      236.0
 34                                  295.0      236.0
 35    1                         1    354.0      236.0
 36                                    0.0      295.0
 37                                   59.0      295.0
 38                                  118.0      295.0
 39                                  177.0      295.0
 40                                  236.0      295.0
 41                                  295.0      295.0
 42    1                         1    354.0      295.0
 43              1                     0.0      354.0
 44                                   59.0      354.0
 45                                  118.0      354.0
 46                                  177.0      354.0
 47              1                   236.0      354.0
 48                                  295.0      354.0
```

```
 49    1                        1     1    354.0      354.0
  1    1    2    9
  1    2    2    2   4000.        .15
                     7.0
  1  29.0E+06  60000.                    .1

  1   10
-3.50    -2.80     -2.10     -1.40     -.70      0.00     0.70     1.40
 2.10    2.80      3.50
  2   10
-3.20    -2.56     -1.92     -1.28     -.64      0.00      .64     1.28
 1.92    2.56      3.20
  1    4    1
  1    1   1.775    .02361    0.
  2    1   1.775    .02361   90.
  3    1  -1.775    .01400    0.
  4    1  -1.775    .01400   90.
  2    4    1
  1    1   1.775    .01400    0.
  2    1   1.775    .01400   90.
  3    1  -1.775    .02833    0.
  4    1  -1.775    .01400   90.
  3    4    1
  1    1   1.775    .04768    0.
  2    1   1.775    .02361   90.
  3    1  -1.775    .01400    0.
  4    1  -1.775    .01400   90.
  4    4    1
  1    1   1.775    .01400    0.
  2    1   1.775    .01400   90.
  3    1  -1.775    .01400    0.
  4    1  -1.775    .02833   90.
  5    2    1
  1    1  -1.775    .01889    0.
  2    1  -1.775    .01889   90.
  6    4    1
  1    1   1.775    .01589    0.
  2    1   1.775    .01400   90.
  3    1  -1.775    .01400    0.
  4    1  -1.775    .02833   90.
  7    4    1
  1    1   1.775    .02361    0.
  2    1   1.775    .04768   90.
  3    1  -1.775    .01400    0.
  4    1  -1.775    .01400   90.
  8    4    1
  1    1   1.775    .01400    0.
  2    1   1.775    .01589   90.
  3    1  -1.775    .02833    0.
  4    1  -1.775    .01400   90.
  9    4    1
  1    1   1.775    .04768    0.
  2    1   1.775    .04768   90.
  3    1  -1.775    .01400    0.
  4    1  -1.775    .01400   90.
```

1	72						
1	1	2	8	1	1	4	-.583
2	2	3	9	1	1	5	-.583
3	3	4	10	1	1	5	-.583
4	4	5	11	1	1	6	-.583
5	5	6	12	1	2	6	-.533
6	6	7	13	1	2	5	-.533
7	2	9	8	1	1	4	-.583
8	3	10	9	1	1	5	-.583
9	4	11	10	1	1	5	-.583
10	5	12	11	1	1	6	-.583
11	6	13	12	1	2	6	-.533
12	7	14	13	1	2	5	-.533
13	8	9	15	1	1	7	-.583
14	9	10	16	1	1	8	-.583
15	10	11	17	1	1	8	-.583
16	11	12	18	1	1	9	-.583
17	12	13	19	1	2	9	-.533
18	13	14	20	1	2	8	-.533
19	9	16	15	1	1	7	-.583
20	10	17	16	1	1	8	-.583
21	11	18	17	1	1	8	-.583
22	12	19	18	1	1	9	-.583
23	13	20	19	1	2	9	-.533
24	14	21	20	1	2	8	-.533
25	15	16	22	1	1	7	-.583
26	16	17	23	1	1	8	-.583
27	17	18	24	1	1	8	-.583
28	18	19	25	1	1	9	-.583
29	19	20	26	1	1	9	-.583
30	20	21	27	1	1	8	-.583
31	16	23	22	1	1	7	-.583
32	17	24	23	1	1	8	-.583
33	18	25	24	1	1	8	-.583
34	19	26	25	1	1	9	-.583
35	20	27	26	1	1	9	-.583
36	21	28	27	1	1	8	-.583
37	22	23	29	1	1	4	-.583
38	23	24	30	1	1	5	-.583
39	24	25	31	1	1	5	-.583
40	25	26	32	1	1	6	-.583
41	26	27	33	1	1	6	-.583
42	27	28	34	1	1	5	-.583
43	23	30	29	1	1	4	-.583
44	24	31	30	1	1	5	-.583
45	25	32	31	1	1	5	-.583
46	26	33	32	1	1	6	-.583
47	27	34	33	1	1	6	-.583
48	28	35	34	1	1	5	-.583
49	29	30	36	1	1	4	-.583
50	30	31	37	1	1	5	-.583
51	31	32	38	1	1	5	-.583
52	32	33	39	1	1	6	-.583
53	33	34	40	1	1	6	-.583

54	34	35	41	1	1	5		-.583	
55	30	37	36	1	1	4		-.583	
56	31	38	37	1	1	5		-.583	
57	32	39	38	1	1	5		-.583	
58	33	40	39	1	1	6		-.583	
59	34	41	40	1	1	6		-.583	
60	35	42	41	1	1	5		-.583	
61	36	37	43	1	1	1		-.583	
62	37	38	44	1	1	2		-.583	
63	38	39	45	1	1	2		-.583	
64	39	40	46	1	1	3		-.583	
65	40	41	47	1	1	3		-.583	
66	41	42	48	1	1	2		-.583	
67	37	44	43	1	1	1		-.583	
68	38	45	44	1	1	2		-.583	
69	39	46	45	1	1	2		-.583	
70	40	47	46	1	1	3		-.583	
71	41	48	47	1	1	3		-.583	
72	42	49	48	1	1	2		-.583	
2	8								
15	8					1			3500000000.
15	16					1			3500000000.
19	12					1			3500000000.
19	20					1			3500000000.
43	36					1			3500000000.
43	44					1			3500000000.
47	40					1			3500000000.
47	48					1			3500000000.
10	20			1.35		10	20		
10	20			-0.35		10	20		
10	20			0.35		10	20		

Appendix D

EXTRACTS OF SAMPLE OUTPUT FILE

EXTRACTS OF SAMPLE OUTPUT

```
NUMBER OF NODAL POINTS                                  49

NUMBER OF ELEMENT TYPES                                  2

NUMBER OF TIME STEPS                                     2

ITERATION TYPE CODE                                      1
    -1 = INITIAL STIFFNESS ONLY
     0 = CONSTANT STIFFNESS IN LOAD STEPS
     N = REFORM STIFFNESS EACH N ITERATIONS

CODE FOR NONLINEAR GEOMETRY                              0
GEOMETRIC STIFFNESS CODE                                 0
     0 = NOT CONSIDERED
     1 = INCLUDED

CREEP ANALYSIS CODE                                      1
SHRINKAGE ANALYSIS CODE                                  1
     0 = ANALYSIS NOT REQUIRED
     1 = ANALYSIS REQUIRED


CONVERGENCE NORM CODE                                    1
     0 = FORCE NORM USED
     1 = DISPLACEMENT NORM USED
     2 = BOTH FORCE AND DISPL NORMS

CONVERGENCE TOLERANCE TYPE CODE                          0
     0 = ABSOLUTE VALUES
     1 = FRACTIONS

PRINCIPAL AXES DIRECTION CODE                            0
     0 = CALCULATED IN PROGRAM
     1 = COINCIDE WITH ELEMENT LOCAL AXES


OUTPUT CONTROL CODES
     0 = NO
     1 = YES

DISPL UNBAL FORCES + STRESSES FOR EACH ITER              2
     2 = ONLY AT END OF TIME STEPS
NODAL DISPL IN LOCAL COORD SYSTEM                        0
STRESS RESULTANTS                                        0
STRAINS                                                  0
DISPL AND UNBAL FORCES FOR EACH ITERATION                0


TOLERANCES TO GET CONVERGENCE
  FORCES                  1.00000
  MOMENTS                10.00000
```

TRANSLATIONS	0.00300
ROTATIONS	0.00300

UPPER LIMITS ON UNBALANCE

FORCES	1000.00
MOMENTS	10000.00
TRANSLATIONS	0.50
ROTATIONS	0.50

ANALYSIS REQD. AT FOLLOWING DAYS AFTER CASTING

3. 5000.

1COMPLETE NODAL POINT DATA

0NODE NUMBER	BOUNDARY CONDITION CODES X	Y	Z	XX	YY	ZZ	NODAL POINT COORDINATES X	Y	Z
1	0	1	0	1	0	1	0.000	0.000	0.000
2	0	1	0	1	0	1	59.000	0.000	0.000
3	0	1	0	1	0	1	118.000	0.000	0.000
4	0	1	0	1	0	1	177.000	0.000	0.000
5	0	1	0	1	0	1	236.000	0.000	0.000
6	0	1	0	1	0	1	295.000	0.000	0.000
7	1	1	0	1	1	1	354.000	0.000	0.000
8	0	0	0	0	0	1	0.000	59.000	0.000
9	0	0	0	0	0	1	59.000	59.000	0.000
10	0	0	0	0	0	1	118.000	59.000	0.000
11	0	0	0	0	0	1	177.000	59.000	0.000
12	0	0	0	0	0	1	236.000	59.000	0.000
13	0	0	0	0	0	1	295.000	59.000	0.000
14	1	0	0	0	1	1	354.000	59.000	0.000
15	0	0	1	0	0	1	0.000	118.000	0.000
16	0	0	0	0	0	1	59.000	118.000	0.000
17	0	0	0	0	0	1	118.000	118.000	0.000
18	0	0	0	0	0	1	177.000	118.000	0.000
19	0	0	1	0	0	1	236.000	118.000	0.000
20	0	0	0	0	0	1	295.000	118.000	0.000
21	1	0	0	0	1	1	354.000	118.000	0.000
22	0	0	0	0	0	1	0.000	177.000	0.000
23	0	0	0	0	0	1	59.000	177.000	0.000
24	0	0	0	0	0	1	118.000	177.000	0.000
25	0	0	0	0	0	1	177.000	177.000	0.000
26	0	0	0	0	0	1	236.000	177.000	0.000
27	0	0	0	0	0	1	295.000	177.000	0.000
28	1	0	0	0	1	1	354.000	177.000	0.000
29	0	0	0	0	0	1	0.000	236.000	0.000
30	0	0	0	0	0	1	59.000	236.000	0.000
31	0	0	0	0	0	1	118.000	236.000	0.000
32	0	0	0	0	0	1	177.000	236.000	0.000
33	0	0	0	0	0	1	236.000	236.000	0.000
34	0	0	0	0	0	1	295.000	236.000	0.000

35	1	0	0	0	1	1	354.000	236.000	0.000
36	0	0	0	0	0	1	0.000	295.000	0.000
37	0	0	0	0	0	1	59.000	295.000	0.000
38	0	0	0	0	0	1	118.000	295.000	0.000
39	0	0	0	0	0	1	177.000	295.000	0.000
40	0	0	0	0	0	1	236.000	295.000	0.000
41	0	0	0	0	0	1	295.000	295.000	0.000
42	1	0	0	0	1	1	354.000	295.000	0.000
43	0	0	1	0	0	1	0.000	354.000	0.000
44	0	0	0	0	0	1	59.000	354.000	0.000
45	0	0	0	0	0	1	118.000	354.000	0.000
46	0	0	0	0	0	1	177.000	354.000	0.000
47	0	0	1	0	0	1	236.000	354.000	0.000
48	0	0	0	0	0	1	295.000	354.000	0.000
49	1	0	0	0	1	1	354.000	354.000	0.000

1 MATERIAL PROPERTIES - CONCRETE AND REINFORCING STEEL

NUMBER OF CONCRETE TYPES	1
NUMBER OF RE STEEL TYPES	1
NUMBER OF CONCRETE LAYER SYSTEMS	2
NUMBER OF RE STEEL LAYER SYSTEMS	9

CONCRETE MATERIAL PROPERTIES

TYPE NO.	1
ELASTIC MATERIAL DATA INPUT INDICATOR	2
CREEP DATA INPUT INDICATOR	2
SHRINKAGE DATA INPUT INDICATOR	2

DATA INPUT INDICATORS - 1 = READ IN VALUES
2 = USE ACI DATA

COMPRESSIVE STRENGTH AT 28 DAYS	0.40000E+04
POISSONS RATIO	0.15000E+00
WEIGHT PER UNIT VOLUME	0.83000E-01
CRACKED SHEAR CONSTANT	0.10000E+01

DAYS AFTER CASTING	3.
COMPRESSIVE STRENGTH	0.26022E+04
TENSILE STRENGTH	0.30685E+03
MODULUS OF ELASTICITY	0.31074E+07
STRAIN AT COMPRESSIVE STRENGTH	0.16748E-02
ULTIMATE STRAIN IN COMPRESSION	0.66993E-02
ULTIMATE STRAIN IN TENSION	0.00000E+00

TENSION STIFFENING MODEL - INCREASED STEEL MODULUS

ULTIMATE SHRINKAGE	-0.80000E-03
SLUMP OF MIX	0.27000E+01
SIZE OF MEMBER	0.68000E+01
RELATIVE HUMIDITY	0.50000E+02

TEMPERATURE COEFFICIENT 0.55000E-05

STEEL MATERIAL PROPERTIES

TYPE	MODULUS	YIELD STRENGTH	BI-MODULUS	ULT STRAIN
1	0.29000E+08	0.60000E+05	0.00000E+00	0.10000E+00

TENSION STIFFENING MODEL - INCREASED STEEL STIFFNESS

FACTORS TO INCREASE STEEL STIFFNESS						MULTIPLES OF CONCRETE CRACKING STRAIN			
4.00	2.70	2.00	1.60	1.15	1.05	1.50	3.00	5.00	8.00

1CONCRETE LAYER SYSTEMS

TYPE NO. 1
Z-COORDINATES =

-3.40000	-2.72000	-2.04000	-1.36000	-0.68000	0.00000	0.68000	1.68000	2.04000	2.72000	3.40000

TYPE NO. 2
Z-COORDINATES =

-3.10000	-2.48000	-1.86000	-1.24000	-0.62000	0.00000	0.62000	1.24000	1.86000	2.48000	3.10000

STEEL LAYER SYSTEMS

TYPE NO. 1
NO. OF 4
ANGLE CODE 1

LAYER	MATERIAL	Z-COORD.	SMEARED THK.	ANGLE
1	1	1.67500	0.02420	0.00000
2	1	1.67500	0.02420	90.00000
3	1	-1.67500	0.01360	0.00000
4	1	-1.67500	0.01360	90.00000

TYPE NO. 2
NO. OF 4
ANGLE CODE 1

LAYER	MATERIAL	Z-COORD.	SMEARED THK.	ANGLE
1	1	1.67500	0.01360	0.00000
2	1	1.67500	0.01360	90.00000
3	1	-1.67500	0.02904	0.00000
4	1	-1.67500	0.01360	90.00000

TYPE NO. 3
NO. OF 4
ANGLE CODE 1

LAYER	MATERIAL	Z-COORD.	SMEARED THK.	ANGLE
1	1	1.67500	0.04887	0.00000
2	1	1.67500	0.02420	90.00000
3	1	-1.67500	0.01360	0.00000
4	1	-1.67500	0.01360	90.00000

TYPE NO. 4
NO. OF 4
ANGLE CODE 1

LAYER	MATERIAL	Z-COORD.	SMEARED THK.	ANGLE
1	1	1.67500	0.01360	0.00000
2	1	1.67500	0.01360	90.00000
3	1	-1.67500	0.01360	0.00000
4	1	-1.67500	0.02904	90.00000

TYPE NO. 5
NO. OF 2
ANGLE CODE 1

LAYER	MATERIAL	Z-COORD.	SMEARED THK.	ANGLE
1	1	-1.67500	0.01936	0.00000
2	1	-1.67500	0.01936	90.00000

TYPE NO. 6
NO. OF 4
ANGLE CODE 1

LAYER	MATERIAL	Z-COORD.	SMEARED THK.	ANGLE
1	1	1.67500	0.01629	0.00000
2	1	1.67500	0.01360	90.00000
3	1	-1.67500	0.01360	0.00000
4	1	-1.67500	0.02904	90.00000

TYPE NO. 7
NO. OF 4
ANGLE CODE 1

LAYER	MATERIAL	Z-COORD.	SMEARED THK.	ANGLE
1	1	1.67500	0.02420	0.00000
2	1	1.67500	0.04887	90.00000
3	1	-1.67500	0.01360	0.00000
4	1	-1.67500	0.01360	90.00000

TYPE NO. 8
NO. OF 4
ANGLE CODE 1

LAYER	MATERIAL	Z-COORD.	SMEARED THK.	ANGLE
1	1	1.67500	0.01360	0.00000

2	1	1.67500	0.01629	90.00000
3	1	-1.67500	0.02904	0.00000
4	1	-1.67500	0.01360	90.00000

TYPE NO. 9
NO. OF 4
ANGLE CODE 1

LAYER	MATERIAL	Z-COORD.	SMEARED THK.	ANGLE
1	1	1.67500	0.04887	0.00000
2	1	1.67500	0.04887	90.00000
3	1	-1.67500	0.01360	0.00000
4	1	-1.67500	0.01360	90.00000

1TRIANGULAR SHELL ELEMENT DATA

NUMBER OF ELEMENTS 72
ELEMENT TYPE OPTION 0
0 = SHELL
1 = MEMBRANE (CST)
2 = PLATE BENDING (RAZZAQUE)
OPTION FOR ELEMENT NODAL LOADS 0
0 = CONSISTENT
1 = TRIBUTARY AREA

GRAVITY LOAD MULTIPLIERS

X	Y	Z
0.000	0.000	0.000

ELEMENT	NODE I	NODE J	NODE K	CONCR	C L S	ST L S	LOCO	ANLO PLAT
1	1	2	8	1	1	4	0	0.00-0.56700E+00
2	2	3	9	1	1	5	0	0.00-0.56700E+00
3	3	4	10	1	1	5	0	0.00-0.56700E+00
4	4	5	11	1	1	6	0	0.00-0.56700E+00
5	5	6	12	1	2	6	0	0.00-0.51700E+00
6	6	7	13	1	2	5	0	0.00-0.51700E+00
7	2	9	8	1	1	4	0	0.00-0.56700E+00
8	3	10	9	1	1	5	0	0.00-0.56700E+00
9	4	11	10	1	1	5	0	0.00-0.56700E+00
10	5	12	11	1	1	6	0	0.00-0.56700E+00
11	6	13	12	1	2	6	0	0.00-0.51700E+00
12	7	14	13	1	2	5	0	0.00-0.51700E+00
13	8	9	15	1	1	7	0	0.00-0.56700E+00
14	9	10	16	1	1	8	0	0.00-0.56700E+00
15	10	11	17	1	1	8	0	0.00-0.56700E+00
16	11	12	18	1	1	9	0	0.00-0.56700E+00
17	12	13	19	1	2	9	0	0.00-0.51700E+00
18	13	14	20	1	2	8	0	0.00-0.51700E+00
19	9	16	15	1	1	7	0	0.00-0.56700E+00
20	10	17	16	1	1	8	0	0.00-0.56700E+00
21	11	18	17	1	1	8	0	0.00-0.56700E+00

22	12	19	18	1	1	9	0	0.00-0.56700E+00
23	13	20	19	1	2	9	0	0.00-0.51700E+00
24	14	21	20	1	2	8	0	0.00-0.51700E+00
25	15	16	22	1	1	7	0	0.00-0.56700E+00
26	16	17	23	1	1	8	0	0.00-0.56700E+00
27	17	18	24	1	1	8	0	0.00-0.56700E+00
28	18	19	25	1	1	9	0	0.00-0.56700E+00
29	19	20	26	1	1	9	0	0.00-0.56700E+00
30	20	21	27	1	1	8	0	0.00-0.56700E+00
31	16	23	22	1	1	7	0	0.00-0.56700E+00
32	17	24	23	1	1	8	0	0.00-0.56700E+00
33	18	25	24	1	1	8	0	0.00-0.56700E+00
34	19	26	25	1	1	9	0	0.00-0.56700E+00
35	20	27	26	1	1	9	0	0.00-0.56700E+00
36	21	28	27	1	1	8	0	0.00-0.56700E+00
37	22	23	29	1	1	4	0	0.00-0.56700E+00
38	23	24	30	1	1	5	0	0.00-0.56700E+00
39	24	25	31	1	1	5	0	0.00-0.56700E+00
40	25	26	32	1	1	6	0	0.00-0.56700E+00
41	26	27	33	1	1	6	0	0.00-0.56700E+00
42	27	28	34	1	1	5	0	0.00-0.56700E+00
43	23	30	29	1	1	4	0	0.00-0.56700E+00
44	24	31	30	1	1	5	0	0.00-0.56700E+00
45	25	32	31	1	1	5	0	0.00-0.56700E+00
46	26	33	32	1	1	6	0	0.00-0.56700E+00
47	27	34	33	1	1	6	0	0.00-0.56700E+00
48	28	35	34	1	1	5	0	0.00-0.56700E+00
49	29	30	36	1	1	4	0	0.00-0.56700E+00
50	30	31	37	1	1	5	0	0.00-0.56700E+00
51	31	32	38	1	1	5	0	0.00-0.56700E+00
52	32	33	39	1	1	6	0	0.00-0.56700E+00
53	33	34	40	1	1	6	0	0.00-0.56700E+00
54	34	35	41	1	1	5	0	0.00-0.56700E+00
55	30	37	36	1	1	4	0	0.00-0.56700E+00
56	31	38	37	1	1	5	0	0.00-0.56700E+00
57	32	39	38	1	1	5	0	0.00-0.56700E+00
58	33	40	39	1	1	6	0	0.00-0.56700E+00
59	34	41	40	1	1	6	0	0.00-0.56700E+00
60	35	42	41	1	1	5	0	0.00-0.56700E+00
61	36	37	43	1	1	1	0	0.00-0.56700E+00
62	37	38	44	1	1	2	0	0.00-0.56700E+00
63	38	39	45	1	1	2	0	0.00-0.56700E+00
64	39	40	46	1	1	3	0	0.00-0.56700E+00
65	40	41	47	1	1	3	0	0.00-0.56700E+00
66	41	42	48	1	1	2	0	0.00-0.56700E+00
67	37	44	43	1	1	1	0	0.00-0.56700E+00
68	38	45	44	1	1	2	0	0.00-0.56700E+00
69	39	46	45	1	1	2	0	0.00-0.56700E+00
70	40	47	46	1	1	3	0	0.00-0.56700E+00
71	41	48	47	1	1	3	0	0.00-0.56700E+00
72	42	49	48	1	1	2	0	0.00-0.56700E+00

BOUNDARY ELEMENTS

NODE	..NODES DEFINING CONSTRAINT DIRECTION...					CODES		DISPLACEMENT
N	NI	NJ	NK	NL	KD	KR	KN	

15	8	0	0	0	0	1	0	0.00000E+00	0.00000E+00
15	16	0	0	0	0	1	0	0.00000E+00	0.00000E+00
19	12	0	0	0	0	1	0	0.00000E+00	0.00000E+00
19	20	0	0	0	0	1	0	0.00000E+00	0.00000E+00
43	36	0	0	0	0	1	0	0.00000E+00	0.00000E+00
43	44	0	0	0	0	1	0	0.00000E+00	0.00000E+00
47	40	0	0	0	0	1	0	0.00000E+00	0.00000E+00
47	48	0	0	0	0	1	0	0.00000E+00	0.00000E+00

NUMBER OF EQUATIONS 213
BANDWIDTH 38

1 CONTROL DATA

NUMBER OF LOAD STEPS	10
NUMBER OF ITERATIONS PERMITTED	20
NUMBER OF LOADED JOINTS	0
FRACTION OF DEAD LOAD	0.0000
FRACTION OF SURFACE LOAD	1.3500
FRACTION OF SPRING LOAD	0.0000
NUMBER OF LOAD STEPS FOR TIME DEP. ANAL.	10
NUMBER OF ITERATIONS FOR TIME DEP. ANAL.	20
ITERATION TYPE CODE	1
NUMBER OF ELEMENTS WITH TEMP CHANGE	0

TIME STEP NUMBER 1
LOAD STEP NUMBER 10
ITERATION NUMBER 10

1JOINT DISPLACEMENTS

NODE	DISPL-X	DISPL-Y	DISPL-Z	ROTAT-X	ROTAT-Y	ROTAT-Z
1	-0.19759E-02	0.00000E+00	-0.10395E+00	0.00000E+00	0.16532E-02	0.00000E+00
2	-0.16391E-02	0.00000E+00	-0.20313E+00	0.00000E+00	0.14574E-02	0.00000E+00
3	-0.70268E-03	0.00000E+00	-0.24764E+00	0.00000E+00	-0.30985E-03	0.00000E+00
4	-0.34910E-03	0.00000E+00	-0.19800E+00	0.00000E+00	-0.13270E-02	0.00000E+00
5	-0.12292E-03	0.00000E+00	-0.13226E+00	0.00000E+00	-0.86270E-03	0.00000E+00
6	0.59022E-04	0.00000E+00	-0.11772E+00	0.00000E+00	0.33322E-03	0.00000E+00
7	0.00000E+00	0.00000E+00	-0.13689E+00	0.00000E+00	0.00000E+00	0.00000E+00
8	-0.26773E-02	-0.40827E-03	-0.54443E-01	0.14394E-02	0.21724E-02	0.00000E+00
9	-0.20083E-02	0.69404E-04	-0.17695E+00	0.64587E-03	0.18739E-02	0.00000E+00
10	-0.80519E-03	0.30288E-03	-0.23301E+00	0.37792E-03	-0.42740E-03	0.00000E+00
6	0.59022E-04	0.00000E+00	-0.11772E+00	0.00000E+00	0.33322E-03	0.00000E+00
7	0.00000E+00	0.00000E+00	-0.13689E+00	0.00000E+00	0.00000E+00	0.00000E+00
8	-0.26773E-02	-0.40827E-03	-0.54443E-01	0.14394E-02	0.21724E-02	0.00000E+00
9	-0.20083E-02	0.69404E-04	-0.17695E+00	0.64587E-03	0.18739E-02	0.00000E+00
10	-0.80519E-03	0.30288E-03	-0.23301E+00	0.37792E-03	-0.42740E-03	0.00000E+00
11	-0.33160E-03	0.74377E-05	-0.16290E+00	0.10960E-02	-0.17874E-02	0.00000E+00
12	0.21149E-04	-0.22172E-03	-0.75666E-01	0.18998E-02	-0.94906E-03	0.00000E+00
13	0.36426E-03	-0.36427E-03	-0.84832E-01	0.73937E-03	0.73937E-03	0.00000E+00
14	0.00000E+00	-0.59030E-04	-0.11772E+00	0.33322E-03	0.00000E+00	0.00000E+00

15	-0.31586E-02	0.11172E-02	0.00000E+00	-0.13887E-04	0.15060E-03	0.00000E+00
16	-0.19283E-02	0.55026E-03	-0.14601E+00	-0.34826E-03	0.31078E-02	0.00000E+00
17	-0.99432E-03	0.54042E-03	-0.22953E+00	-0.34216E-03	-0.31058E-03	0.00000E+00
18	-0.41818E-03	0.21943E-03	-0.12635E+00	-0.75427E-04	-0.30141E-02	0.00000E+00
19	0.12394E-03	-0.12395E-03	0.00000E+00	-0.39031E-04	-0.39031E-04	0.00000E+00
20	0.22172E-03	-0.21169E-04	-0.75666E-01	-0.94906E-03	0.18998E-02	0.00000E+00
21	0.00000E+00	0.12291E-03	-0.13226E+00	-0.86270E-03	0.00000E+00	0.00000E+00
22	-0.29886E-02	0.10944E-02	-0.59911E-01	-0.21578E-02	0.29074E-02	0.00000E+00
23	-0.25841E-02	0.10367E-02	-0.21410E+00	-0.16419E-02	0.23579E-02	0.00000E+00
24	-0.11045E-02	0.75668E-03	-0.27537E+00	-0.10987E-02	-0.33129E-03	0.00000E+00
25	-0.11462E-02	0.11462E-02	-0.19949E+00	-0.16314E-02	-0.16314E-02	0.00000E+00
26	-0.21945E-03	0.41816E-03	-0.12635E+00	-0.30141E-02	-0.75422E-04	0.00000E+00
27	-0.74461E-05	0.33158E-03	-0.16290E+00	-0.17874E-02	0.10950E-02	0.00000E+00
28	0.00000E+00	0.34907E-03	-0.19800E+00	-0.13270E-02	0.00000E+00	0.00000E+00
29	-0.31221E-02	0.57821E-03	-0.15464E+00	-0.81055E-03	0.22820E-02	0.00000E+00
30	-0.31024E-02	0.13147E-02	-0.28334E+00	-0.66038E-03	0.19161E-02	0.00000E+00
31	-0.11445E-02	0.11445E-02	-0.32926E+00	-0.37297E-03	-0.37296E-03	0.00000E+00
32	-0.75670E-03	0.11045E-02	-0.27537E+00	-0.33129E-03	-0.10987E-02	0.00000E+00
33	-0.54043E-03	0.99430E-03	-0.22953E+00	-0.31059E-03	-0.34215E-03	0.00000E+00
34	-0.30289E-03	0.80517E-03	-0.23301E+00	-0.42739E-03	0.37792E-03	0.00000E+00
35	0.00000E+00	0.70266E-03	-0.24764E+00	-0.30984E-03	0.00000E+00	0.00000E+00
36	-0.39091E-02	0.16958E-02	-0.96341E-01	0.25380E-02	0.26794E-02	0.00000E+00
37	-0.33285E-02	0.33285E-02	-0.24020E+00	0.19223E-02	0.19223E-02	0.00000E+00
38	-0.13146E-02	0.31023E-02	-0.28334E+00	0.19161E-02	-0.66037E-03	0.00000E+00
39	-0.10367E-02	0.25841E-02	-0.21410E+00	0.23579E-02	-0.16419E-02	0.00000E+00
40	-0.55026E-03	0.19282E-02	-0.14601E+00	0.31078E-02	-0.34825E-03	0.00000E+00
41	-0.69410E-04	0.20083E-02	-0.17695E+00	0.18739E-02	0.64587E-03	0.00000E+00
42	0.00000E+00	0.16391E-02	-0.20313E+00	0.14574E-02	0.00000E+00	0.00000E+00
43	-0.31376E-02	0.31376E-02	0.00000E+00	0.58116E-04	0.58116E-04	0.00000E+00
44	-0.16958E-02	0.39091E-02	-0.96341E-01	0.26794E-02	0.25380E-02	0.00000E+00
45	-0.57820E-03	0.31221E-02	-0.15464E+00	0.22820E-02	-0.81055E-03	0.00000E+00
46	-0.10944E-02	0.29886E-02	-0.59911E-01	0.29074E-02	-0.21578E-02	0.00000E+00
47	-0.11172E-02	0.31586E-02	0.00000E+00	0.15060E-03	-0.13887E-04	0.00000E+00
48	0.40827E-03	0.26772E-02	-0.54443E-01	0.21724E-02	0.14394E-02	0.00000E+00
49	0.00000E+00	0.19759E-02	-0.10395E+00	0.16532E-02	0.00000E+00	0.00000E+00

TIME STEP NUMBER 1
LOAD STEP NUMBER 10
ITERATION NUMBER 3
1JOINT DISPLACEMENTS

NODE	DISPL-X	DISPL-Y	DISPL-Z	ROTAT-X	ROTAT-Y	ROTAT-Z
1	0.31408E+00	0.00000E+00	-0.43893E+00	0.00000E+00	0.13548E-01	0.00000E+00
2	0.26280E+00	0.00000E+00	-0.11875E+01	0.00000E+00	0.12073E-01	0.00000E+00
3	0.21553E+00	0.00000E+00	-0.15366E+01	0.00000E+00	-0.28149E-02	0.00000E+00
4	0.16410E+00	0.00000E+00	-0.11231E+01	0.00000E+00	-0.11331E-01	0.00000E+00
5	0.11262E+00	0.00000E+00	-0.59366E+00	0.00000E+00	-0.63553E-02	0.00000E+00
6	0.58541E-01	0.00000E+00	-0.55084E+00	0.00000E+00	0.43857E-02	0.00000E+00
7	0.00000E+00	0.00000E+00	-0.73736E+00	0.00000E+00	0.00000E+00	0.00000E+00
8	0.31081E+00	-0.59763E-01	-0.27731E+00	0.58194E-02	0.10891E-01	0.00000E+00
9	0.25998E+00	-0.55362E-01	-0.99863E+00	0.45544E-02	0.12580E-01	0.00000E+00
10	0.21422E+00	-0.53065E-01	-0.13682E+01	0.49647E-02	-0.27919E-02	0.00000E+00
11	0.16347E+00	-0.56518E-01	-0.90399E+00	0.70743E-02	-0.12084E-01	0.00000E+00
12	0.11238E+00	-0.54972E-01	-0.33501E+00	0.81524E-02	-0.64523E-02	0.00000E+00

13	0.61278E-01	-0.61277E-01	-0.35535E+00	0.46038E-02	0.46037E-02	0.00000E+00
14	0.00000E+00	-0.58541E-01	-0.55084E+00	0.43857E-02	0.00000E+00	0.00000E+00
15	0.31516E+00	-0.99849E-01	0.00000E+00	-0.44958E-04	0.19149E-03	0.00000E+00
16	0.26189E+00	-0.10665E+00	-0.79038E+00	-0.24832E-02	0.16957E-01	0.00000E+00
17	0.21480E+00	-0.10713E+00	-0.12478E+01	-0.14796E-02	-0.20515E-02	0.00000E+00
18	0.16453E+00	-0.11012E+00	-0.67143E+00	0.21737E-03	-0.15892E-01	0.00000E+00
19	0.11107E+00	-0.11107E+00	0.00000E+00	-0.93617E-04	-0.93621E-04	0.00000E+00
20	0.54973E-01	-0.11238E+00	-0.33501E+00	-0.64523E-02	0.81524E-02	0.00000E+00
21	0.00000E+00	-0.11262E+00	-0.59366E+00	-0.63552E-02	0.00000E+00	0.00000E+00
22	0.31099E+00	-0.15810E+00	-0.33418E+00	-0.12799E-01	0.16084E-01	0.00000E+00
23	0.25867E+00	-0.15787E+00	-0.12525E+01	-0.11955E-01	0.14904E-01	0.00000E+00
24	0.21525E+00	-0.16117E+00	-0.16028E+01	-0.97296E-02	-0.29826E-02	0.00000E+00
25	0.15837E+00	-0.15837E+00	-0.10996E+01	-0.10150E-01	-0.10150E-01	0.00000E+00
26	0.11012E+00	-0.16453E+00	-0.67143E+00	-0.15891E-01	0.21736E-03	0.00000E+00
27	0.56519E-01	-0.16346E+00	-0.90398E+00	-0.12084E-01	0.70742E-02	0.00000E+00
28	0.00000E+00	-0.16410E+00	-0.11231E+01	-0.11330E-01	0.00000E+00	0.00000E+00
29	0.31104E+00	-0.21809E+00	-0.91665E+00	-0.58937E-02	0.16112E-01	0.00000E+00
30	0.25412E+00	-0.21275E+00	-0.18019E+01	-0.60821E-02	0.13734E-01	0.00000E+00
31	0.21365E+00	-0.21365E+00	-0.20894E+01	-0.41838E-02	-0.41838E-02	0.00000E+00
32	0.16117E+00	-0.21524E+00	-0.16028E+01	-0.29827E-02	-0.97296E-02	0.00000E+00
33	0.10713E+00	-0.21480E+00	-0.12478E+01	-0.20515E-02	-0.14797E-02	0.00000E+00
34	0.53066E-01	-0.21421E+00	-0.13682E+01	-0.27920E-02	0.49647E-02	0.00000E+00
35	0.00000E+00	-0.21553E+00	-0.15365E+01	-0.28149E-02	0.00000E+00	0.00000E+00
36	0.30671E+00	-0.26577E+00	-0.61145E+00	0.15962E-01	0.15289E-01	0.00000E+00
37	0.25308E+00	-0.25307E+00	-0.15344E+01	0.13477E-01	0.13477E-01	0.00000E+00
38	0.21275E+00	-0.25412E+00	-0.18019E+01	0.13734E-01	-0.60820E-02	0.00000E+00
39	0.15787E+00	-0.25867E+00	-0.12525E+01	0.14904E-01	-0.11955E-01	0.00000E+00
40	0.10665E+00	-0.26189E+00	-0.79038E+00	0.16957E-01	-0.24832E-02	0.00000E+00
41	0.55363E-01	-0.25998E+00	-0.99863E+00	0.12580E-01	0.45544E-02	0.00000E+00
42	0.00000E+00	-0.26280E+00	-0.11875E+01	0.12073E-01	0.00000E+00	0.00000E+00
43	0.31497E+00	-0.31497E+00	0.00000E+00	0.93113E-04	0.93114E-04	0.00000E+00
44	0.26577E+00	-0.30671E+00	-0.61145E+00	0.15289E-01	0.15962E-01	0.00000E+00
45	0.21809E+00	-0.31104E+00	-0.91665E+00	0.16112E-01	-0.58937E-02	0.00000E+00
46	0.15810E+00	-0.31099E+00	-0.33419E+00	0.16084E-01	-0.12799E-01	0.00000E+00
47	0.99850E-01	-0.31516E+00	0.00000E+00	0.19148E-03	-0.44957E-04	0.00000E+00
48	0.59764E-01	-0.31081E+00	-0.27731E+00	0.10891E-01	0.58194E-02	0.00000E+00
49	0.00000E+00	-0.31408E+00	-0.43893E+00	0.13548E-01	0.00000E+00	0.00000E+00

Appendix E

RESULTS OF THE COMPUTER ANALYSIS

Table E.1: Deflections for Square Slabs Using ACI-209 Recommendations

Slab ID	Clear span (ins)	Slab Thickness (ins)	Live-Load to Dead-Load Ratio	Computed Deflections (ins)											
				Mid-panel Deflections						Deflections Along Column Lines					
				Interior (Node 7)			Exterior (Node 31)			Node 17			Node 45		
				Δ_{tot}	Δ_{inst}	Δ_{incr}	Δ_{tot}	Δ_{inst}	Δ_{incr}	Δ_{tot}	Δ_{inst}	Δ_{incr}	Δ_{tot}	Δ_{inst}	Δ_{incr}
ACI-S1	210	6.00	0.50	1.735	0.563	1.172	2.473	0.861	1.612	1.592	0.572	1.020	1.269	0.409	0.860
ACI-S2	210	6.00	1.00	1.380	0.414	0.966	1.693	0.616	1.077	1.077	0.412	0.665	0.818	0.289	0.529
ACI-S3	210	6.00	1.50	1.189	0.371	0.818	1.490	0.540	0.950	0.927	0.370	0.557	0.741	0.262	0.479
ACI-S4	210	8.00	0.50	1.244	0.428	0.816	1.417	0.554	0.863	0.893	0.364	0.529	0.679	0.261	0.418
ACI-S5	210	8.00	1.00	0.980	0.253	0.727	1.131	0.379	0.752	0.689	0.252	0.437	0.510	0.175	0.335
ACI-S6	210	8.00	1.50	0.805	0.166	0.639	0.971	0.321	0.650	0.557	0.202	0.355	0.431	0.146	0.285

Table E.2: Computed Deflections for Square Slabs Loaded at 3 Days

Slab ID	Clear span (ins)	Slab Thickness (ins)	Computed Deflections (ins)												Perm. Defl. (l/240) (ins)
			Mid-panel Deflections						Deflections Along Column Lines						
			Interior (Node 7)			Exterior (Node 31)			Node 17			Node 45			
			Δ_{tot}	Δ_{inst}	Δ_{incr}	Δ_{tot}	Δ_{inst}	Δ_{incr}	Δ_{tot}	Δ_{inst}	Δ_{incr}	Δ_{tot}	Δ_{inst}	Δ_{incr}	
SS-A1	210	7.00	1.152	0.197	0.955	2.408	0.419	1.989	1.361	0.242	1.119	1.100	0.196	0.904	0.875
SS-A2	210	8.40	0.778	0.111	0.667	1.682	0.209	1.473	1.040	0.133	0.907	0.699	0.092	0.607	0.875
SS-A3	210	8.60	0.716	0.102	0.614	1.471	0.186	1.285	0.716	0.102	0.614	0.603	0.082	0.521	0.875
SS-A4	210	8.20	0.795	0.114	0.681	1.806	0.225	1.581	1.142	0.144	0.998	0.742	0.098	0.644	0.875
SS-A5	210	8.50	0.691	0.101	0.590	1.644	0.202	1.442	1.027	0.128	*0.899*	0.681	0.089	0.592	0.875
SS-B1	314	13.4	1.550	0.196	1.354	4.092	0.491	3.601	2.464	0.323	2.141	1.832	0.222	1.610	1.310
SS-B2	314	15.8	0.908	0.116	0.792	2.694	0.351	2.343	1.588	0.224	1.364	1.239	0.168	1.071	1.310
SS-B3	314	16.0	0.870	0.111	0.759	2.583	0.346	2.237	1.520	0.220	*1.300*	1.186	0.164	1.022	1.310
SS-C1	432	21.6	1.272	0.147	1.125	3.936	0.663	3.273	2.448	0.449	1.999	1.838	0.327	1.511	1.800
SS-C2	432	22.3	1.129	0.134	0.995	3.707	0.637	3.070	2.268	0.427	1.841	1.705	0.314	1.391	1.800
SS-C3	432	22.5	1.074	0.128	0.946	3.648	0.628	3.020	2.260	0.422	1.838	1.675	0.310	1.365	1.800
SS-C4	432	22.7	1.035	0.124	0.911	3.596	0.623	2.973	2.220	0.417	*1.803*	1.650	0.309	1.341	1.800

Table E.3: Computed Deflections for Square Slabs Loaded at 4 Days

Slab ID	Clear span (ins)	Slab Thickness (ins)	Computed Deflections (ins)												Perm. Defl. (l/240) (ins)
			Mid-panel Deflections						Deflections Along Column Lines						
			Interior (Node 7)			Exterior (Node 31)			Node 17			Node 45			
			Δ_{tot}	Δ_{inst}	Δ_{incr}	Δ_{tot}	Δ_{inst}	Δ_{incr}	Δ_{tot}	Δ_{inst}	Δ_{incr}	Δ_{tot}	Δ_{inst}	Δ_{incr}	
SS-A6	210	7.00	0.903	0.144	0.759	1.876	0.265	1.611	1.194	0.171	1.023	0.780	0.117	0.663	0.875
SS-A7	210	8.00	0.713	0.120	0.593	1.448	0.216	1.232	0.886	0.137	0.749	0.595	0.095	0.500	0.875
SS-A8	210	7.60	0.840	0.140	0.700	1.739	0.528	1.211	1.085	0.165	0.920	0.721	0.114	0.607	0.875
SS-A9	210	7.80	0.769	0.129	0.640	1.575	0.234	1.341	0.957	0.148	0.809	0.664	0.104	0.560	0.875
SS-A10	210	7.70	0.802	0.133	0.669	1.679	0.249	1.430	1.036	0.159	*0.877*	0.703	0.110	0.593	0.875
SS-B4	314	13.0	1.413	0.193	1.220	3.561	0.487	3.074	2.154	0.320	1.834	1.601	0.222	1.379	1.310
SS-B5	314	14.6	0.947	0.144	0.803	2.744	0.404	2.340	1.609	0.257	1.352	1.252	0.189	1.063	1.310
SS-B6	314	14.7	0.946	0.139	0.807	2.699	0.398	2.301	1.589	0.253	1.336	1.235	0.188	1.047	1.310
SS-B7	314	14.8	0.893	0.131	0.762	2.599	0.389	2.210	1.534	0.248	*1.286*	1.205	0.184	1.021	1.310
SS-C5	432	19.0	1.628	0.224	1.404	4.631	0.786	3.845	2.822	0.530	2.292	2.163	0.379	1.784	1.800
SS-C6	432	21.0	1.152	0.150	1.002	3.688	0.675	3.013	2.301	0.454	1.847	1.697	0.332	1.365	1.800
SS-C7	432	21.8	1.092	0.143	0.949	3.399	0.637	2.762	2.121	0.426	1.695	1.568	0.316	1.252	1.800
SS-C8	432	21.2	1.131	0.147	0.984	3.635	0.668	2.967	2.267	0.449	1.818	1.672	0.329	1.343	1.800
SS-C9	432	21.3	1.166	0.154	1.012	3.541	0.657	2.884	2.210	0.440	*1.770*	1.649	0.326	1.323	1.800

Table E.4: Computed Deflections for Square Slabs Loaded at 7 Days

Slab ID	Clear span (ins)	Slab Thickness (ins)	Computed Deflections (ins)												Perm. Defl. (l/240) (ins)
			Mid-panel Deflections						Deflections Along Column Lines						
			Interior (Node 7)			Exterior (Node 31)			Node 17			Node 45			
			Δ_{tot}	Δ_{inst}	Δ_{incr}	Δ_{tot}	Δ_{inst}	Δ_{incr}	Δ_{tot}	Δ_{inst}	Δ_{incr}	Δ_{tot}	Δ_{inst}	Δ_{incr}	
SS-A11	210	6.00	1.150	0.244	0.906	3.062	0.603	2.459	1.838	0.372	1.466	1.415	0.280	1.135	0.875
SS-A12	210	6.60	0.844	0.175	0.669	2.295	0.435	1.860	1.310	0.255	1.055	1.050	0.206	0.844	0.875
SS-A13	210	7.00	0.781	0.157	0.624	1.447	0.272	1.175	0.890	0.175	0.715	0.602	0.120	0.482	0.875
SS-A14	210	6.80	0.855	0.174	0.681	1.677	0.313	1.364	1.053	0.203	*0.850*	0.712	0.141	0.571	0.875
SS-B8	314	9.0	2.789	0.486	2.303	5.413	0.906	4.507	3.559	0.643	2.916	2.902	0.494	2.408	1.310
SS-B9	314	10.0	2.183	0.356	1.827	4.669	0.777	3.892	2.848	0.495	2.353	2.183	0.377	1.806	1.310
SS-B10	314	12.0	1.364	0.230	1.134	3.152	0.548	2.604	1.876	0.356	1.520	1.475	0.256	1.219	1.310
SS-B11	314	12.9	1.139	0.190	0.949	2.757	0.487	2.270	1.620	0.310	*1.310*	1.256	0.226	1.030	1.310
SS-C10	432	16.0	2.011	0.423	1.588	4.906	1.109	3.797	2.992	0.725	2.267	2.347	0.537	1.811	1.800
SS-C11	432	17.8	1.573	0.262	1.311	4.222	0.825	3.397	2.552	0.548	2.004	1.925	0.360	1.565	1.800
SS-C12	432	18.5	1.407	0.231	1.176	3.841	0.773	3.068	2.366	0.515	1.851	1.775	0.378	1.397	1.800
SS-C13	432	18.7	1.302	0.212	1.089	3.773	0.762	3.011	2.325	0.507	*1.818*	1.742	0.373	1.369	1.800

Table E.5: Computed Deflections for Square Slabs Loaded at 14 Days

Slab ID	Clear span (ins)	Slab Thickness (ins)	Computed Deflections (ins)												Perm. Defl. (l/240) (ins)
			Mid-panel Deflections						Deflections Along Column Lines						
			Interior (Node 7)			Exterior (Node 31)			Node 17			Node 45			
			Δ_{tot}	Δ_{inst}	Δ_{incr}	Δ_{tot}	Δ_{inst}	Δ_{incr}	Δ_{tot}	Δ_{inst}	Δ_{incr}	Δ_{tot}	Δ_{inst}	Δ_{incr}	
SS-A15	210	6.00	0.900	0.199	0.701	1.686	0.352	1.334	1.041	0.233	0.808	0.720	0.162	0.558	0.875
SS-A16	210	5.80	0.951	0.216	0.735	1.978	0.421	1.557	1.302	0.291	1.012	0.824	0.186	0.638	0.875
SS-A17	210	5.90	0.916	0.206	0.710	1.685	0.310	1.375	1.103	0.225	*0.878*	0.762	0.173	0.589	0.875
SS-B12	314	12.0	1.037	0.197	0.840	2.553	0.501	2.052	1.511	0.320	1.191	1.187	0.237	0.950	1.310
SS-B13	314	11.6	1.191	0.224	0.967	2.741	0.541	2.200	1.608	0.345	1.263	1.267	0.254	1.013	1.310
SS-B14	314	11.4	1.264	0.237	1.027	2.862	0.561	2.301	1.694	0.361	1.333	1.310	0.262	1.048	1.310
SS-B15	314	11.5	1.192	0.225	0.967	2.814	0.551	2.263	1.677	0.355	*1.322*	1.282	0.257	1.025	1.310
SS-C14	432	18.0	1.164	0.215	0.949	3.415	0.710	2.705	2.119	0.482	1.637	1.572	0.355	1.217	1.800
SS-C15	432	17.4	1.364	0.249	1.115	3.624	0.750	2.874	2.245	0.510	1.735	1.677	0.375	1.302	1.800
SS-C16	432	17.1	1.367	0.235	1.132	3.798	0.775	3.023	2.351	0.527	1.824	1.753	0.386	1.367	1.800
SS-C17	432	17.2	1.329	0.245	1.084	3.716	0.766	2.950	2.308	0.521	*1.787*	1.730	0.384	1.346	1.800

Table E.6: Computed Deflections for Square Slabs Loaded at 28 days

Slab ID	Clear span (ins)	Slab Thickness (ins)	Computed Deflections (ins)												Perm. Defl. (l/240) (ins)
			Mid-panel Deflections						Deflections Along Column Lines						
			Interior (Node 7)			Exterior (Node 31)			Node 17			Node 45			
			Δ_{tot}	Δ_{inst}	Δ_{incr}	Δ_{tot}	Δ_{inst}	Δ_{incr}	Δ_{tot}	Δ_{inst}	Δ_{incr}	Δ_{tot}	Δ_{inst}	Δ_{incr}	
SS-A18	210	5.40	0.998	0.190	0.808	1.811	0.335	1.476	1.173	0.254	0.919	0.762	0.162	0.600	0.875
SS-A19	210	5.60	0.904	0.173	0.731	1.620	0.300	1.320	1.016	0.226	0.790	0.684	0.144	0.540	0.875
SS-A20	210	5.50	0.936	0.177	0.759	1.699	0.307	1.392	1.084	0.233	*0.851*	0.706	0.148	0.558	0.875
SS-B16	314	10.0	1.599	0.279	1.320	3.253	0.609	2.644	1.920	0.430	1.490	1.544	0.308	1.236	1.310
SS-B17	314	10.4	1.206	0.236	0.970	2.776	0.553	2.223	1.663	0.387	1.276	1.291	0.276	1.015	1.310
SS-B18	314	10.3	1.321	0.255	1.066	2.809	0.561	2.248	1.674	0.392	*1.282*	1.311	0.280	1.031	1.310
SS-C18	432	15.7	1.342	0.230	1.112	3.559	0.873	2.686	2.238	0.630	1.608	1.603	0.434	1.169	1.800
SS-C19	432	15.5	1.465	0.261	1.204	3.674	0.898	2.776	2.310	0.651	1.659	1.663	0.447	1.216	1.800
SS-C20	432	15.0	1.554	0.280	1.274	3.892	0.940	2.952	2.460	0.681	*1.779*	1.766	0.468	1.298	1.800

Table E.7: Computed Deflections for Square Slabs Loaded at 3 Days (f'_c = 3500 psi)

Slab ID	Clear span (ins)	Slab Thickness (ins)	Computed Deflections (ins)												Perm. Defl. (l/240) (ins)
			Mid-panel Deflections						Deflections Along Column Lines						
			Interior (Node 7)			Exterior (Node 31)			Node 17			Node 45			
			Δ_{tot}	Δ_{inst}	Δ_{incr}	Δ_{tot}	Δ_{inst}	Δ_{incr}	Δ_{tot}	Δ_{inst}	Δ_{incr}	Δ_{tot}	Δ_{inst}	Δ_{incr}	
SS-A21	210	7.80	0.672	0.116	0.556	1.408	0.217	1.191	0.883	0.141	0.742	0.588	0.096	0.492	0.875
SS-A22	210	7.40	0.740	0.129	0.611	2.058	0.316	1.742	1.230	0.192	1.038	0.927	0.149	0.778	0.875
SS-A23	210	7.60	0.709	0.123	0.586	1.545	0.237	1.308	1.001	0.158	*0.843*	0.661	0.107	0.558	0.875
SS-B19	314	14.4	0.838	0.149	0.689	2.311	0.417	1.894	1.398	0.265	1.133	1.066	0.196	0.870	1.310
SS-B20	314	13.8	1.052	0.179	0.873	2.607	0.460	2.147	1.612	0.297	*1.315*	1.187	0.213	0.974	1.310

Table E.8: Computed Deflections for Square Slabs Loaded at 3 Days ($f'_c = 4000$ psi)

Slab ID	Clear span (ins)	Slab Thickness (ins)	Computed Deflections (ins)												Perm. Defl. ($l/240$) (ins)
			Mid-panel Deflections						Deflections Along Column Lines						
			Interior (Node 7)			Exterior (Node 31)			Node 17			Node 45			
			Δ_{tot}	Δ_{inst}	Δ_{incr}	Δ_{tot}	Δ_{inst}	Δ_{incr}	Δ_{tot}	Δ_{inst}	Δ_{incr}	Δ_{tot}	Δ_{inst}	Δ_{incr}	
SS-A24	210	7.50	0.600	0.120	0.480	1.189	0.217	0.972	0.732	0.139	0.593	0.491	0.096	0.395	0.875
SS-A25	210	6.60	0.871	0.169	0.702	2.257	0.421	1.836	1.365	0.262	1.103	0.989	0.192	0.797	0.875
SS-A26	210	6.80	0.737	0.149	0.588	2.089	0.383	1.706	1.248	0.233	1.015	0.916	0.176	0.740	0.875
SS-A27	210	7.00	0.713	0.143	0.570	1.560	0.281	1.279	1.012	0.187	*0.825*	0.647	0.124	0.523	0.875
SS-B21	314	14.0	0.743	0.155	0.588	2.097	0.431	1.666	1.254	0.270	0.984	0.985	0.201	0.784	1.310
SS-B22	314	12.8	1.116	0.214	0.902	2.605	0.529	2.076	1.640	0.344	*1.296*	1.163	0.241	0.922	1.310

Table E.9: Computed Deflections for Square Slabs with Drop Panels Loaded at 7 Days

Slab ID	Clear span (ins)	Slab Thickness (ins)	Computed Deflections (ins)												Perm. Defl. (l/240) (ins)
			Mid-panel Deflections						Deflections Along Column Lines						
			Interior (Node 7)			Exterior (Node 31)			Node 17			Node 45			
			Δ_{tot}	Δ_{inst}	Δ_{incr}	Δ_{tot}	Δ_{inst}	Δ_{incr}	Δ_{tot}	Δ_{inst}	Δ_{incr}	Δ_{tot}	Δ_{inst}	Δ_{incr}	
DP-A1	216	6.40	0.730	0.131	0.599	1.281	0.235	1.046	0.737	0.143	0.594	0.536	0.104	0.432	0.875
DP-A2	216	5.60	0.967	0.183	0.784	1.889	0.357	1.532	1.151	0.228	0.923	0.798	0.158	0.640	0.875
DP-A3	216	5.80	0.896	0.166	0.730	1.657	0.311	1.346	0.998	0.197	0.801	0.697	0.137	0.560	0.875
DP-A4	216	5.70	0.913	0.172	0.741	1.769	0.334	1.435	1.085	0.214	*0.871*	0.731	0.145	0.586	0.875
DP-B1	324	12.6	0.833	0.142	0.691	1.734	0.347	1.387	1.018	0.215	0.803	0.747	0.160	0.587	1.310
DP-B2	324	10.7	1.282	0.217	1.065	2.978	0.569	2.409	1.715	0.338	1.377	1.363	0.265	1.098	1.310
DP-B3	324	10.8	1.166	0.207	0.959	2.912	0.552	2.360	1.656	0.327	1.329	1.336	0.256	1.080	1.310
DP-B4	324	10.9	1.149	0.202	0.947	2.735	0.521	2.214	1.574	0.312	*1.262*	1.229	0.239	0.990	1.310
DP-C1	442	18.0	0.666	0.179	0.487	3.012	0.693	2.319	1.834	0.459	1.375	1.366	0.350	1.016	1.800
DP-C2	442	16.8	0.871	0.230	0.641	3.371	0.755	2.616	2.057	0.500	1.557	1.574	0.386	1.188	1.800
DP-C3	442	15.6	1.600	0.286	1.314	3.963	0.827	3.136	2.354	0.528	1.826	1.778	0.393	1.385	1.800
DP-C4	442	15.7	1.586	0.283	1.303	3.925	0.820	3.105	2.334	0.524	*1.810*	1.768	0.391	1.377	1.800

Table E.10: Computed Deflections for Rectangular Slabs with Aspect Ratio 1.5 Loaded at 4 Days

Slab ID	Clear Span Y-Dir. (ins)	Slab Thickness (ins)	Computed Deflections (ins)												Perm. Defl. (l/240) (ins)
			Mid-panel Deflections						Deflections Along Column Lines						
			Interior (Node 7)			Exterior (Node 31)			X-Dir. (Node 17)			Y-Dir. (Node 33)			
			Δ_{tot}	Δ_{inst}	Δ_{incr}	Δ_{tot}	Δ_{inst}	Δ_{incr}	Δ_{tot}	Δ_{inst}	Δ_{incr}	Δ_{tot}	Δ_{inst}	Δ_{incr}	
RS-A1	210	6.20	0.846	0.134	0.712	1.779	0.268	1.511	0.347	0.057	0.290	1.724	0.263	1.461	0.875
RS-A2	210	6.40	0.769	0.122	0.647	1.630	0.243	1.387	0.308	0.050	0.258	1.565	0.237	1.328	0.875
RS-A3	210	6.60	0.729	0.114	0.615	1.161	0.173	0.988	0.277	0.045	0.232	1.093	0.166	0.927	0.875
RS-A4	210	7.00	0.657	0.100	0.557	0.943	0.141	0.802	0.224	0.036	0.188	0.864	0.133	0.731	0.875
RS-A5	210	6.80	0.690	0.106	0.584	1.033	0.154	0.879	0.256	0.041	0.215	0.954	0.146	0.808	0.875
RS-A6	210	6.70	0.708	0.110	0.598	1.073	0.160	0.913	0.264	0.042	0.222	0.993	0.153	*0.840*	0.875
RS-B1	314	12.0	1.038	0.160	0.878	1.986	0.314	1.672	0.417	0.075	0.342	1.909	0.303	1.606	1.310
RS-B2	314	12.6	0.809	0.135	0.674	1.769	0.283	1.486	0.366	0.068	0.298	1.707	0.271	1.436	1.310
RS-B3	314	12.8	0.772	0.130	0.642	1.706	0.273	1.433	0.336	0.064	0.272	1.657	0.263	1.394	1.310
RS-B4	314	13.0	0.740	0.128	0.612	1.700	0.289	1.411	0.323	0.067	0.256	1.637	0.276	1.361	1.310
RS-B5	314	13.2	0.689	0.118	0.571	1.541	0.252	1.289	0.309	0.060	0.249	1.513	0.243	*1.270*	1.310
RS-C1	432	18.0	1.042	0.178	0.864	2.440	0.480	1.960	0.557	0.122	0.435	2.319	0.458	1.861	1.800
RS-C2	432	18.3	0.989	0.169	0.820	2.373	0.469	1.904	0.547	0.119	0.428	2.249	0.449	*1.800*	1.800

Table E.11: Computed Deflections for Rectangular Slabs with Aspect Ratio 1.5 Loaded at 7 Days

Slab ID	Clear Span Y-Dir. (ins)	Slab Thickness (ins)	Computed Deflections (ins)												Perm. Defl. (l/240) (ins)
			Mid-panel Deflections						Deflections Along Column Lines						
			Interior (Node 7)			Exterior (Node 31)			X-Dir. (Node 17)			Y-Dir. (Node 33)			
			Δ_{tot}	Δ_{inst}	Δ_{incr}	Δ_{tot}	Δ_{inst}	Δ_{incr}	Δ_{tot}	Δ_{inst}	Δ_{incr}	Δ_{tot}	Δ_{inst}	Δ_{incr}	
RS-A7	210	7.00	0.521	0.110	0.411	0.700	0.151	0.549	0.154	0.039	0.115	0.628	0.142	0.486	0.875
RS-A8	210	6.40	0.619	0.115	0.504	0.865	0.160	0.705	0.208	0.042	0.166	0.800	0.152	0.648	0.875
RS-A9	210	6.00	0.702	0.133	0.569	1.025	0.191	0.834	0.249	0.050	0.199	0.952	0.183	0.769	0.875
RS-A10	210	5.80	0.745	0.144	0.601	1.140	0.214	0.926	0.278	0.056	0.222	1.071	0.206	*0.865*	0.875
RS-B6	314	10.0	1.251	0.235	1.016	2.276	0.447	1.829	0.486	0.104	0.382	2.197	0.436	1.761	1.310
RS-B7	314	11.0	0.896	0.175	0.721	1.865	0.348	1.517	0.393	0.083	0.310	1.809	0.338	1.471	1.310
RS-B8	314	11.6	0.747	0.150	0.597	1.653	0.310	1.343	0.332	0.073	0.259	1.622	0.300	1.322	1.310
RS-B9	314	11.7	0.734	0.147	0.587	1.603	0.304	1.299	0.330	0.072	0.258	1.564	0.293	*1.271*	1.310
RS-C3	432	15.0	1.527	0.289	1.238	3.070	0.637	2.433	0.728	0.165	0.563	2.884	0.608	2.276	1.800
RS-C4	432	16.2	1.138	0.223	0.915	2.464	0.542	1.922	0.573	0.139	0.434	2.347	0.519	1.828	1.800
RS-C5	432	16.3	1.114	0.221	0.893	2.451	0.539	1.912	0.565	0.138	0.427	2.330	0.516	1.814	1.800
RS-C6	432	16.4	1.103	0.214	0.889	2.409	0.528	1.881	0.542	0.135	0.407	2.304	0.506	*1.798*	1.800

Table E.12: Computed Deflections for Rectangular Slabs with Aspect Ratio 1.5 Loaded at 14 Days

Slab ID	Clear Span Y-Dir. (ins)	Slab Thickness (ins)	Computed Deflections (ins)												Perm. Defl. (l/240) (ins)
			Mid-panel Deflections						Deflections Along Column Lines						
			Interior (Node 7)			Exterior (Node 31)			X-Dir. (Node 17)			Y-Dir. (Node 33)			
			Δ_{tot}	Δ_{inst}	Δ_{incr}	Δ_{tot}	Δ_{inst}	Δ_{incr}	Δ_{tot}	Δ_{inst}	Δ_{incr}	Δ_{tot}	Δ_{inst}	Δ_{incr}	
RS-A11	210	5.40	0.725	0.150	0.575	1.010	0.210	0.800	0.252	0.058	0.194	0.937	0.203	0.734	0.875
RS-A12	210	5.00	0.827	0.177	0.650	1.851	0.410	1.441	0.329	0.077	0.252	1.804	0.410	1.394	0.875
RS-A13	210	5.20	0.774	0.164	0.610	1.117	0.235	0.882	0.282	0.065	0.217	1.045	0.228	*0.817*	0.875
RS-B10	314	10.7	0.738	0.154	0.584	1.562	0.335	1.227	0.318	0.077	0.241	1.493	0.324	1.169	1.310
RS-B11	314	10.2	0.849	0.175	0.674	1.766	0.370	1.396	0.355	0.085	0.270	1.702	0.358	1.344	1.310
RS-B12	314	10.3	0.827	0.171	0.656	1.720	0.363	1.357	0.354	0.084	0.270	1.655	0.351	*1.304*	1.310
RS-C7	432	15.2	1.081	0.225	0.856	2.338	0.542	1.796	0.522	0.140	0.382	2.242	0.527	1.715	1.800
RS-C8	432	14.8	1.218	0.247	0.971	2.468	0.567	1.901	0.578	0.149	0.429	2.360	0.550	*1.810*	1.800

Table E.13: Computed Deflections for Rectangular Slabs with Aspect Ratio 1.5 Loaded at 28 Days

Slab ID	Clear Span Y-Dir. (ins)	Slab Thickness (ins)	Computed Deflections (ins)												Perm. Defl. (l/240) (ins)
			Mid-panel Deflections						Deflections Along Column Lines						
			Interior (Node 7)			Exterior (Node 31)			X-Dir. (Node 17)			Y-Dir. (Node 33)			
			Δ_{tot}	Δ_{inst}	Δ_{incr}	Δ_{tot}	Δ_{inst}	Δ_{incr}	Δ_{tot}	Δ_{inst}	Δ_{incr}	Δ_{tot}	Δ_{inst}	Δ_{incr}	
RS-A14	210	5.40	0.640	0.112	0.528	0.831	0.155	0.676	0.191	0.045	0.146	0.760	0.152	0.608	0.875
RS-A15	210	4.70	0.818	0.151	0.667	1.207	0.221	0.986	0.301	0.068	0.233	1.138	0.220	0.918	0.875
RS-A16	210	4.80	0.793	0.144	0.649	1.130	0.208	0.922	0.279	0.063	0.216	1.056	0.208	*0.848*	0.875
RS-B13	314	9.00	0.976	0.187	0.789	2.012	0.398	1.614	0.419	0.106	0.313	1.951	0.402	1.549	1.310
RS-B14	314	9.60	0.844	0.162	0.682	1.730	0.346	1.384	0.355	0.091	0.264	1.666	0.348	*1.318*	1.310
RS-C9	432	13.0	1.554	0.272	1.282	2.825	0.649	2.176	0.635	0.178	0.457	2.682	0.646	2.036	1.800
RS-C10	432	13.6	1.336	0.246	1.090	2.550	0.600	1.950	0.579	0.167	0.412	2.431	0.600	1.831	1.800
RS-C11	432	13.7	1.337	0.239	1.098	2.510	0.592	1.918	0.574	0.165	0.409	2.398	0.593	*1.805*	1.800

Table E.14: Computed Deflections for Rectangular Slabs with Aspect Ratio 2.0 Loaded at 4 Days

Slab ID	Clear Span Y-Dir. (ins)	Slab Thickness (ins)	Computed Deflections (ins)												Perm. Defl. (l/240) (ins)
			Mid-panel Deflections						Deflections Along Column Lines						
			Interior (Node 7)			Exterior (Node 31)			X-Dir. (Node 17)			Y-Dir. (Node 33)			
			Δ_{tot}	Δ_{inst}	Δ_{incr}	Δ_{tot}	Δ_{inst}	Δ_{incr}	Δ_{tot}	Δ_{inst}	Δ_{incr}	Δ_{tot}	Δ_{inst}	Δ_{incr}	
RS-A17	210	6.00	0.901	0.139	0.762	1.625	0.252	1.373	0.109	0.019	0.090	1.634	0.254	1.380	0.875
RS-A18	210	6.60	0.734	0.122	0.612	0.908	0.151	0.757	0.079	0.015	0.064	0.893	0.151	0.742	0.875
RS-A19	210	6.40	0.769	0.117	0.652	0.956	0.146	0.810	0.082	0.015	0.067	0.951	0.148	0.803	0.875
RS-A20	210	6.20	0.816	0.126	0.690	1.043	0.161	0.882	0.091	0.016	0.075	1.040	0.163	*0.877*	0.875
RS-B15	314	12.0	0.855	0.132	0.723	1.402	0.224	1.178	0.105	0.022	0.083	1.408	0.227	1.181	1.310
RS-B16	314	11.5	0.956	0.146	0.810	1.589	0.248	1.341	0.122	0.025	0.097	1.603	0.252	1.351	1.310
RS-B17	314	11.6	0.880	0.147	0.733	1.579	0.267	1.312	0.111	0.025	0.086	1.594	0.270	*1.324*	1.310
RS-C12	432	17.6	1.125	0.167	0.958	2.128	0.375	1.753	0.180	0.040	0.140	2.141	0.382	1.759	1.800
RS-C13	432	17.5	1.141	0.170	0.971	2.151	0.379	1.772	0.182	0.041	0.141	2.168	0.386	*1.782*	1.800

Table E.15: Computed Deflections for Rectangular Slabs with Aspect Ratio 2.0 Loaded at 7 Days

Slab ID	Clear Span Y-Dir. (ins)	Slab Thickness (ins)	Computed Deflections (ins)												Perm. Defl. (l/240) (ins)
			Mid-panel Deflections						Deflections Along Column Lines						
			Interior (Node 7)			Exterior (Node 31)			X-Dir. (Node 17)			Y-Dir. (Node 33)			
			Δ_{tot}	Δ_{inst}	Δ_{incr}	Δ_{tot}	Δ_{inst}	Δ_{incr}	Δ_{tot}	Δ_{inst}	Δ_{incr}	Δ_{tot}	Δ_{inst}	Δ_{incr}	
RS-A21	210	7.00	0.466	0.084	0.382	0.569	0.104	0.465	0.055	0.011	0.044	0.555	0.104	0.451	0.875
RS-A22	210	5.60	0.806	0.170	0.636	1.030	0.217	0.813	0.092	0.022	0.070	1.028	0.219	0.809	0.875
RS-A23	210	5.40	0.868	0.187	0.681	1.088	0.234	0.854	0.098	0.024	0.074	1.090	0.236	*0.854*	0.875
RS-B18	314	10.0	1.078	0.206	0.872	1.935	0.378	1.557	0.142	0.033	0.109	1.948	0.382	1.566	1.310
RS-B19	314	10.6	1.058	0.183	0.875	1.864	0.334	1.530	0.140	0.030	0.110	1.865	0.338	1.527	1.310
RS-B20	314	11.0	0.963	0.167	0.796	1.718	0.307	1.411	0.125	0.028	0.097	1.722	0.311	1.411	1.310
RS-B21	314	11.1	0.941	0.163	0.778	1.671	0.299	1.372	0.120	0.027	0.093	1.683	0.303	1.380	1.310
RS-B22	314	11.2	0.904	0.158	0.746	1.522	0.270	1.252	0.117	0.026	0.091	1.533	0.274	*1.259*	1.310
RS-C14	432	15.0	1.528	0.293	1.235	2.487	0.527	1.960	0.225	0.057	0.168	2.490	0.534	1.956	1.800
RS-C15	432	15.4	1.529	0.256	1.273	2.596	0.493	2.103	0.236	0.054	0.182	2.598	0.501	2.097	1.800
RS-C16	432	16.2	1.328	0.220	1.108	2.308	0.444	1.864	0.207	0.048	0.159	2.321	0.451	1.870	1.800
RS-C17	432	16.3	1.298	0.218	1.080	2.289	0.440	1.849	0.204	0.048	0.156	2.298	0.447	1.851	1.800
RS-C18	432	16.5	1.272	0.215	1.057	2.214	0.428	1.786	0.200	0.047	0.153	2.223	0.435	*1.788*	1.800

Table E.16: Computed Deflections for Rectangular Slabs with Aspect Ratio 2.0 Loaded at 14 Days

Slab ID	Clear Span Y-Dir. (ins)	Slab Thickness (ins)	Computed Deflections (ins)												Perm. Defl. (l/240) (ins)
			Mid-panel Deflections						Deflections Along Column Lines						
			Interior (Node 7)			Exterior (Node 31)			X-Dir. (Node 17)			Y-Dir. (Node 33)			
			Δ_{tot}	Δ_{inst}	Δ_{incr}	Δ_{tot}	Δ_{inst}	Δ_{incr}	Δ_{tot}	Δ_{inst}	Δ_{incr}	Δ_{tot}	Δ_{inst}	Δ_{incr}	
RS-A24	210	5.00	0.799	0.168	0.631	0.956	0.205	0.751	0.089	0.021	0.068	0.946	0.207	0.739	0.875
RS-A25	210	4.80	0.859	0.184	0.675	1.084	0.236	0.848	0.100	0.025	0.075	1.084	0.241	0.843	0.875
RS-A26	210	4.70	0.906	0.196	0.710	1.142	0.251	0.891	0.106	0.026	0.080	1.143	0.256	*0.887*	0.875
RS-B23	314	10.2	0.841	0.168	0.673	1.379	0.288	1.091	0.108	0.028	0.080	1.386	0.293	1.093	1.310
RS-B24	314	9.60	0.985	0.195	0.790	1.784	0.368	1.416	0.129	0.032	0.097	1.795	0.373	1.422	1.310
RS-B25	314	9.90	0.899	0.178	0.721	1.601	0.335	1.266	0.119	0.030	0.089	1.620	0.341	*1.279*	1.310
RS-C19	432	14.8	1.176	0.235	0.941	2.020	0.465	1.555	0.175	0.049	0.126	2.044	0.475	1.569	1.800
RS-C20	432	14.0	1.471	0.292	1.179	2.385	0.534	1.851	0.210	0.057	0.153	2.403	0.543	1.860	1.800
RS-C21	432	14.2	1.337	0.265	1.072	2.298	0.515	1.783	0.201	0.054	0.147	2.320	0.524	*1.796*	1.800

Table E.17: Computed Deflections for Rectangular Slabs with Aspect Ratio 2.0 Loaded at 28 Days

Slab ID	Clear Span Y-Dir. (ins)	Slab Thickness (ins)	Computed Deflections (ins)												Perm. Defl. (l/240) (ins)
			Mid-panel Deflections						Deflections Along Column Lines						
			Interior (Node 7)			Exterior (Node 31)			X-Dir. (Node 17)			Y-Dir. (Node 33)			
			Δ_{tot}	Δ_{inst}	Δ_{incr}	Δ_{tot}	Δ_{inst}	Δ_{incr}	Δ_{tot}	Δ_{inst}	Δ_{incr}	Δ_{tot}	Δ_{inst}	Δ_{incr}	
RS-A27	210	5.20	0.624	0.107	0.517	0.739	0.138	0.601	0.073	0.017	0.056	0.729	0.141	0.588	0.875
RS-A28	210	4.60	0.811	0.140	0.671	0.974	0.182	0.792	0.092	0.022	0.070	0.967	0.187	0.780	0.875
RS-A29	210	4.40	0.892	0.156	0.736	1.117	0.207	0.910	0.102	0.024	0.078	1.120	0.214	0.906	0.875
RS-A30	210	4.50	0.855	0.150	0.705	1.039	0.193	0.846	0.099	0.023	0.076	1.035	0.199	*0.836*	0.875
RS-B26	314	9.00	0.973	0.176	0.797	1.689	0.328	1.361	0.129	0.034	0.095	1.703	0.340	1.363	1.310
RS-B27	314	9.20	0.921	0.166	0.755	1.600	0.310	1.290	0.121	0.032	0.089	1.613	0.322	*1.291*	1.310
RS-C22	432	14.0	1.067	0.195	0.872	1.990	0.470	1.520	0.172	0.052	0.120	2.000	0.485	1.515	1.800
RS-C23	432	13.2	1.365	0.251	1.114	2.262	0.523	1.739	0.200	0.059	0.141	2.272	0.543	1.729	1.800
RS-C24	432	13.0	1.425	0.261	1.164	2.389	0.545	1.844	0.214	0.061	0.153	2.408	0.566	1.842	1.800
RS-C25	432	13.1	1.394	0.255	1.139	2.340	0.536	1.804	0.204	0.060	0.144	2.355	0.557	*1.798*	1.800